

9-12-2013 12:00 AM

Development of Microfabrication Process for Micro Inductive Sensors

Xueguang Han, *The University of Western Ontario*

Supervisor: Dr. Jun Yang, *The University of Western Ontario*

A thesis submitted in partial fulfillment of the requirements for the Master of Engineering Science degree in Mechanical and Materials Engineering

© Xueguang Han 2013

Follow this and additional works at: <https://ir.lib.uwo.ca/etd>



Part of the [Electro-Mechanical Systems Commons](#)

Recommended Citation

Han, Xueguang, "Development of Microfabrication Process for Micro Inductive Sensors" (2013). *Electronic Thesis and Dissertation Repository*. 1632.

<https://ir.lib.uwo.ca/etd/1632>

This Dissertation/Thesis is brought to you for free and open access by Scholarship@Western. It has been accepted for inclusion in Electronic Thesis and Dissertation Repository by an authorized administrator of Scholarship@Western. For more information, please contact wlsadmin@uwo.ca.

DEVELOPMENT OF MICROFABRICATION PROCESS FOR MICRO INDUCTIVE
SENSORS

(Thesis format: Monograph)

by

Xueguang Han

Graduate Program in Mechanical and Materials Engineering

A thesis submitted in partial fulfillment
of the requirements for the degree of
Master of Engineering Science

The School of Graduate and Postdoctoral Studies
The University of Western Ontario
London, Ontario, Canada

© Xueguang Han 2013

Abstract

Inductive position/angle sensors are widely used in vehicles and have very bright market prospects. However, the current sensor designs often suffer from high space consuming which increases the assembly size of vehicle parts. In addition, the high emission of traditional inductive sensors can cause the interference with other electronic components. In this dissertation, a novel and reliable microfabrication process was developed to fabricate a newly designed miniaturized inductive sensor for gas pedal use. The ANSYS HFSS simulation (High Frequency Structural Simulator) has proved that the newly developed inductive sensor could provide sufficient sensitivity to meet the sensing requirements. The performance of the sensor was well studied by the quality ensuring inter-process tests, the performance test and the system integration tests. The final prototype was developed and the test results showed that the properties of the devices were consistent with the simulation. This research project has led to a better understanding of developing miniaturized inductive sensor and microfabrication processes for fabricating vehicle sensors.

Keywords: Inductive sensor, microfabrication, photolithography, sputtering, electroplating, wet etching

Acknowledgments

First of all, I would like to thank my supervisor, Dr. Jun Yang, who gave me this great opportunity to join his team and this project. He introduced me to this exciting research area, and offered me a lot of help and freedom to do research.

I also would like to thank Lingmin Shao, who offered me a lot of help and advice during the research. His patient explanation helped me to understand the research as well as the simulation better than ever.

My thanks also go to KSR company, Larry Willemsen, Ryan Elliott and Don O'Neill offered great support during the research and tests.

My colleagues and cleanroom stuffs are very supportive during my research, I owe them tremendous gratitude.

Finally, I would like to express my sincere gratitude to my family and my girlfriend. Thanks a lot for your trust and support.

Table of Contents

Abstract.....	ii
Acknowledgments.....	iii
Table of Contents.....	iv
List of Tables	vii
List of Figures	viii
Chapter 1	1
1 Introduction.....	1
1.1 Position sensors overview.....	1
1.2 Motivation of using micro inductive sensors.....	6
1.3 Scope and research objective	11
1.4 Outline of thesis	12
Chapter 2.....	14
2 Introduction of microfabrication process and prototype simulation.....	14
2.1 Background.....	14
2.2 Introduction of microfabrication process.....	15
2.2.1 Substrate selection	15
2.2.2 Photolithography.....	16
2.2.3 Sputtering.....	22
2.2.4 Electroplating in microfabrication	25
2.2.5 Wet etching for metals.....	28
2.3 Prototype simulation	30
2.4 Conclusion	34
Chapter 3.....	36
3 Microfabrication process for the micro inductive sensor.....	36

3.1	Introduction.....	36
3.2	Critical parameter calculation and process selection	37
3.3	Photomask design and optimization	58
3.4	Microfabrication steps	61
3.4.1	Substrate pretreatment	61
3.4.2	Seeding layer sputtering.....	62
3.4.3	First layer micromold photolithography	64
3.4.4	Electroplating.....	71
3.4.5	Strip photoresist	78
3.4.6	Etching seed layer	78
3.4.7	Insulating layer preparation	80
3.4.8	Sulfuric acid etch	87
3.4.9	Second seed layer sputtering.....	87
3.4.10	Second layer copper coil fabrication.....	88
3.5	Conclusions.....	91
Chapter 4.....		92
4	Quality characterization	92
4.1	Introduction.....	92
4.2	Inter-procedure test and low frequency test by LCR meter	92
4.3	High frequency test by impedance analyzer	96
4.4	Circuit integration	100
4.5	Conclusion	112
Chapter 5.....		114
5	Conclusions	114
5.1	Summary of results	114

5.2 Thesis contributions	117
5.3 Suggestions for future research.....	117
References.....	119

List of Tables

Table 2.1 Resistance result with different copper thickness.....	34
Table 3.1 Parameters for electroplating.....	77
Table 3.2 Physical properties of the HD4100 negative tone Polyimide [43].	81
Table 4.1 Test result of first copper coils	95
Table 4.2 Test result of the device.....	96
Table 4.3 Comparison of simulation results and test results.	100
Table 4.4 Bonding parameter.....	104

List of Figures

Figure 1.1 Application for position/angle sensors in each vehicle. (Adapted from [2])	2
Figure 1.2 Schematic drawing of the variable resistor-based position/angle sensor. (Adapted from [4]).....	3
Figure 1.3 Hall Effect and the assembly of Hall effect sensor. (Adapted from [5, 6]).....	4
Figure 1.4 AMR unit and assembly of AMR angle sensor. (Adapted from [8, 9])	5
Figure 1.5 Inductive sensor components. PCB (bottom) and Coupler/Rotor (up)	8
Figure 1.6 Assembly schematic of inductive sensor. (Adapted from [15])	9
Figure 1.7 Simplified operation principle	9
Figure 2.1 Lithography process flow.	19
Figure 2.2 Schematic illustration of three systems of photolithography: (a) contact; (b) proximity; and (c) projection. (Adapted from [28]).....	20
Figure 2.3 Steps of photolithography, comparison of positive and negative photoresist.	21
Figure 2.4 Illustration of mechanisms when ion strikes the target surface. (Adapted from [30]).....	23
Figure 2.5 Illustration of sputtering process. (Adapted from [31]).....	24
Figure 2.6 Principle of electroplating.	27

Figure 2.7 Chemical reaction process of wet etch.	28
Figure 2.8 Undercut in the wet etch.....	30
Figure 2.9 Design of the inductive sensor coil.	31
Figure 2.10 Model of prototype created by HFSS.....	32
Figure 2.11 Plot of magnetic field generated by the excitation coil.	33
Figure 2.12 Resistance simulation result.	33
Figure 2.13 Inductance simulation result.....	34
Figure 3.1 Cross-section view of the inductive sensor device.....	36
Figure 3.2 Step coverage of sputtering.	40
Figure 3.3 Bi-layer lift-off process. (Copied from [37]).....	41
Figure 3.4 Undercut in bi-layer method under microscope.	42
Figure 3.5 SEM image of surface using bi-layer method.	43
Figure 3.6 SEM image of the cross-section using bi-layer method.....	43
Figure 3.7 The electroplating process using photoresist as micro mold.....	46
Figure 3.8 Over-plating in the electroplating process.....	47
Figure 3.9 Cracks round the patterns in SU-8.....	50
Figure 3.10 Cross-section view of the coil.	51

Figure 3.11 Electroplating growth mechanism of via holes.	53
Figure 3.12 Outline of the process for device.....	58
Figure 3.13 Filleted corners in the mask.....	59
Figure 3.14 50X magnification of the mask features.....	59
Figure 3.15 Transparent window of the mask.	60
Figure 3.16 Mask designed for electroplating.	61
Figure 3.17 Photograph of Edwards Auto500 sputter deposition system. (Copied from [45])	62
Figure 3.18 Wafer with copper seed layer.	63
Figure 3.19 Structures of novolac resin. (Copied from [27])	64
Figure 3.20 Photochemical reaction of DNQ upon exposure. (Copied from [27])	65
Figure 3.21 Spinning speed vs thickness. (Copied from [49])	66
Figure 3.22 The difference between ink side facing glass and facing substrate.....	68
Figure 3.23 Karl SussMA6 mask aligner for photolithography.	69
Figure 3.24 Layout of mask 1	69
Figure 3.25 Part of the patterned micromold under microscope	71
Figure 3.26 IKO electroplating system. (Copied from [52])	74

Figure 3.27 Sample holder	75
Figure 3.28 Defects caused by excessive current.	76
Figure 3.29 Copper grown by electroplating in micromold.	78
Figure 3.30 Details of the first layer copper	80
Figure 3.31 Spinning curve of HD4100 (Copied from [43]).	82
Figure 3.32 Layout of Mask 2 used in Polyimide photolithography.	84
Figure 3.33 Microscope image of a well developed via area.	86
Figure 3.34 Layout of Mask 3.....	88
Figure 3.35 Images of two layer structure under the microscope.	89
Figure 3.36 Image of finished sample.....	90
Figure 3.37 Image of devices after dicing.	90
Figure 4.1 The circuit schematics of the first layer coil.	93
Figure 4.2 Probe station and LCR meter used in the measurement.	94
Figure 4.3 Agilent 4294A impedance analyzer.	97
Figure 4.4 Resistance of the eclipse coil.....	98
Figure 4.5 Inductance of the eclipse coil.	98
Figure 4.6 Resistance of the round excitation coil.....	99

Figure 4.7 Inductance of the round excitation coil.	99
Figure 4.8 Layout of PCB.	101
Figure 4.9 Schematic circuitry of excitation coil, LC coupler and sensing coil.	102
Figure 4.10 Wire bonder used to bond device to PCB.	103
Figure 4.11 Morphology of good bonding result and the bonding parameter-setting panel.	104
Figure 4.12 Pin definitions of AA800B.	105
Figure 4.13 Image of the sensors assemblies.	106
Figure 4.14 Screenshot of the waveform of the excitation coil alone	107
Figure 4.15 Screenshot of the waveform of the excitation coil with coupler.	108
Figure 4.16 Waveform of the sensing coil.	109
Figure 4.17 Sensor output measured from PPS port.	112

Chapter 1

1 Introduction

1.1 Position sensors overview

The sensors act as a messenger between vehicle and central control unit. Nowadays, a large number of sensors are installed inside each vehicle. Acting as a perception unit, the sensors convert physical or chemical variables, for example, angle, pressure or temperature, into electrical signals to control the vehicle operations and diagnose the conditions of the vehicle. Taking inductive sensor as an example, when the gas pedal is pressed, the position sensor installed senses the rotating angle of the pedal, converts and sends the signal to control unit, which will then “tell” the motor to increase or decrease the gas throttle accordingly.

In one vehicle, there are variety types of sensors, e.g. Hall sensor, inductive sensor, ultrasonic transducer and thermal resistor. Among these, angle and position sensors are widely used for applications such as pedal position sensing, throttle control, transmissions and steering wheels (as shown in **Figure 1.1**). While the vehicle is in operation, the electronics systems need to get the physical feedback from the sensors. Meanwhile, these signals will be immediately processed and sent back to the other sensors to control the vehicle. As the automotive electronics systems are becoming more intelligent, drivers’ safety and comfort, gas efficiency and performance are becoming more and more important. Therefore, the number of sensors inside each vehicle is growing significantly during last few decades. In 1995, there were only about 10 sensors

working in one vehicle [1], recently, the number has reached approximately 30 and is still increasing.

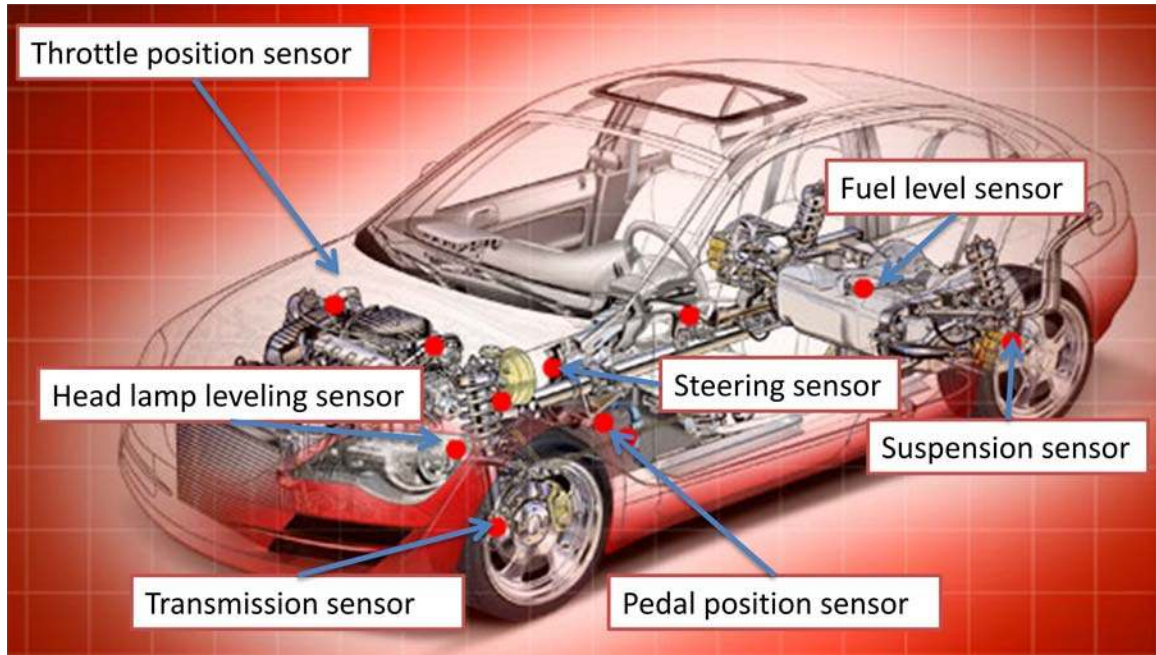


Figure 1.1 Application for position/angle sensors in each vehicle. (Adapted from [2])

Most vehicles are used in a harsh environment, like continuous vibration, variable temperature, dust and humidity, so the motor vehicle sensors must meet the following requirements: (1). Reliable, (2). Accurate, (3). Compact, small dimension, (4). Functional under extreme conditions, (5). Low cost, (6). Interchangeable, (7). electromagnetic compatible [3]. In this study, the materials and fabrication methods were carefully selected to make sure that the micro inductive sensor meet s these requirements.

Currently, there are several popular kinds of commercialized position/angle sensors. The early stage angle sensors are based on variable resistor [4].

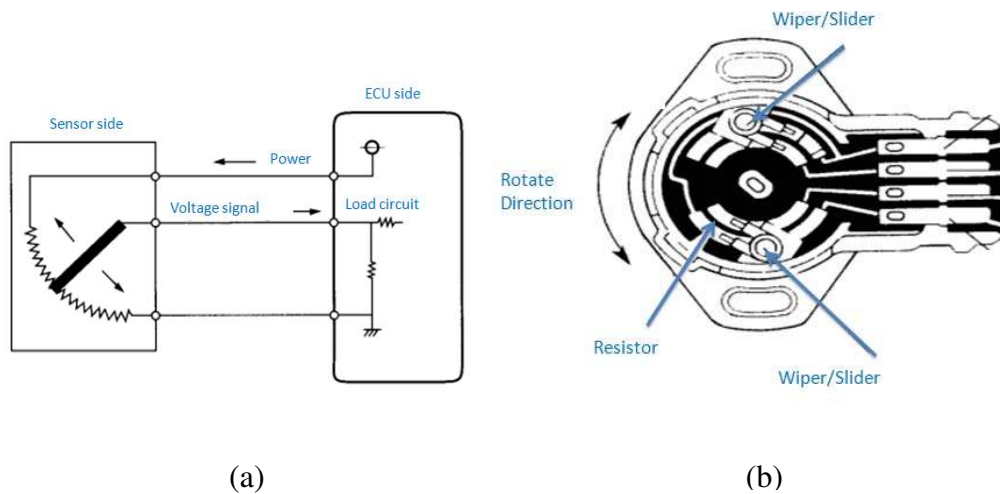


Figure 1.2 Schematic drawing of the variable resistor-based position/angle sensor.

(Adapted from [4])

Variable resistor based sensor is a typical contact type sensor. The working principle is shown in **Figure 1.2(a)**. Briefly, a wiper arm (slider) is mechanically connected to a moving part of the vehicle, such as the accelerate pedal. As the part moves, so does the slider, which is connected with a resistor. The layout of this type of sensor is shown in **Figure 1.2(b)**. As the wiper moves, any movement will induce resistance change of the resistor, resulting in voltage change as the output signal. This kind of sensor is easy to manufacture and calibrate. However, the contact area of the resistor is likely to wear out after a long-term usage, which makes the sensor's output unreliable.

Another widely used sensor is Hall Effect sensor. It is a contactless type of sensor and the principle of the sensor is illustrated in **Figure 1.3**.

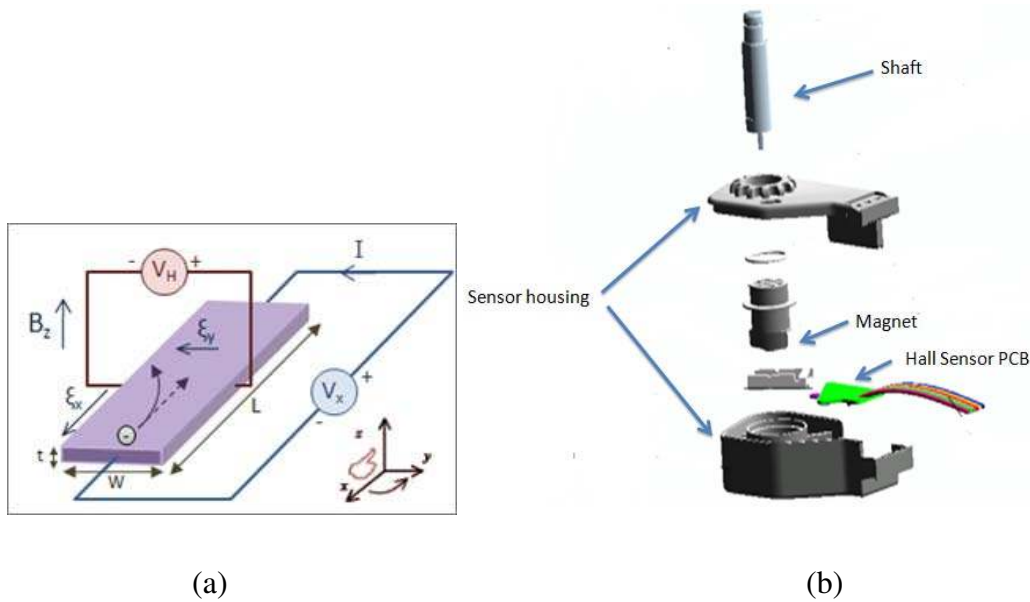


Figure 1.3 Hall Effect and the assembly of Hall effect sensor. (Adapted from [5, 6])

The working principle of Hall sensor is explained as follows. As shown in **Figure 1.3(a)**, a current is passing through a thin sheet semiconductor, when no magnetic field presents, the output Hall voltage is zero. When a magnet approaches, Lorentz force exerts on the current. The current distribution is disturbed, resulting in a potential difference across the output [7]. The cross-section view of the sensor assembly is shown in **Figure 1.3(b)**, magnet is installed on the moving shaft, when shaft rotates, and sensing part in the sensor housing can sense the rotation angle of the shaft. Contactless, long life span, highly repeatable operation are the reasons for using Hall Effect in a sensor. However, in a Hall Effect sensor, magnet is an indispensable part. It is well known that vibration and heat can cause a magnet to demagnetize. As mentioned before, in a moving vehicle, in which the sensor will have to endure high temperature and sudden impact, it is highly possible the sensor will fail due to magnet failure.

There is another kind of magnetic sensor, which is based on AMR (Anisotropic Magnet Resistance)/GMR (Giant Magnet Resistance) materials.

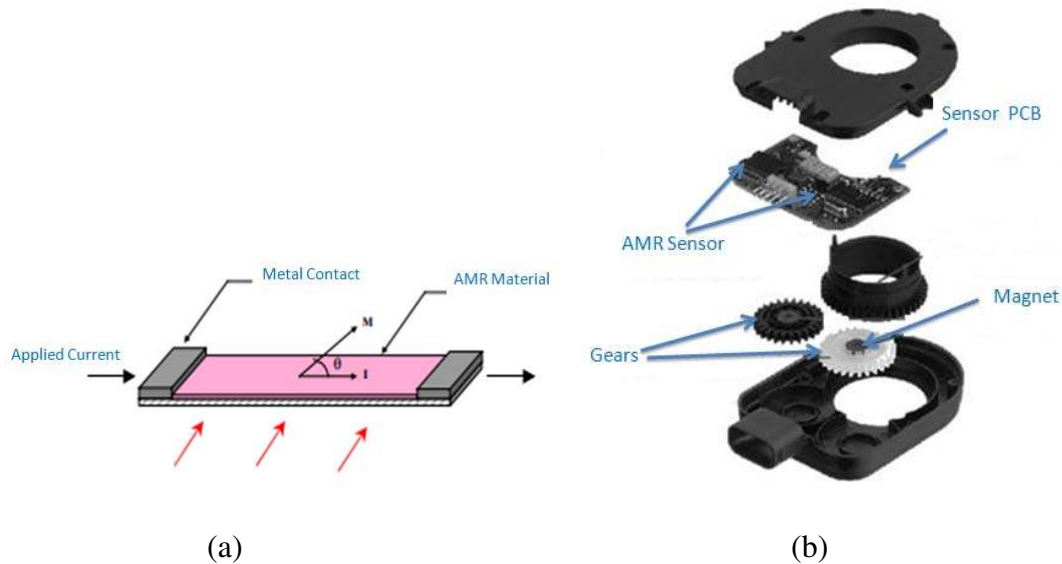


Figure 1.4 AMR unit and assembly of AMR angle sensor. (Adapted from [8, 9])

The working principle of AMR sensor is shown in **Figure 1.4(a)**, AMR materials can be manufactured into a thin strip to perform as a resistive element. When the angle θ between magnetic moment \mathbf{M} vector and the current flow \mathbf{I} changes, the resistance of the AMR element changes accordingly. The cross-section view of the sensor assembly is shown in **Figure 1.4(b)**, magnet is installed on moving gears, AMR elements can sense how much the gears rotate. The AMR/GMR sensors are also contactless and wear-free, however, like Hall Effect sensors, the disadvantage of the sensors is their indispensability of magnet.

In summary, position/angle sensors can be divided into two categories, contact and contactless. Most of the contact position sensors evolved from early variable resistor sensors, which suffer from short life span. The recent contactless magnetic sensors are

more attractive because of their improved robustness, precision and reliability, nevertheless, their dimension is also smaller. However, for the magnetic sensors, magnet is the Achilles heel; the shortcoming of the magnet often causes sensors to be unreliable in an extreme or unexpected environment. In addition, automotive manufactures are continuously making efforts to reduce the cost of car components; however, the cost of the magnet is too high which is another big concern.

1.2 Motivation of using micro inductive sensors

The inductive coil sensor, based on electromagnetic method, is one of the most widely used electro-magnetic sensors. The inductive sensor commonly includes an activating induction loop, a pick-up loop and a coupler/rotor. The activating induction loop generates alternating magnetic field which induces the eddy current in the coupler, and the eddy current also generates an alternating magnetic field, then the sensing loop can detect the changing magnetic field from the coupler. Thanks to their touchless, robustness and high sensitivity, inductive sensors prevail in the many different areas. The inductive sensors have a wide application not only in automobile [10] but also biomedical applications [11], space physic investigations [12], earth studies [13], and geophysics studies [14].

Comparing to the other kind of sensors, (e.g. Hall sensor, magnet-resistive, fluxgate-type or variable resistive sensors), the coil based inductive sensor could be easily manufactured on a PCB, and easily tuned as needed. In addition, the inductive sensors have a number of advantages, such as wide operating temperature, mechanical variability (Linear, rotational, arc, axis can go across the sensor, etc) and robustness.

The fundamental operating principles of coil sensors are based on Maxwell's equations:

$$\oint E \cdot dA = \frac{q}{\varepsilon_0} \quad \text{Eq 1.1}$$

$$\oint B \cdot dA = 0 \quad \text{Eq 1.2}$$

$$\oint E \cdot dS = -\frac{d\phi_B}{dt} \quad \text{Eq 1.3}$$

$$\oint B \cdot dS = \mu_0 i + \mu_0 \varepsilon_0 \frac{d\phi_E}{dt} \quad \text{Eq 1.4}$$

In which, E is the vector of electric field in the cross-section area of the coil, A is the cross-section area of the coil, q is quantity of electric charge, ε_0 is permittivity of air, B is vector of magnetic field, dS denotes the differential vector element of surface area S normal to surface, ϕ_B is the magnetic flux, μ_0 is permeability of air, i is electric current, t is time.

The basic principle of pick-up coil in inductive sensor is from the Faraday's law of induction, the transfer function is:

$$V = f(B) = -n \cdot \frac{d\phi}{dt} = -n \cdot A \cdot \frac{dB}{dt} = -\mu_0 \cdot n \cdot A \cdot \frac{dH}{dt} \quad \text{Eq 1.5}$$

$$\phi = nA\mu_0 H \quad \text{Eq 1.6}$$

In which A is the cross-section area of the coil, n the number of turns, ϕ is the magnetic flux passing through the coil, B is vector of magnetic field, μ_0 is permeability of air, H is the magnetic field, t is time.

The most popular design of the contactless inductive sensors includes PCB coil and a coupler/rotor (manufactured by Hella KG Hueck&Co, Germany), as shown in **Figure 1.5**, The excitation coil and receiver/pick-up coil sit on the PCB board, the peripheral electronic components such as resistors, capacitors and data processing ASIC (Application-Specific Integrated Circuit) chip are mounted on the PCB as well. The coupler/rotor could be a closed winding or a metal sheet with a specific geometry, as shown in **Figure 1.6**.

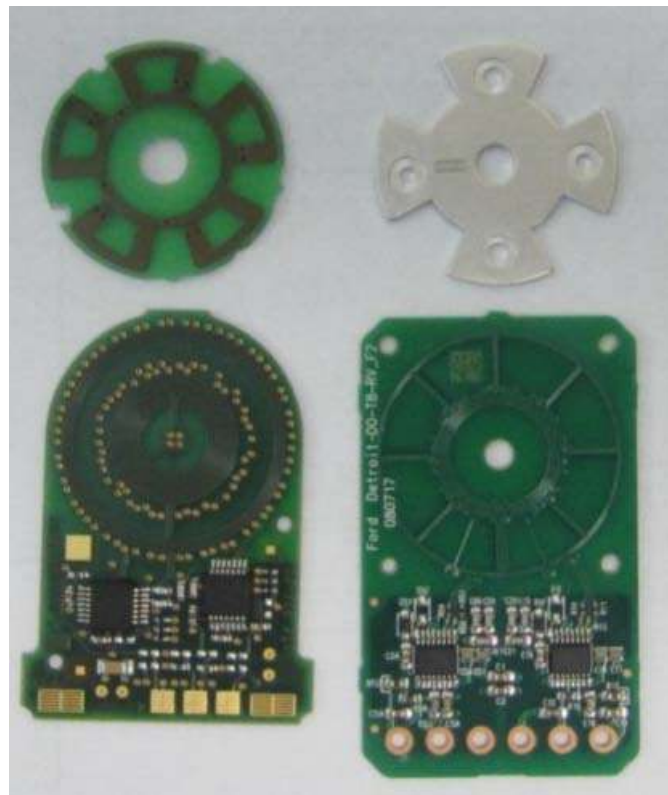


Figure1.5 Inductive sensor components.PCB (bottom) and Coupler/Rotor (up)

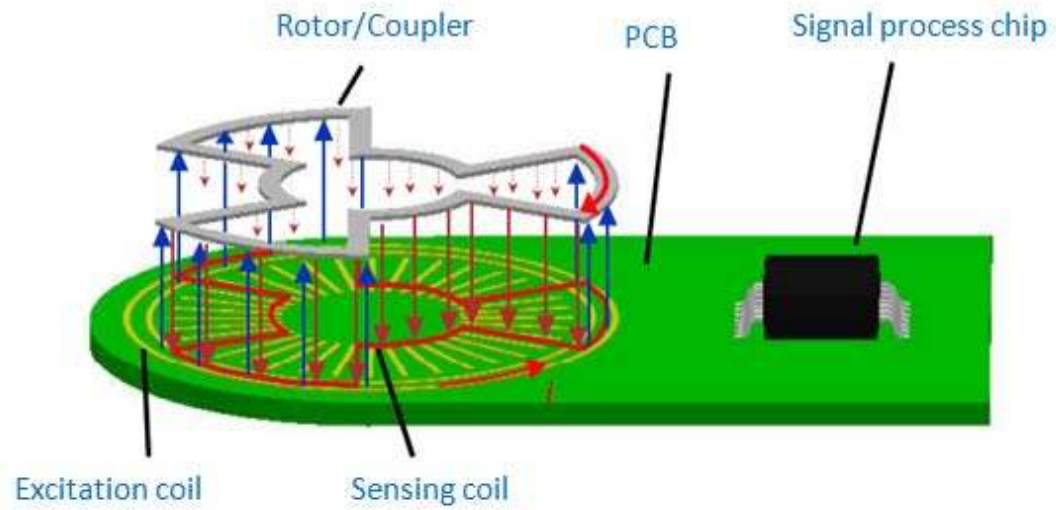


Figure 1.6 Assembly schematic of inductive sensor. (Adapted from [15])

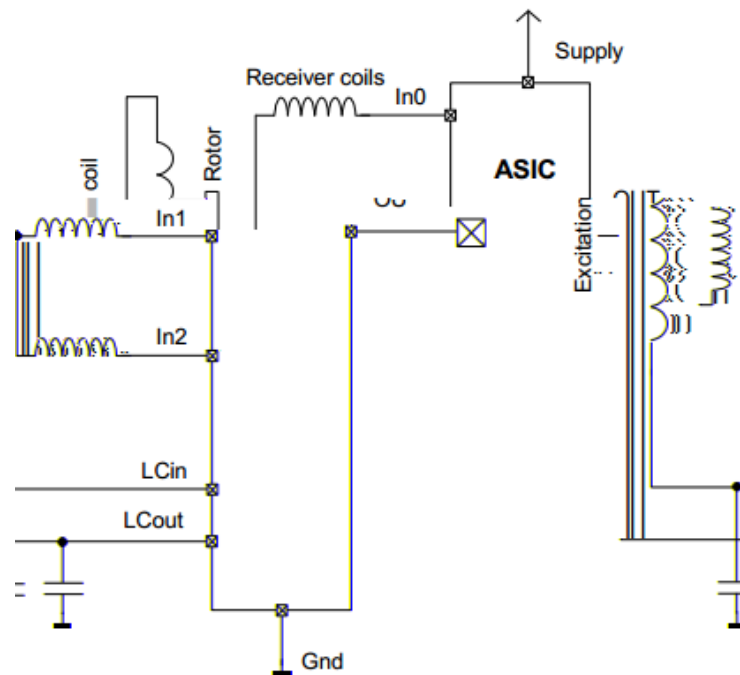


Figure 1.7 Simplified operation principle

The schematic of the signal process circuitry is shown in **Figure 1.7**. The working principle of the circuitry could be summarized as follows: the excitation coil is driven by the oscillator driving circuit in the ASIC to generate an alternating magnetic field, which results in eddy current on the metallic coupler/rotor. The alternating eddy current generates a secondary magnetic field, which will induces signal change in the picked-up coils by Faraday's law (Equation 1.5). The signals then are transferred into ASIC, processed and output in form of voltage or PWM signals (Pulse Width Modulation).

The inductive sensor is contact-less, in addition, it does not require a magnet as the essential function component. Therefore, the inductive sensor is more reliable than magnetic position/angle sensor, especially in a harsh environment such as high temperature or severe vibration. This feature is extremely important for vehicles operated in mines, rural area or high temperature region.

Although the sensor coils can be easily fabricated on PCB by modern electronic technology, the PCB based inductive sensors still have some weakness. For example, in order to generate a sufficient magnetic field, the activating loop often needs many turns. Therefore, the dimension of sensors is always very large due to the low resolution of PCB process. Only limited coil turns are allowed because the best resolution PCB technology can reach is 50 μm [16]. As a consequence, the large dimension will result in large assembly size of the pedal or wheel, which is a big issue for vehicles with a limited space. Nevertheless, the large size will cause high emission of the magnetic field. The magnetic field may interfere with the other electronics, causing them to work improperly.

From an assessment of the limitations and drawbacks of the existing sensors, in this study, the micro-fabrication technology was introduced to fabricate the excitation coil and the coupler coil for a newly designed micro inductive sensor. In the traditional design, the magnitude of eddy current in the metal coupler is big enough to generate the reflective magnetic field because the metal trace in PCB can sustain large current, however, in the micro inductive sensor; the width of the trace is too small to sustain larger current. Thus, another LC loop was introduced to resonate with the excitation coil to reduce the driving energy. In this design, there is no eddy current, which means there is less energy dissipation, so less energy is required to drive the excitation circuit. In theory, the resolution of micro-fabrication lithography can reach 1 μm , therefore, the width of the coil wire can be significantly reduced and more turns can be fabricated. Micro-fabrication technology allows the sensor to shrink down whilst keep a sufficient number of coil turns. Moreover, it allows the sensor to shrink down even further by adding a magnetic circuit to enhance the signal strength. With micro-fabrication technology, it is expected that sensor size can be reduced to 10% of the PCB prototype size; hence, the EMC performance of the sensor can be greatly improved.

1.3 Scope and research objective

The purpose of this research is to develop a novel fabrication process for the miniaturized inductive sensor for automotive application using cutting-edge micro fabrication technology. The micro-fabrication process, including lithography, sputtering, electroplating and wet etch will be investigated thoroughly. The following aspects will be investigated:

- Design micro inductive structure suitable for micro-fabrication, especially the mask design.
- Develop a proper lithography process suitable for the coil, and optimize parameter for photolithography.
- Find a proper way for the coil fabrication, to fulfill the thickness requirement of the coils.
- Find a proper insulating layer for the double-layer coils.
- Find a way for fabricating multilayer coils with inter-connections.
- Validate the performance of the coils, and compare the data with the simulation results.

1.4 Outline of thesis

This dissertation is divided into five chapters, which is organized in the following as:

Chapter 1 introduces existing position/angle sensors, including their advantages and disadvantages. The motivation for selecting the inductive sensors and the reason for using micro-fabrication instead of PCB technology are also discussed. The scope, research objective and outline of thesis are provided as well.

Chapter 2 introduces the several microfabrication processes that will be used in this project. Their principles and operating mechanisms are described. Latter part of this chapter introduces the design of the inductive sensor and the simulation of the prototype.

Chapter 3 describes the procedures for device fabrication in detail, including the deposition of seed layer, the lithography of the micromold, electroplating of the copper

layer, preparation of the insulating layer and fabrication of the second copper layer.

Chapter 4 introduces tests which were performed during the process, after the process and upon system integration. The tests include, the inter-procedure tests performed by LCR meter and probe station, the devices tests performed by impedance analyzer upon completion, system integration tests performed by oscilloscope.

Chapter 5 gives a summary of the thesis, and suggestions for future work.

Chapter 2

2 Introduction of microfabrication process and prototype simulation

2.1 Background

Microfabrication is a process to produce devices and structures with dimensions in millimeter, micrometer, even nanometer scale. It utilizes the same established semiconductor fabrication processes, including photo-lithography, sputtering, together with some other processes such as RIE, wet etch and CVD [17-19], which are widely in Integrated Circuits (IC) industry.

Microfabrication processes can be used to fabricate varieties of microstructures and devices. These microstructures and devices includes but not limited to: moving parts such as cantilevers, static structures such as micro-fluidic channels, biological surfaces such as proteins and cells, and electronics devices such as resistors, transistors and capacitors [20].

Microfabrication process, also well known as a batch yield processing, can effectively produce a single device or thousands of devices at the same time. This particular feature of the microfabrication not only dramatically reduces the unit cost of the devices, also reduces the quality difference between each device, enabling large volume of production with minimum tolerance. The success of the modern IC industry, which is the most significant revolution in information technology (IT) age, has demonstrated the effectiveness and efficiency of microfabrication.

With microfabrication technique, we can achieve the following advantages: small dimension of devices, the possibility of batch process, the ability of integrating electronic components, and some other features thanks to the precise geometry control. There are a number of commercialized and mature micro-sensors, such as pressure sensors and accelerometers, prepared by micro-fabrication, which has also demonstrated that microfabrication is suitable for high volume mass production.

To fabricate a functional device, a sequence of microfabrication processes are involved, including design, fabrication, packaging and testing. Some of them can be originated from the standard semiconductor fabrication technology; however, some other micro-machining processes are very specific due to the deviation of applications and materials. Every process has to be carefully designed and operated.

In the following section, the microfabrication processes adopted in this project are briefly introduced.

2.2 Introduction of microfabrication process

2.2.1 Substrate selection

Silicon is the most commonly used substrate in IC industry. Therefore, for microfabrication process, the first choice of substrate is also silicon. Silicon wafers are supplied in different diameters and different crystal orientations. By using silicon as substrate, it is possible to integrate transducer and electronic circuitry to build system-on-chip or system-in-package devices. Hence, silicon is a high-reliability, high-strength, high-precision material which can provide a solid support for the structures built on it

[21]. In addition, there are varieties of micromachining method which can be adopted to produce desirable structures in the silicon substrate [22-24].

Glass is another option because of its good dielectric and optical properties. Glasses are supplied in different shapes, e.g., sheet form or wafer form, and different sizes. Since they are transparent, glasses are especially suitable for optical usage.

Ceramics and polymers are two other options for substrate materials. Ceramics such as ferrite can be used as functional materials to enhance signal strength [25, 26]. Polymers are also attracting more and more attention because of their lightweight and the application of special processes such as hot embossing, laser machining and injection molding.

2.2.2 Photolithography

Photolithography is a process that can transfer patterns from a mask onto a substrate by UV light. It usually uses photoresist as structure material to form micron or nanometer scale patterns.

Photoresist

Photoresists are light-sensitive materials being used to form patterned coating on a substrate. Photoresists for semiconductor industry were introduced in the 1950s. There are two types of photoresists: negative photoresists which were commercially developed by Kodak and positive photoresists which were firstly developed by Shipley. Currently, various kinds of photoresists which can meet different requirements are manufactured by Shipley, AZ electronic materials, Microchem and some research institutes.

There are several general requirements for the photoresist:

1. Photoresist polymers must be dispersed in solvent in order to be coated onto a substrate.
2. The adhesion between photoresist and substrate must be strong enough to ensure the edge acuity, minimize undercutting, and avoid peeling off during the following procedures.
3. The photoresist must be sensitive to particular wavelength light; otherwise it would be exposed by any light source, including the natural light or room light.

Photoresist contains four basic components: the polymer, the solvent, the photo-sensitizer and additives. Although photoresists are both polymer-based chemicals, the properties of polymers are quite different for positive photoresist and negative photoresist. Polymers in negative photoresist are not chemically bonded to each other before exposure, the polymers crosslink or polymerize upon exposure; while positive photoresist polymers are insoluble in developer before exposure, upon exposure to light, the polymers become photo-soluble [27]. Solvent is the carrier of all the other chemicals, and allows the photoresist to stay in a liquid state to be spin-coated. Non-polar organic solvents such as toluene, xylene are usually used as the solvent in negative photoresist. In positive photoresist, ethyl cellosolve acetate, diglyme or cyclohexanone are frequently used. The sensitizer is used to control the photochemical reaction and different additives are used to facilitate the photochemical process.

Process of photolithography

To begin with, the user needs to design the patterns that they want to transfer. Then the patterns are printed on a photomask. The mask could be a glass plate with a thin layer of metal (typically chromium), or thin transparent plastic sheet. For glass plate mask, a sequence of optical or electron-beam lithography is used to process the metal to generate the patterns. For the plastic sheet, high-resolution printing is used to print a black ink onto the sheet to form a pattern. Usually the plastic mask cannot be used in high-resolution lithography due to their rough edge (Caused by the natural weakness of printing).

The process flow of the photolithography is shown in **Figure 2.11**.

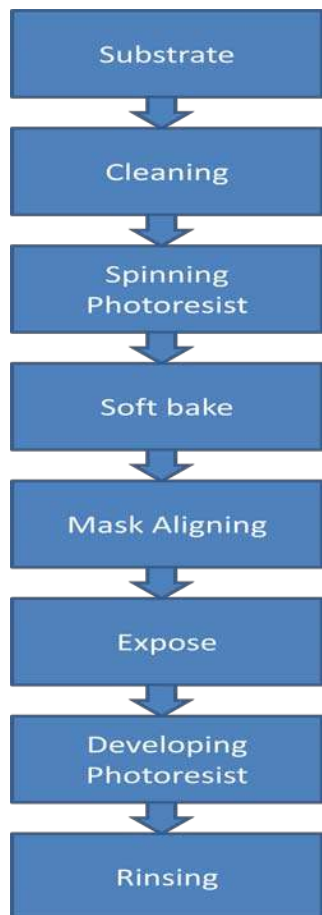


Figure 2.1 Lithography process flow.

The whole process begins with cleaning the substrate to remove any residual particles. Then the substrate is put into a spin-coater to coat photoresist. A layer of adhesion promoter, such as hexamethyldisilazane (HMDS) can be deposit on the substrate before the photoresist spinning if needed. The thickness of the photoresist is determined by the viscosity of the photoresist and can be controlled by the spinning speed. After the spinning, the substrate is put onto a hotplate or in an oven for soft-baking. Soft-bake removes the solvent in the resist and enhances adhesion. Afterwards, the substrate is put in the mask aligner to align with the mask, right afterwards the photoresist is exposed by ultra-violet (UV) light source.

Depending on which kind of photoresist is used, the exposure will result in different outcome. As shown in **Figure 2.3**, if positive photoresist is used, the exposed area can be dissolved in the following development procedure by a developer. On the contrary, if negative photoresist is used, the exposed area will be cross-linked and remain on the substrate, the un-exposed area is removed by the following development procedure. For negative photoresist, there is usually a post-bake step prior to development to expedite the cross-link.

There are three different exposure systems depending on the distance between the mask and the substrate: contact, proximity and projection (**Figure 2.2**). As implied by the name, contact means the mask and the substrate contact with each other, proximity mean there is a small distance between the mask and the substrate, projection means a dual-lens optical system is used to project the mask pattern onto the substrate. The pattern made by contact mode is usually better than proximity mode because the UV light does not scatter after passing the mask, however, the contact of the mask with the photoresist may damage the mask or the photoresist layer.

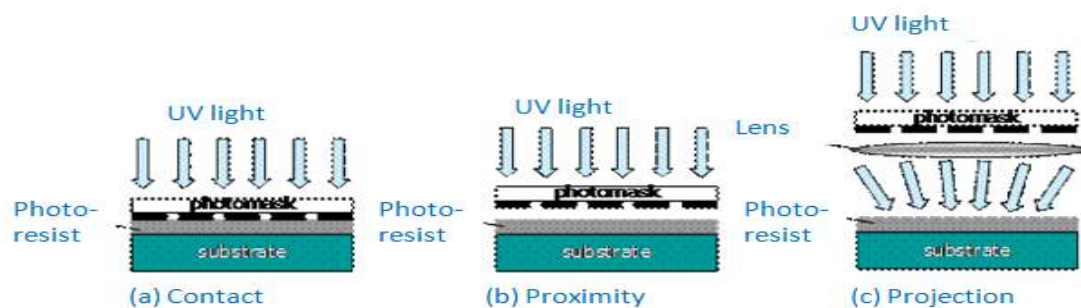


Figure 2.2 Schematic illustration of three systems of photolithography: (a) contact; (b) proximity; and (c) projection. (Adapted from [28])

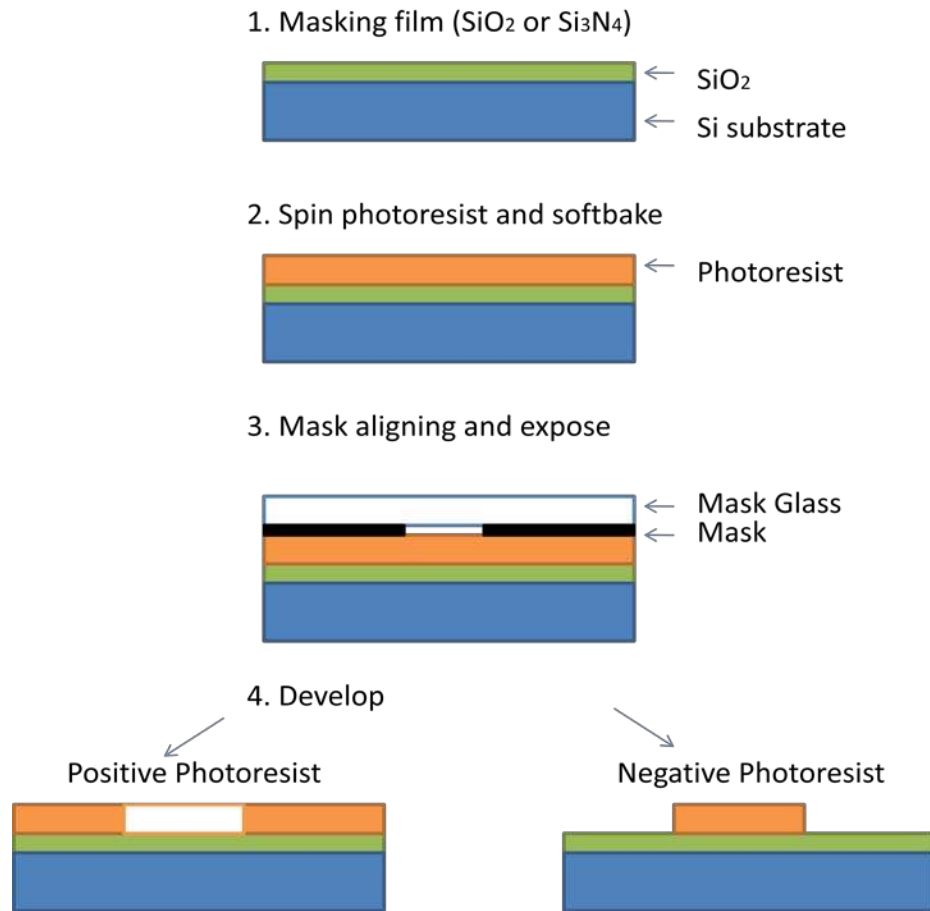


Figure 2.3 Steps of photolithography, comparison of positive and negative photoresist.

Depending on what kind of Photoresist is used, different result can be achieved. If positive photoresist is used, the exposed area can be washed away by developer; if negative photoresist is used, the exposed area will solidify and remains (**Figure 2.3**).

After the development, the desired patterns are revealed. The remaining photoresist can act as a mask for the following etching procedure, or as a lift-off layer for the following thin film deposition.

2.2.3 Sputtering

Sputtering is a widely used microfabrication process, which is mainly used to deposit metal films such as Au, Cu, Ag, etc. and dielectric films such as SiO₂. Sputtering is a term used to describe the mechanism in which atoms are ejected from a target material due to bombardment by the energetic particles [29]. Sputtering is usually performed in a vacuum chamber, in which plasma is formed by a large bias voltage across the closely spaced cathode and anode pair. The target (material to be deposited) is mounted on the cathode. The ions come from an inert gas in the chamber. Depending on the energy of the ions, different mechanisms would happen when ions strike the target surface. The ions may bounce off the surface, or be absorbed by the material to produce heat, or penetrate the surface to increase the energy in the target. Some of the ions with enough energy will hit the surface and create a cascade of collisions, due to momentum exchange, target atoms that gained enough energy in the collision will eject from the surface. Then the ejected atoms are transported to the surface of the substrate, and then they condense and form a thin film. Process of sputtering is shown in **Figure 2.4**.

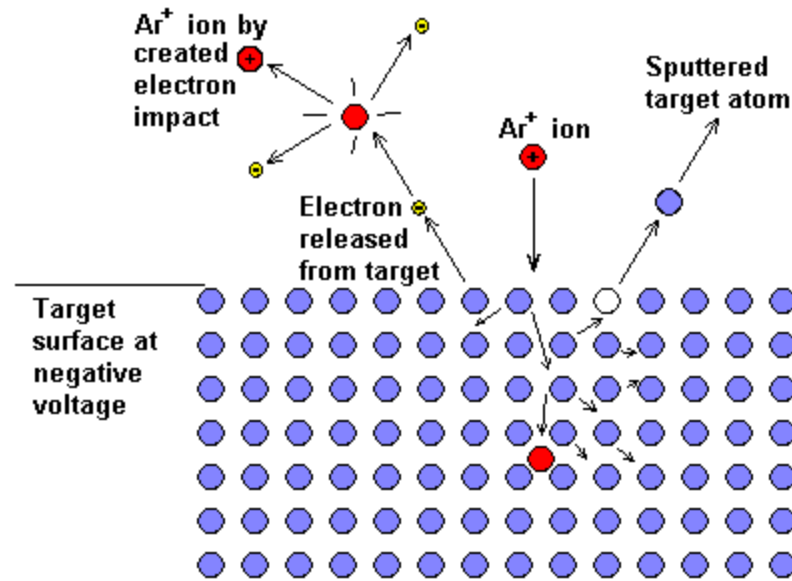


Figure 2.4 Illustration of mechanisms when ion strikes the target surface. (Adapted from [30])

Due to the energy exchange in the sputtering process, sputtered atoms have high energy and high surface mobility. As a result, the step coverage is better than evaporation or some other deposition methods.

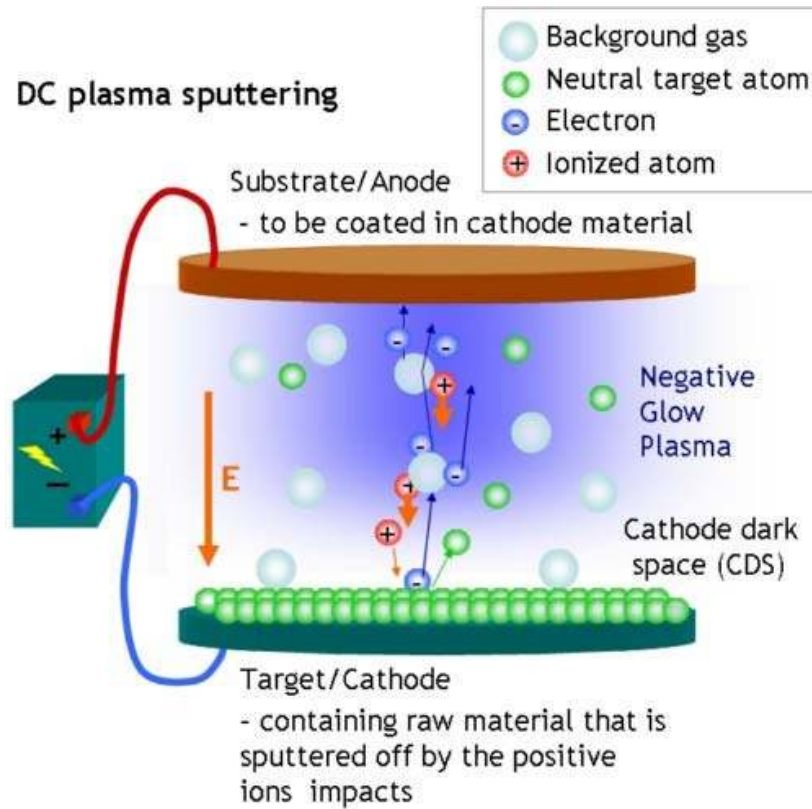


Figure 2.5 Illustration of sputtering process. (Adapted from [31])

Figure 2.5 shows the process of a sputtering. Argon is a preferred inert gas in the sputtering because of its high atomic weight will enhance the energy exchange during the collisions. When a high voltage is applied, the argon will arc to plasma state. The argon ions run towards the cathode with high speed and strike the target. The target atoms or molecular are knocked out and deposited on the substrate.

A sputtering machine usually has two sputtering mode: DC sputtering and RF sputtering. For a conductive material, both of the modes can be used. In DC mode, the ions are accelerated by the constant bias voltage to bombardment velocity. As ions strike the target, the resulting charges can move freely in the material to prevent charge build-up. However, for a non-conductive material like SiO_2 , free charge cannot move freely. As

the ions strike the target surface, the resulting charges stay on the surface and build up an electric field. As a result, the Argon ions cannot bombard the target any more. To prevent this phenomenon, it is necessary to apply AC or pulsed power to make sure the built-up ions charges are expelled during the positive or neutral phase. Because the RF bias contains half-positive voltage and half-negative voltage, deposit rates are lower than DC.

Sputtering has the following advantages:

1. The quality of the sputtering film is good, and the thickness difference varies very little over the whole wafer.
2. Film thickness can be easily controlled by adjusting operating parameters such as deposition time, bias voltage and flow rate of Argon.
3. Two or more targets can be sputtered together to deposit alloy.
4. Substrate can be cleaned prior to sputtering by reversing the DC bias.

2.2.4 Electroplating in microfabrication

Electroplating commonly refers to the application of a dense, uniform, and adherent metal coating to a metallic or conductive surface by applying electric current. As a microfabrication process, electroplating is used to fabricate thicker metal layers, the thickness of which is often beyond the capability of sputtering or evaporation.

In electroplating process, the wafer to be electroplated is connected to the cathode (negative terminal), while the anode can be either of sacrificial anode (dissolvable anode) or permanent anode (inert anode) [32]. The sacrificial anodes are made of the metal to be

plated. In this case, the anode acts as a source of fresh metal to replenish the metal ions that have been extracted from the solution. The permanent anodes, however, stay intact during the process. For the permanent anode, Platinum or carbon is often used. Both of the cathode and anode are immersed in an electrolyte solution bath, and current is passing through the cathode, bath and anode. The current is carried by ions in the electrolyte solution. When electric current is applied, the positive ions in the electrolyte will move towards the cathode and the negative ions move towards the anode. At the cathode, electrons provided by the power source will neutralize the positively charged metal ions, the metal ions then turn into metal atom and deposit on the cathode. The sacrificial electroplating process can be represented by the following equations:

At the cathode:



At the anode:



For an inert anode, at the cathode:



At the anode:



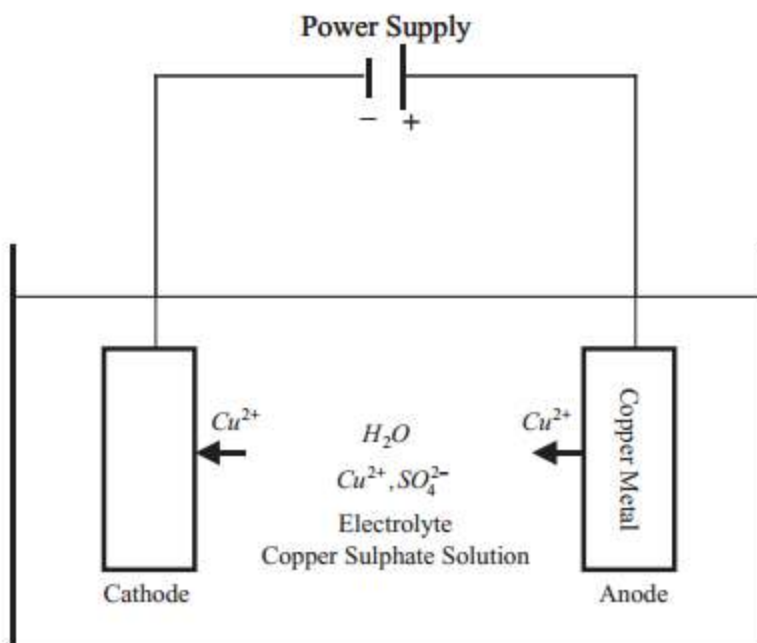


Figure 2.6 Principle of electroplating.

Figure 2.6 shows a simplified configuration of an electroplating unit which is used to electroplate copper. As stated by the previous chemical equations, copper ions are neutralized by the electrons at the cathode, concurrently, the same amount of copper atoms lose electrons and dissolve in the solution.

The actual configuration is more complicated. The power source itself can be programmed to be regulated by current or voltage. Some of the power source can be programmed into a pulse-reverse mode rather than DC. The compounds of electrolyte solutions are complicated, taking copper electroplating as an example, the formula of the plating bath is not only copper sulfate, in the solution, sulfuric acid and hydrochloric acid are added to stabilize the pH. Some other chemicals like brightener, carrier are also added to ensure the quality of the plating copper. These two additives, brightener and carrier,

can increase the number of nucleation, meanwhile, keep the nucleation seed small to form a smooth surface [33], it is very important for microstructure fabrication. Microscopic current distribution also needs to be taken into consideration, the total current need to be regulated very carefully in order to produce metal film with good quality.

2.2.5 Wet etching for metals

Wet etching is a chemical process, which can be used to etch Si, metals or some other compounds in microfabrication. The process of wet etching is very straightforward. The sample is placed into the solution that attacks the film to be etched, while the mask protects the areas to be kept as structures for the device. The chemical process of wet etching is explained by the **Figure 2.7**.

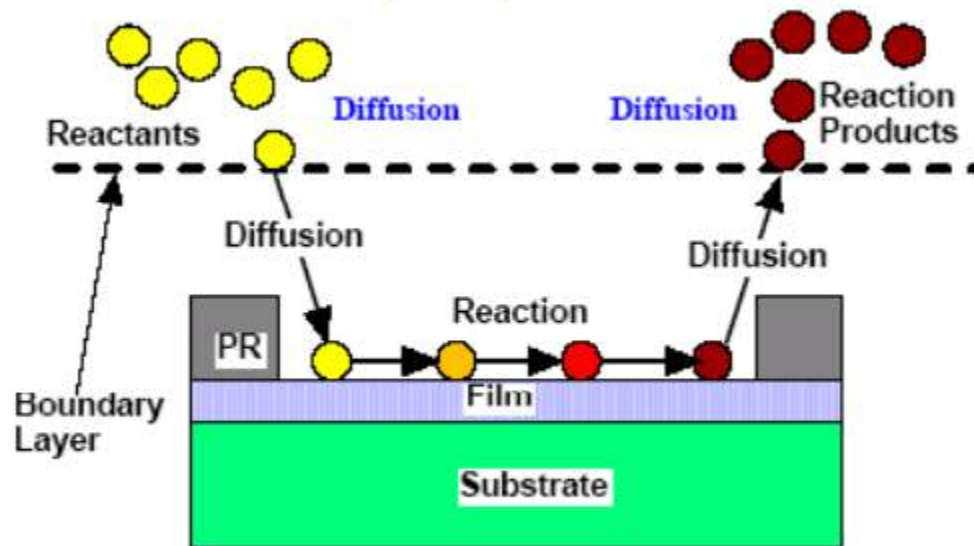


Figure 2.7 Chemical reaction process of wet etch.

Once the sample is immersed in the etching solution, the reactants in the liquid diffuse through the boundary layer to the surface of sample, and then react with the film. Hereafter, the reaction products diffuse away from the sample surface, through the boundary layer into the liquid.

Wet etching has the advantages such as low cost and good selectivity. However, the method also has some disadvantages: it is hard to control critical feature dimension; the etching rate decreases as reactant is consumed; the reaction product and the etching solution is hazardous and difficult to handle. Sometimes, the reaction could produce toxic fume and the process need to be done in a well-vented fume hood and full protection, like gowning, is required by the operator.

The wet etching process is mainly monitored by observing the color change during the reaction. The etch rate provided by the solution company can only be considered as a reference because the actual etch rate differs due to temperature or density change. If the sample is over etched, undercut will be formed in the sample (as shown in **Figure 2.8**).

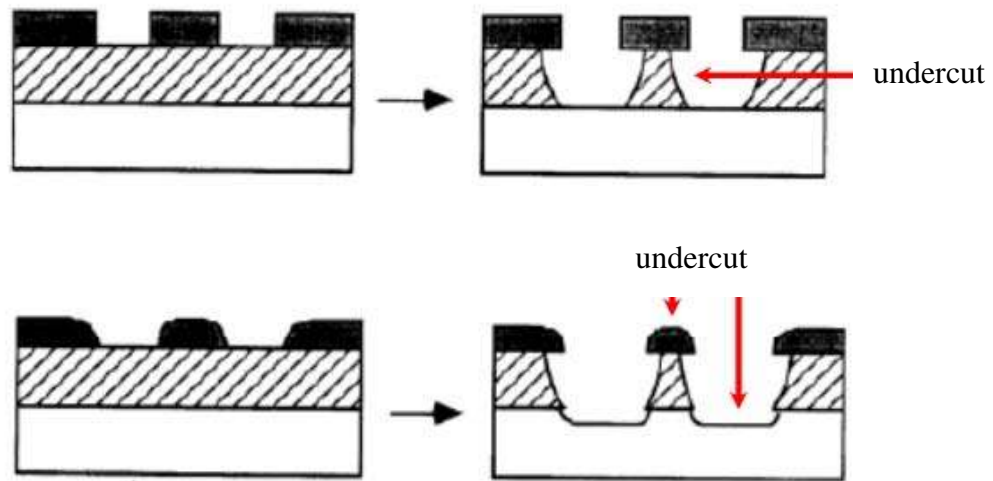


Figure 2.8 Undercut in the wet etch.

Undercut will deteriorate the adhesion between layers and lead to profile changes. The films may peel off due to undercut; moreover, some of the structures may not function well due to profile change. Therefore, the control of the wet etching is very critical.

2.3 Prototype simulation

The design of the inductive sensor prototype is provided by KSR International Co. In the design, there are an excitation coil, a sensing coil and a coupler eclipse coil. The excitation coil can be driven by the LC oscillate driver circuit to generate alternating magnetic field. The magnetic field will couple with another LC loop that contains the eclipse coil, and then resonance will occur. The resonance alternating electro-magnetic field generates alternating electric field in the sensing coil. The electrical signal can be measured and processed by ASIC (Application-Specific Integrated Circuit). The drawing of inductive sensor prototype is shown in **Figure 2.9**:

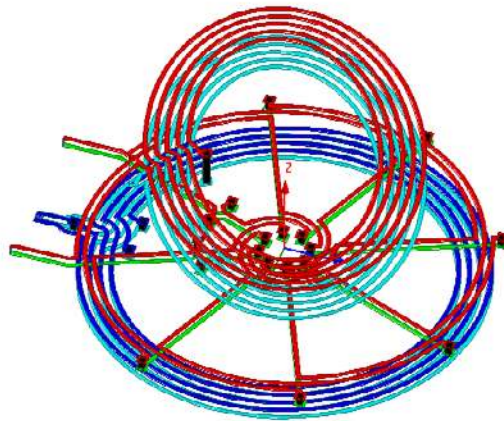


Figure 2.9 Design of the inductive sensor coil.

Before fabrication process, simulation needs to be done to calculate the parameters and performance of the device. By comparing with the later electrical test results, the correctness of every fabrication process can be verified. As shown in the **Figure 2.10**, a 1:1 scale model of the device was developed in HFSS (high frequency structural simulator). HFSS is an electromagnetic field simulation software based on finite element [34]. In general, electric field and magnetic field are different form of electromagnetic field. In HFSS, the current, voltage and magnetic field are considered as electromagnetic field transmitted in different medium. Using Maxwell equations, the distribution of the magnetic field, the inductance and resistance can be calculated.

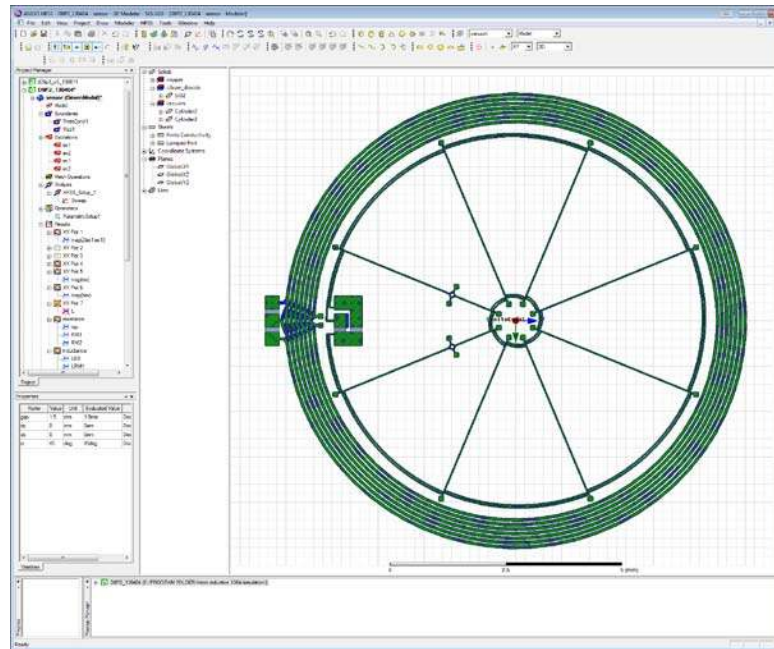


Figure 2.10 Model of prototype created by HFSS.

Lumped port is assigned in the HFSS as excitation. In analyzing settings, sweeping is added to analyze the frequency response under different frequency. The copper layer is created as sheet model; the thickness parameter is assigned during the simulation. The plot of magnetic field generated by the excitation coil is shown below, although current or voltage magnitude does not assigned by lumped port excitation, the distribution of the magnetic field can be seen, as shown in **Figure 2.11**.

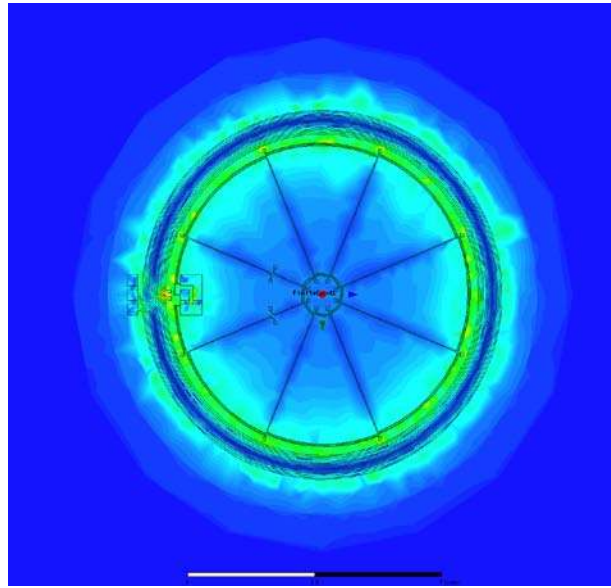


Figure 2.11 Plot of magnetic field generated by the excitation coil.

The inductance and resistance simulation results with the copper thickness of 10 μm are shown in **Figure 2.12** and **Figure 2.13**.

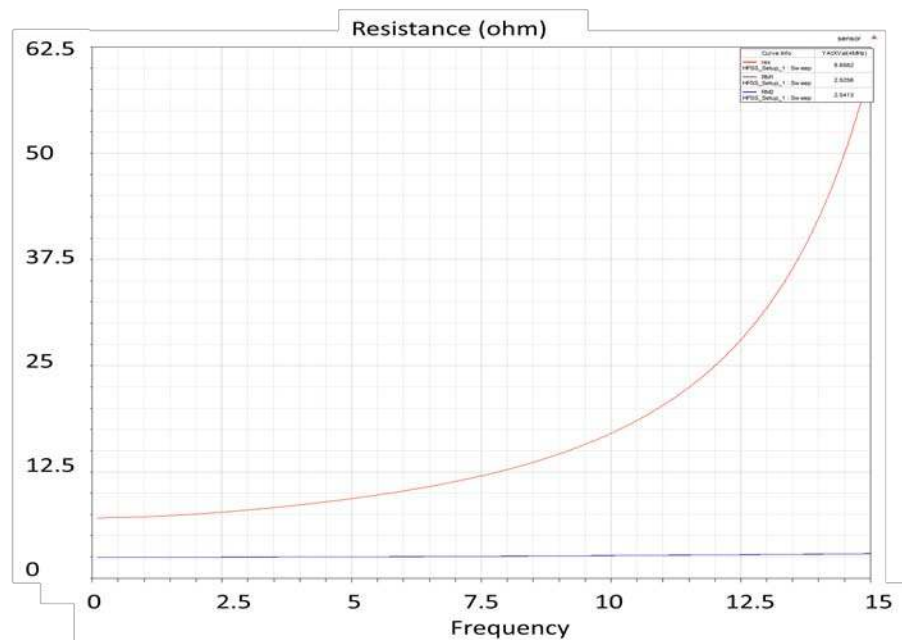


Figure 2.12 Resistance simulation result.

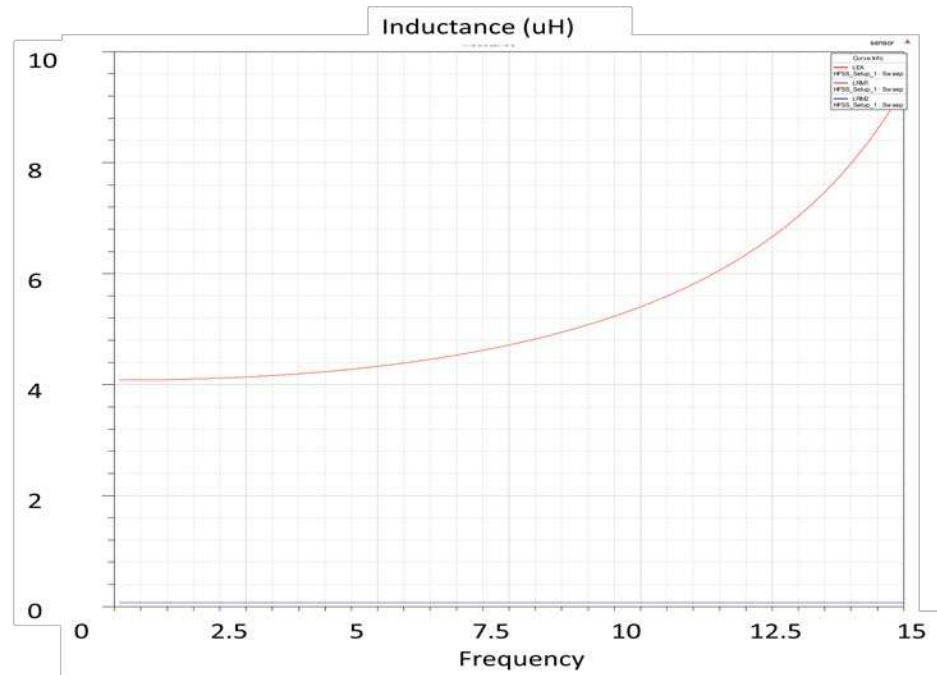


Figure 2.13 Inductance simulation result.

The values of resistance with different copper thickness are listed below:

Table 2.1 Resistance result with different copper thickness

Copper thickness	5 μm	10 μm	15 μm	20 μm	25 μm
Resistance (Ω)	53.79	26.89	17.93	10.55	8.44

During the process and at the end of the process, we can measure the inductance or resistance of the devices and compare them with the simulation results, to verify the correctness of every step, as well as optimize the fabrication procedures.

2.4 Conclusion

This chapter introduced some key microfabrication processes, such as photolithography, sputtering, electroplating and wet etching, which will be used in our device fabrication.

Their principles and procedures are explained; their limitations and disadvantages are also briefly discussed. The simulation for the prototype gives a general idea for parameters selection for the following design. The device simulation is done by HFSS software; the parameters such as inductance and resistance are calculated for the future experimental verification.

Chapter 3

3 Microfabrication process for the micro inductive sensor

3.1 Introduction

It is desired to extend the developed techniques for future industrial application; therefore, designing a fast, simple and reliable procedure for the micro-fabrication is very important. In addition, using the accessible microfabrication tools, which are scalable for mass production, is crucial for automotive industry. In Chapter 2, several microfabrication processes were briefly introduced. The tools including mask-aligner, sputtering machine, electroplating machine and some supplementary test equipment are all available in Western Nanofab.

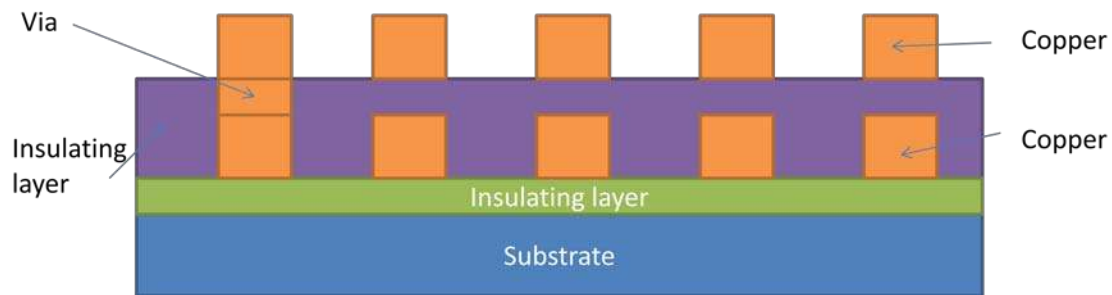


Figure 3.1 Cross-section view of the inductive sensor device.

The coils are essential components for the micro inductive sensor. In order to better understand the configuration of the device, the cross-section view of the device is shown in Figure 3.1. There are three layers for the coils from the bottom to top: the first layer of copper coil; an insulating layer with via holes, which also insulates the first and second layer copper coil and offers a support for the second copper layer; and the second copper

layer. After analyzing the layer structure, we can conclude that the fabrication process of the device should consist of three major steps:

1. Fabricate the first copper layer.
2. Prepare an insulating layer, fabricate via holes in the insulating layer.
3. Fabricate second copper layer and vias.

This chapter explores the feasibility of a novel microfabrication process that can produce a multiple layers 3D devices. The following section will explain the process step by step.

3.2 Critical parameter calculation and process selection

Substrate selection

The substrate is the support for the copper coils. The basic requirements for the substrate include low-cost, firm, reliable, non-dissolvable in acids, most importantly, non-conductive.

Si and glass are good candidates for the purpose at the first thought. They are not expensive, and commonly the top choice in microfabrication. However, Si is a semiconductor, although the resistance of Si is relatively large, current can still go through. Glass is transparent, and reacts with HF acid. Considering the datasheet of photoresists are all calibrated on Si substrate, the exposure procedure for the glass wafer has to be re-calibrated. In addition, in the following steps, metal etchant containing HF is used to remove the metal layer, meanwhile, the glass substrate will be eroded. In conclusion, both Si and glass are not suitable for our purpose.

Taking into account the non-conductive, non-transparent and non-dissolvable properties, Si substrate with a thermal grown SiO₂ layer is the best choice. Not only this kind of substrate has the same advantages as Si substrate, also HF will not erode the substrate too much because of the relatively low etch rate of SiO₂ in HF. As a result, the 4-inch Si wafer with 2μm SiO₂ is chosen as substrate in this study.

Line width and copper thickness calculation

The target size of the inductive sensor design is around 1 cm×1 cm. In order to generate adequate signal strength, also considering the packaging in the future, the line width of the coil is set to be 50 μm, the gap between two line is set to be 20μm to avoid fabrication failure caused by mis-alignment or roughness of the edge. Same parameters are also applicable for the eclipse coils. AC current will be applied in the coils to generate alternating magnetic field. Because of skin effect, the AC current will mainly go through the surface of the copper coils. The skin depth is calculated as:

$$\delta = \sqrt{\frac{2}{\omega\mu\gamma}} \quad \text{Eq 3.1}$$

For copper, $\gamma=58 \times 10^6 \Omega \cdot \text{m}$, $\mu=4\pi \times 10^{-7} \text{ H/m}$, assuming the operating frequency is 4MHz. Considering the current density allowed in the copper wire, along with the average current running through the coil, the calculation of the coil thickness is shown below.

$$\frac{V}{\rho \frac{l}{a \cdot b}} \cdot \frac{\sqrt{2}}{2} = I(Allow) \times (2 \cdot a \cdot \delta + 2 \cdot b \cdot \delta) \quad \text{Eq 3.2}$$

In Equation 3.2, a is the width of the coil, b is the thickness, δ is the skin depth, $I(Allow)$ refers to the maximum current density allowed in copper, the number is 15-25 A/mm², ρ is resistivity of the copper, l is the length of the coil. After calculation, we have a conclusion that the thickness for the coil should be over 10 μ m.

Now the thickness of the copper coil is determined, another problem rises up: How can we fabricate the 10 μ m copper layer?

Sputtering Vs Electroplating

E-beam evaporation, sputtering and electroplating are the three commonly used methods for fabricating metal layers. The film quality grown by the e-beam evaporation is very good [35]. However, the growth rate of the e-beam evaporation is very slow: the common growth rate is about 1-2 Angstrom/s, so that it will take 10 more hours to complete the process, which is not acceptable for industrial applications. Moreover, the step coverage is very poor due to its uni-directional growth mechanism [36].

The growth rate of sputtering is much higher than e-beam evaporation, but the step coverage is so uniform that it will block the lift-off solution to infiltrate, as show in **Figure 3.2**, making it impossible to lift off the photoresist.

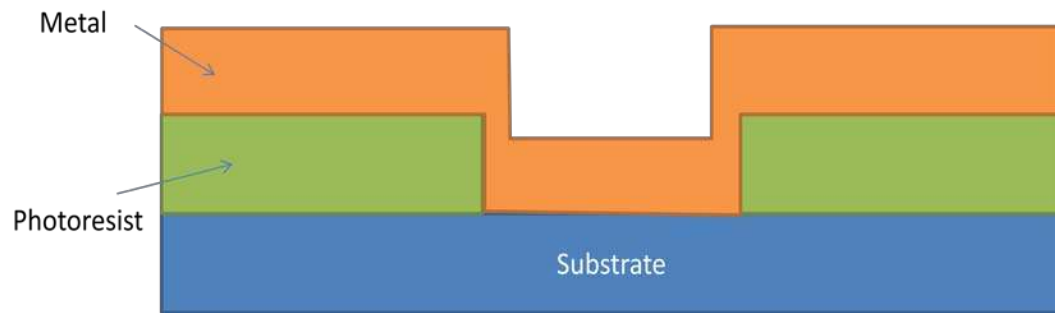


Figure 3.2 Step coverage of sputtering.

In order to lift off the photoresist after metal deposition, a bi-layer lift-off method is adopted. Using LOR30B (manufactured by MicroChem®) as an example, the procedures are shown below:

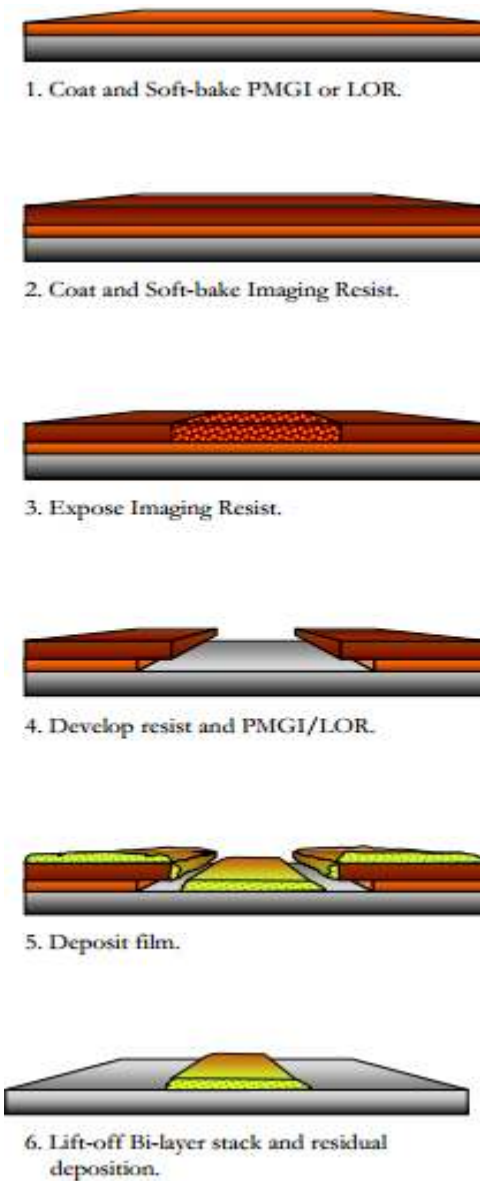


Figure 3.3 Bi-layer lift-off process. (Copied from [37]).

As shown in **Figure 3.3**, the dissolving rates of the two layers are different in developer. With a faster dissolving rate of LOR30B (lift-off resist) than that of photoresist, an undercut is formed after development. After depositing metal, small gap will formed between the metal and the photoresist, which will allow the lift-off solution such as

Acetone or PG-remover to infiltrate. Therefore, the lift-off will be much easier using bi-layer method than using single layer method.

However, the thickness of the metal is limited by the thickness of the lift-off resist. If the thickness of the metal is larger than the thickness of the lift-off resist, the gap will be covered and the lift-off cannot continue in this case. We have the primary test using bi-layer resist method. The morphology of the bi-layer structure is shown in **Figure 3.4**:

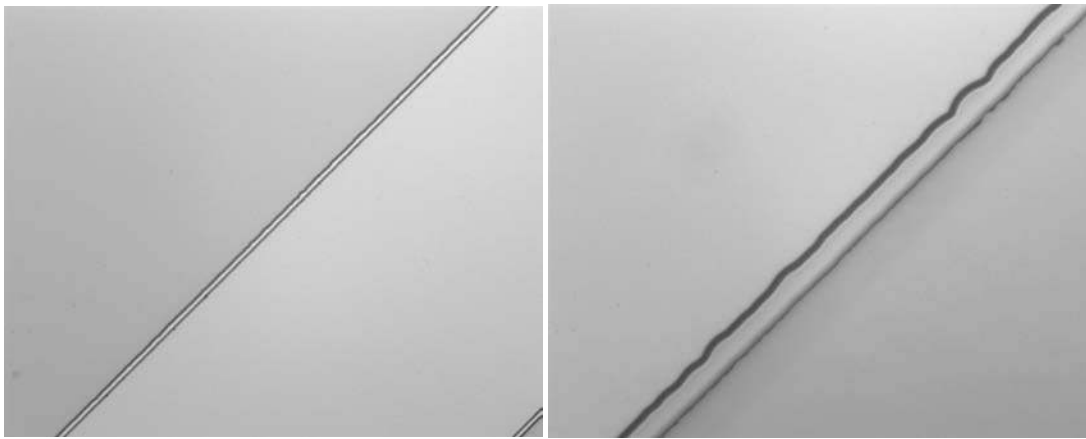


Figure 3.4 Undercut in bi-layer method under microscope.

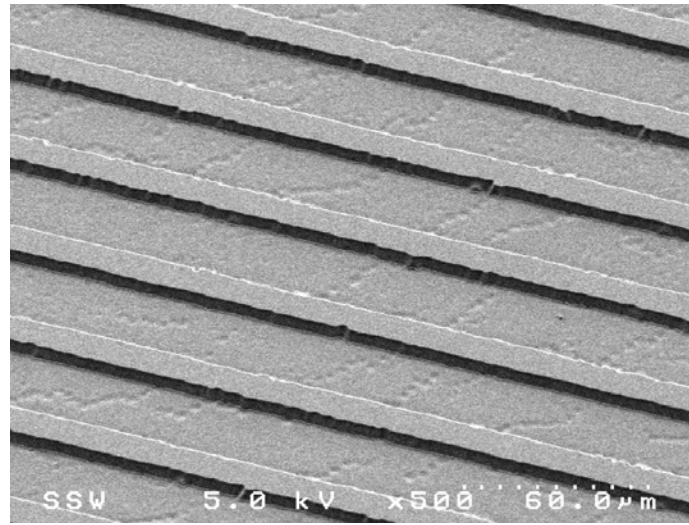


Figure 3.5 SEM image of surface using bi-layer method.

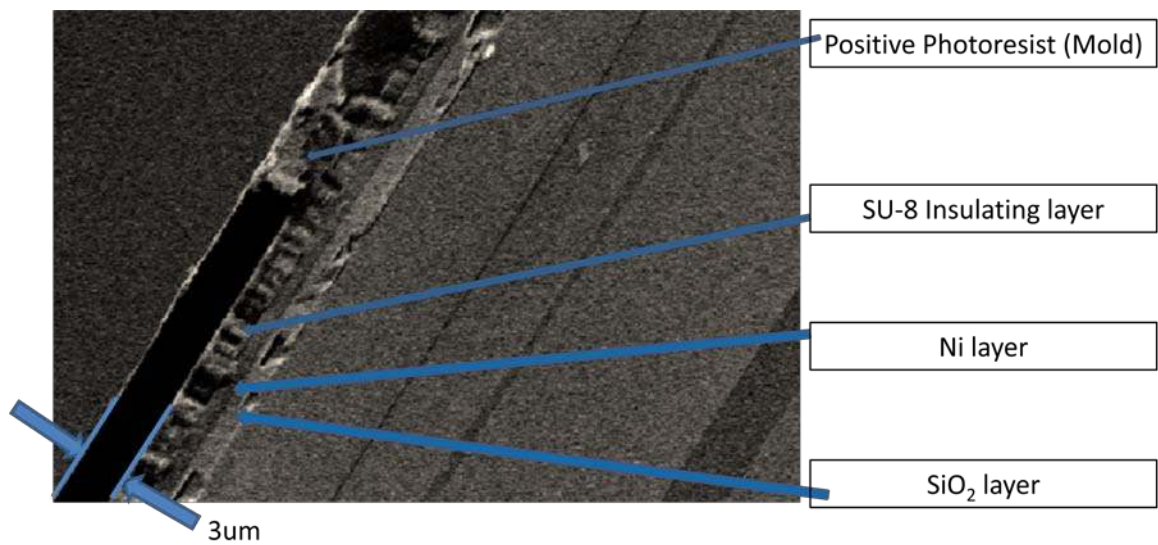


Figure 3.6 SEM image of the cross-section using bi-layer method.

The SEM image of micromold fabricated by bi-layer method is shown in **Figure 3.5**. The image of cross section view of the micromold is shown in **Figure 3.6**. In this preliminary test, Ni was used as adhesion layer. From the cross-section view, the shape of the undercut is clearly shown. In this case, the spinning speed of LOR30B is 1000rpm, and

the maximum thickness of LOR30B layer we can reach is $3\mu\text{m}$ according to the datasheet. 1000rpm is the lowest spinning speed that can be used, since the film quality will be unacceptable if the spinning speed is less than 1000rpm.

From the preliminary test, it is obvious that the sputtering is not suitable for the $10\mu\text{m}$ copper fabrication. Therefore, electroplating was brought up and tried.

Electroplating is usually used for metal coating, but in this project, electroplating is used to fabricate the copper microstructure. There are two prerequisite for the electroplating process: (1). A conductive wafer, on which the structure will be grown on and current can go through. (2). A micromold, in which the copper will grow, also confine the vertical shape of the copper. The conductive wafer can be easily achieved by sputtering a conductive layer onto the wafer. The micro mold should be easily patterned and thick enough to meet the thickness requirement. Moreover, it should be easy to be removed afterwards. A thick positive photoresist with high resolution clearly is the best choice. The procedures for electroplating on a structured micro mold are:

1. Sputtering a conductive seeding layer on the wafer.
2. Spinning photoresist on the wafer.
3. Photolithography and developing.
4. Electroplating.
5. Striping the photoresist.
6. Removing the seed layer.

The seed layer should be removed after the electroplating, otherwise the structures are electrically shorted. The thickness of the seeding layer should be far smaller than the thickness of the electroplated metal (hundreds of nanometres comparing to several micron), so the seed layer can disappear before the plated metal is eroded.

The procedures of electroplating using patterned photoresist as the plating mold are shown in **Figure 3.7**:

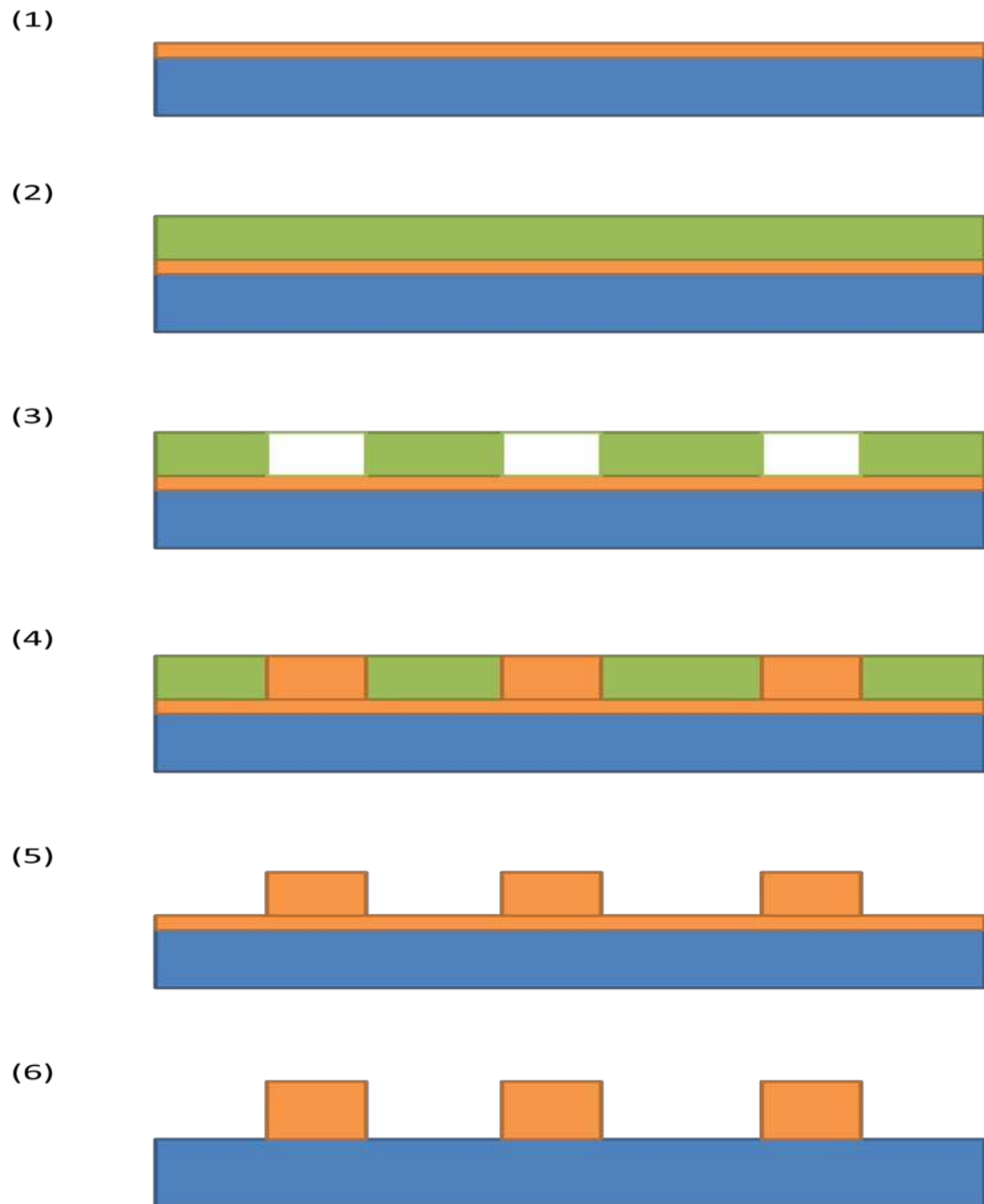


Figure 3.7 The electroplating process using photoresist as micro mold.

Unlike sputtering, over-plating in electroplating process is allowed if the process is carefully monitored to avoid shortage. Over-plating will form a mushroom shaped structure above the photoresist, as shown in **Figure 3.8**.

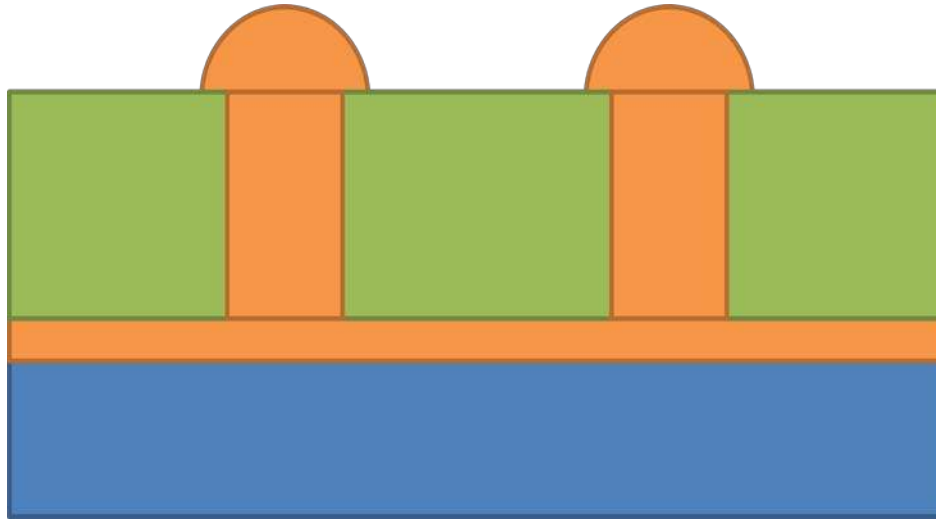


Figure 3.8 Over-plating in the electroplating process.

In summary, among the three metal deposition methods, electroplating is the best choice for copper fabrication because that it is the most suitable and economic method. More importantly, electroplating technique has been widely used in industrial application, it is expected the developed technique can be transferred to mass production seamlessly.

Photoresist selection

A proper photoresist has to be selected to fabricate the patterned micro mold for the electroplating process. The most widely used thick photoresists, such as SU-8 [38] or KMPR [39], are negative tone photoresist, therefore, they are very difficult to be removed after exposure. A positive photoresist, however, can be easily removed by solvent such as Acetone or PG-remover after exposure. In addition, the thickness of the photoresist

remaining after developing has to be over 10 μ m to fulfill the requirement of the electroplating micro mold. Some other requirements such as good adhesion and high resolution also have to be met.

The positive photoresist available from UWO cleanroom, Shipley S1805, S1827 cannot meet the thickness requirement. Therefore, we ordered AZ9260 positive photoresist from AZ Electronic Materials. The maximum thickness of the photoresist by single coating can reach 12 μ m. The aspect ratio can reach 3:1, which is ideal for our developed process. Thus, AZ9260 is used in the process as the micro mold for electroplating.

Insulating layer material selection

The insulating layer is used to separate the two copper layers, as well as a structure layer to support the second copper layer. Several requirements have to be met for the insulating materials:

1. Non-conductive, this is also the insulating layer's basic function.
2. Insoluble in acid or base such as Sulfuric acid, Hydrogen fluoride or Ammonium persulfate.
3. Compatible with the microfabrication process, which means the process of the insulating layer is better to be performed in cleanroom. In addition, the material should be able to be etched or photo-patterned in order to form the via holes.
4. Good mechanical properties, does not crack or peel off due to shrinkage; good adhesion with the substrate.

At the beginning, we considered SiO_2 and negative photoresist SU-8. The preparation methods for SiO_2 are sputtering and PECVD. However, the problem for sputtering is the deposition speed. In order to fully cover the copper layer, the SiO_2 layer should be over $10\mu\text{m}$ thick, it would take several hours to complete. Likewise, PECVD is a high-temperature process, during the deposition, the stress in SiO_2 will build up [40] and finally lead to crack if the film is too thick. The maximum thickness of SiO_2 can be deposited by PECVD is less than $1\mu\text{m}$. SiO_2 is not suitable due to the process limit.

SU-8 is a polymer based negative photoresist, so it is non-conductive. Moreover, it can be photo-patterned, therefore, deposition and patterning could be done in one step, etching is not needed afterwards. Using different spinning speed, the thickness ranging from $0.1\mu\text{m}$ to 2mm can be achieved [41]. It seems that SU-8 is a good candidate and we tried to use SU-8 at first. Unfortunately, the mechanical property of SU-8 is so poor that it cracks instantly when it was dipped into some other liquid such as solvent or acid. **Figure 3.9** shows the crack forms around the patterns. As a result, the SU-8 film cracks or peels off from the wafer. Obviously, SU-8 is not a good option.

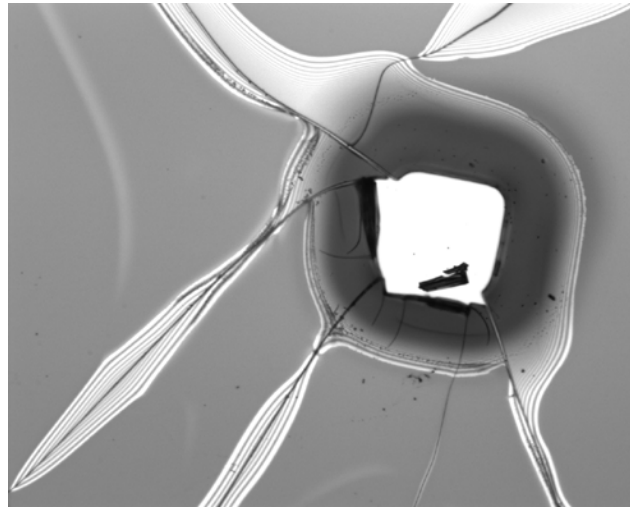


Figure 3.9 Cracks round the patterns in SU-8.

Another optional polymer-based material used in microfabrication is polyimide. The advantages of polyimide include: lightweight, flexible, resistant to chemicals and high temperature. In electronics industry, they are used for producing flexible PCB. In semiconductor industry, polyimide is used as inter-layer dielectric, high-temperature adhesive, mechanical stress buffer or protective overcoat [42]. Some of the polyimide materials are photo-definable. They can be classified as positive tone or negative tone, the same way as the normal photoresist, and they can be processed in the same way as the normal photoresist. For the positive tone polyimide, the exposed area can be removed by developer. For the negative tone polyimide, the exposed area crosslink and remain, the un-exposed area can be removed by developer. Both positive and negative polyimides are able to produce fine features with high aspect ratio. Most importantly, the tensile strength of polyimide (200Mpa) [43] is much bigger than SU-8 (73Mpa) [44], which means polyimide is less likely to crack.

Based on those reasons, we ordered both positive (HD8820) and negative tone (HD4100) polyimide. In the initial test, the positive polyimide seems to be very fragile, because it cracks easily during curing. On the contrary, the negative polyimide is very robust; it survived in high-temperature cure and remains intact in metal etchant. The resolution of the polyimide is also very satisfactory; we can obtain 15 μ m thick polyimide after cure with fine photo-defined features. In the end, the negative tone polyimide (HD4100) is chosen as the inter-layer dielectric material.

Via holes fabrication

There are two layers of copper in the device. Most part of the two layers of copper should be electrically separated by dielectric layer and connected at specific point by the via holes. The structures are in **Figure 3.10**:

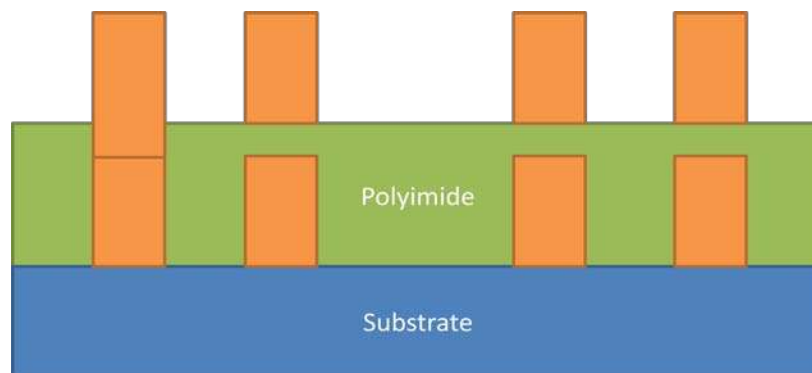


Figure 3.10 Cross-section view of the coil.

Electroplating is still the first choice for the second layer copper fabrication. The seed layer for electroplating is still needed. As long as we use sputtering to deposit the seed layer, we can take advantage of the good step coverage of sputtering. After photolithography of polyimide, the via holes are formed in polyimide film and the contact area of the first layer copper is uncovered. Due to the good step coverage of sputtering, copper will cover the bottom and the sidewalls of the via holes, as well as the surface of the polyimide without any gaps or blanks. During electroplating, the current can go through the thin film of copper that covers the surface of polyimide, sidewall and bottom of the via holes, therefore, the growth will occur everywhere simultaneously. After removing the seed layer, an electrical connection will be formed by the via. The electroplating growth process for fabricating via holes and second layer copper is shown in **Figure 3.11**.

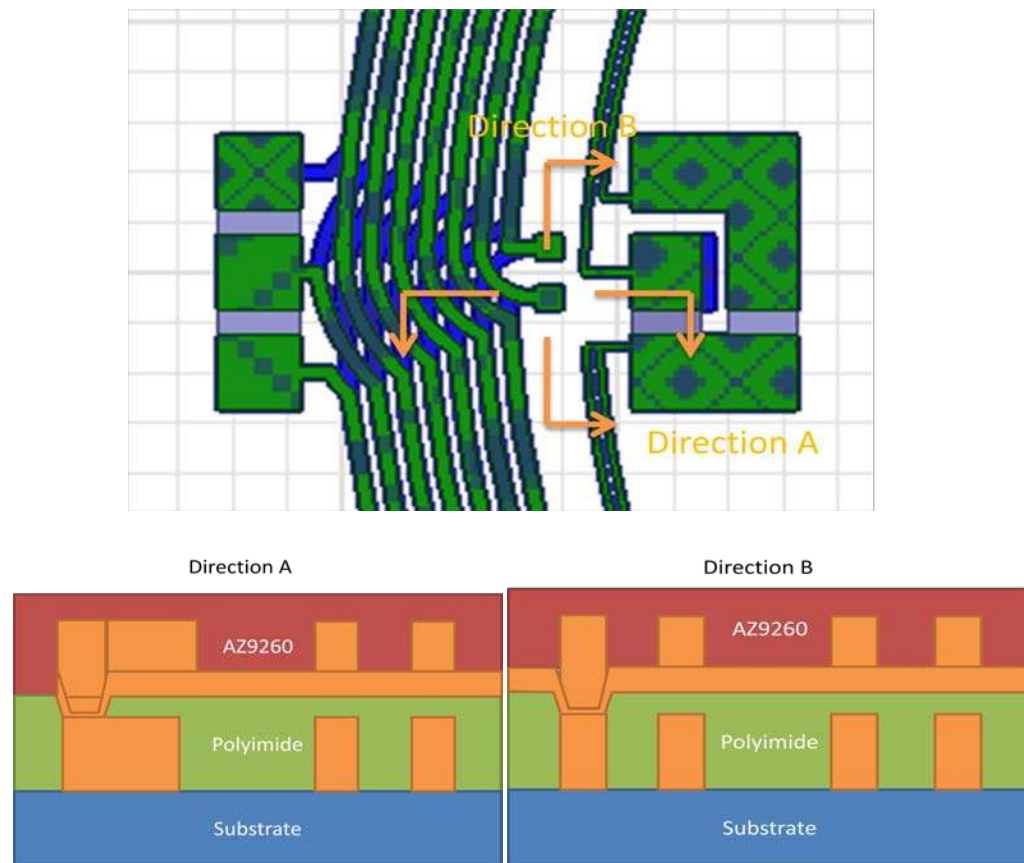
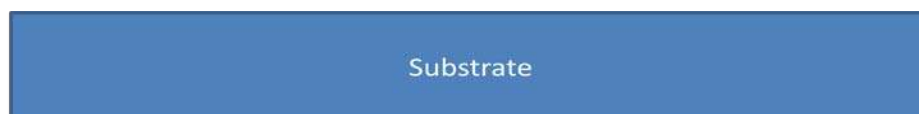


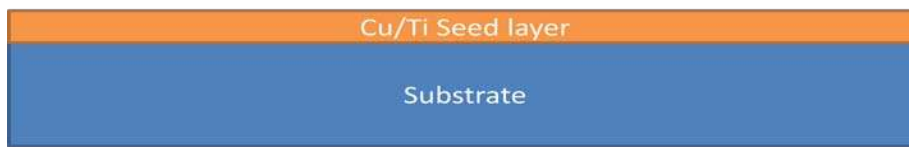
Figure 3.11 Electroplating growth mechanism of via holes.

Outline of the microfabrication process

As every essential parameter, process and material is determined, outline of the process is summarized below:



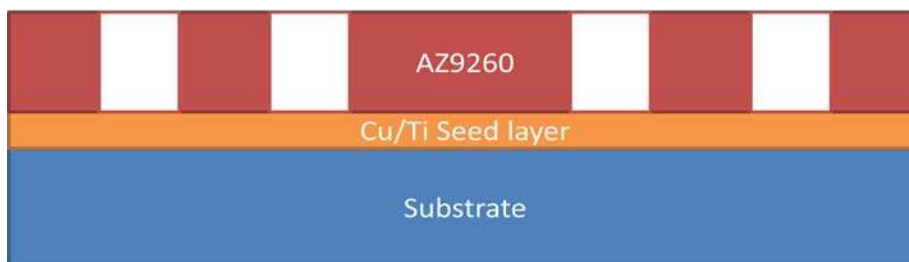
Step 1. The Silicon substrate with SiO₂ layer is thoroughly cleaned.



Step 2. Cu/Ti seed layer is deposited by sputtering.



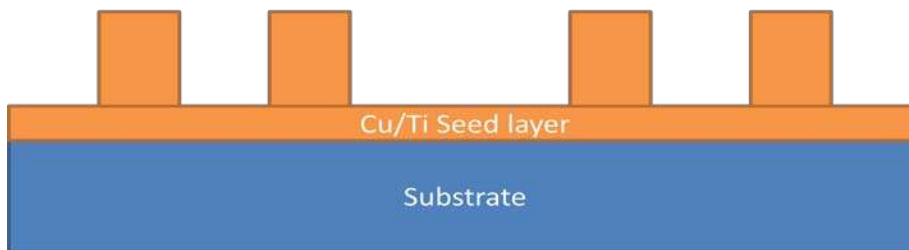
Step 3. Spin coat AZ9260 photoresist.



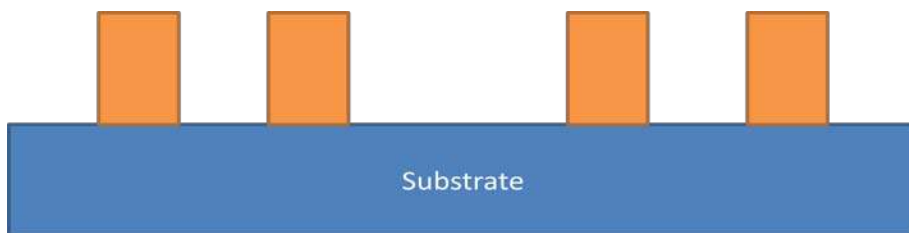
Step 4. Expose and develop.



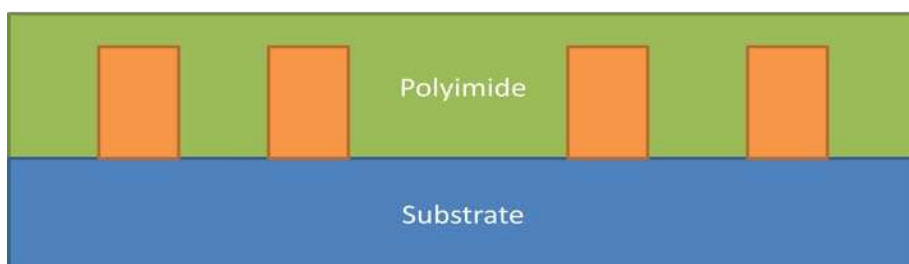
Step 5. Electroplate copper



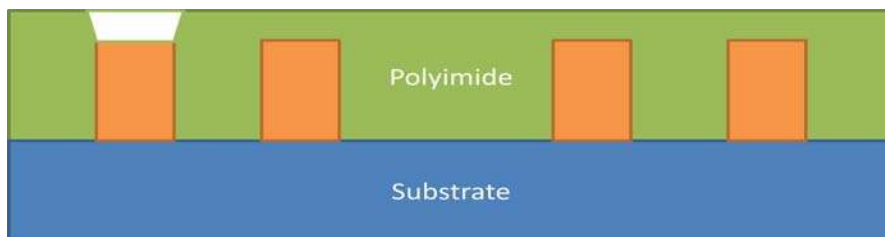
Step 6. Strip photoresist.



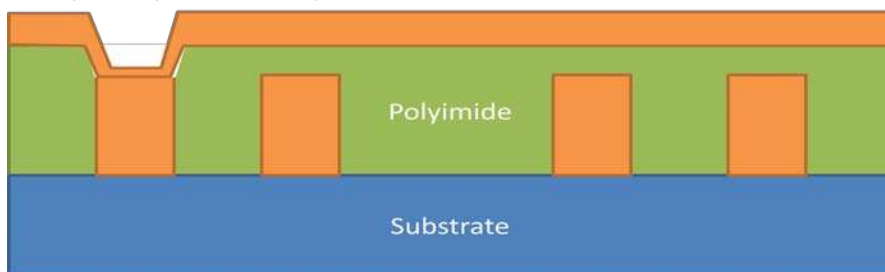
Step 7. Remove seed layer by wet etch.



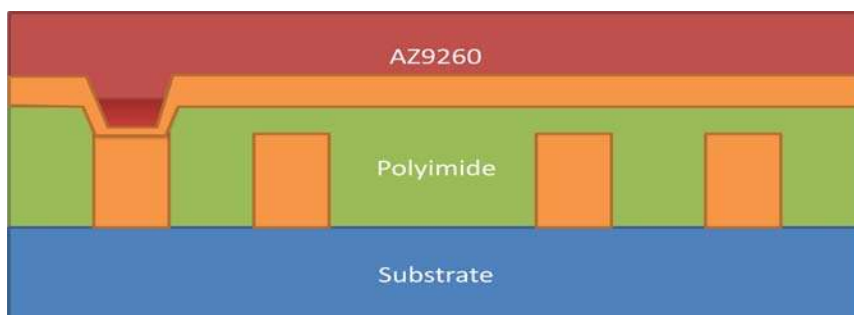
Step 8. Spin coat HD4100 negative tone polyimide.



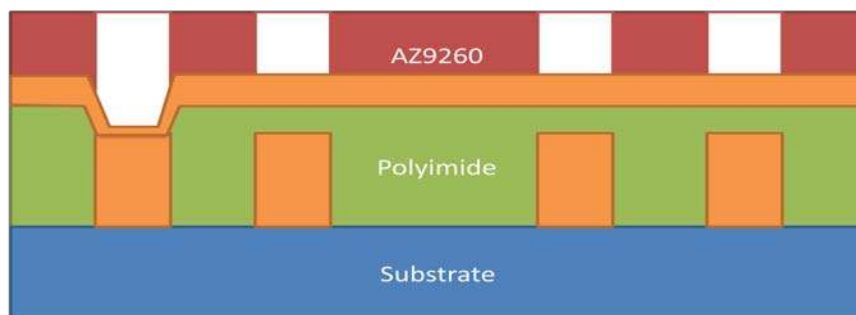
Step 9. Expose, develop and cure.



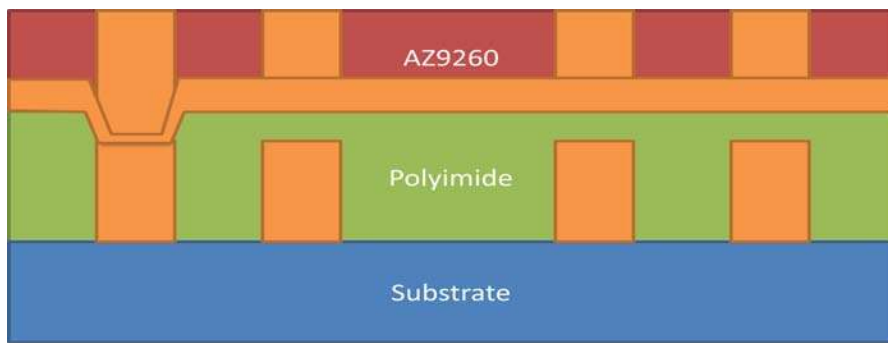
Step 10. Sputter Cu/Ti seed layer.



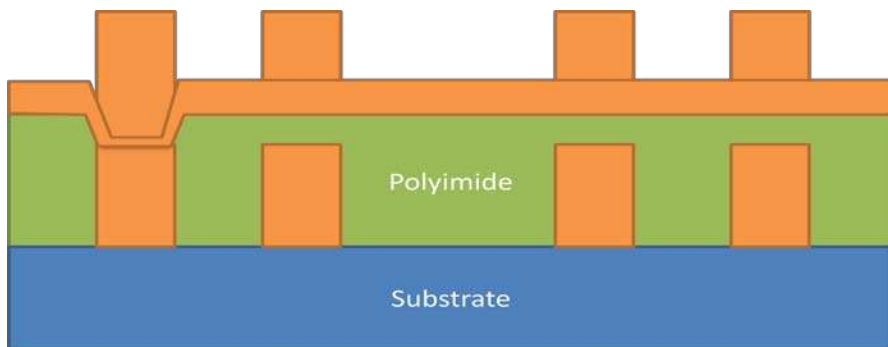
Step 11. Spin coat second AZ9260 photoresist film.



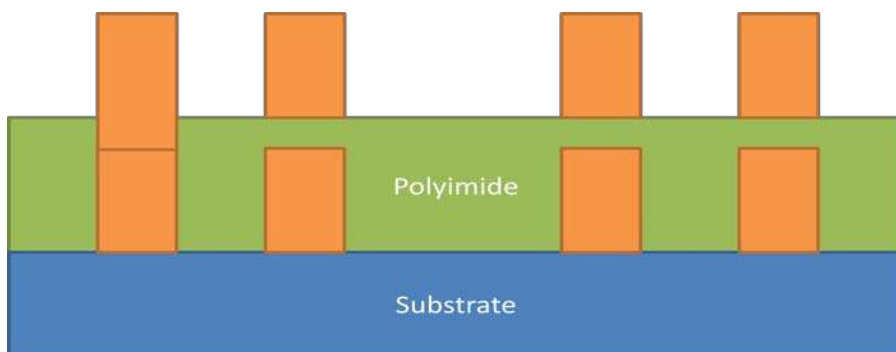
Step 12. Expose and develop.



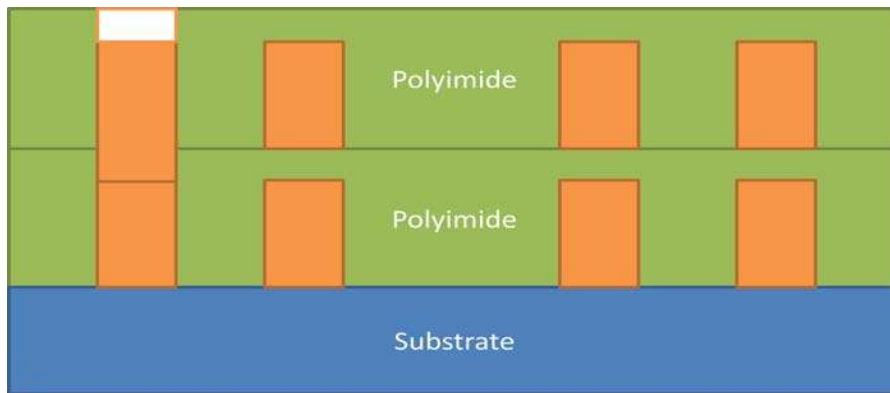
Step 13. Electroplate copper.



Step 14. Strip Photoresist.



Step 15. Remove seed layer by wet etch.



Step 15. Spin coat second polyimide layer, expose, develop and cure. Top polyimide layer is used to protect the copper coil.

Figure 3.12 Outline of the process for device.

3.3 Photomask design and optimization

Photomask design is a very important part in the lithography process. A well designed mask will ensure the functionality of the device, also reduce the failure probability during the process.

In this project, there are three masks in total. Mask 1 and Mask 3 were used to fabricate the first coil layer and second coil layer, while Mask 2 was used to process the insulating layer. For the mask design, there are some improvements accomplished in the project development. These improvements will also be very useful in the future mask designing.

In microfabrication process, sharp corners need to be avoided to make sure the microstructures do not crack because of stress concentration. In the mask design, sharp corners are rounded to avoid sharp angles (**Figure 3.13**). The radius of the fillets is set to be $5\mu\text{m}$.

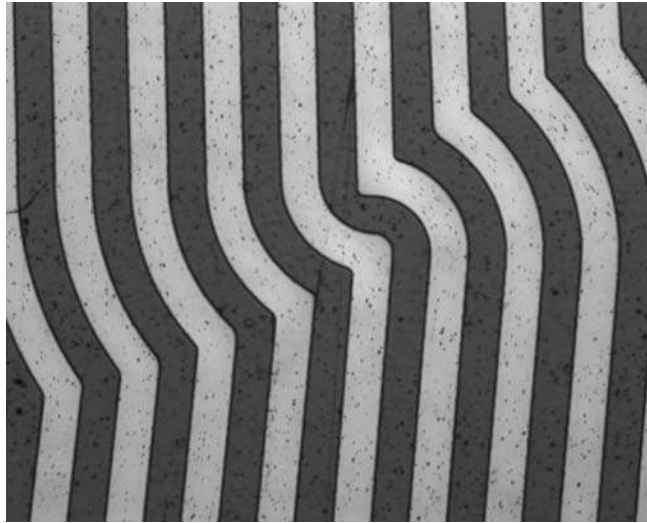


Figure 3.13 Filleted corners in the mask.

For the primary validation stage, the plastic masks are chosen to reduce the cost. The masks are prepared by CAD/Art Service Inc., using the highest resolution (2000DPI) they can print. However, the edge is not very smooth comparing to Chromium mask (**Figure 3.14**).

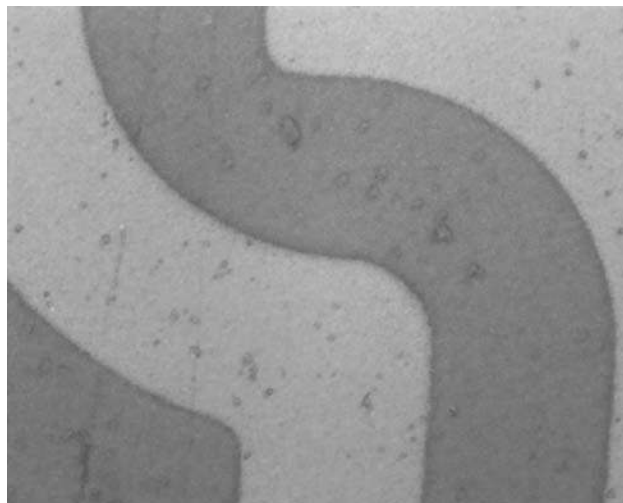


Figure 3.14 50X magnification of the mask features.

The mask 1 and mask 3 are for positive photoresist, so most area of the mask is opaque (no structure area). In addition, the line width of the alignment mark is only $20\mu\text{m}$. Therefore, it is very difficult to do alignment under the microscope because the scope is quite limited. In order to assist the alignment, transparent windows are created at the corners of the features (**Figure 3.15**). By adding these transparent windows, the alignment is much easier.

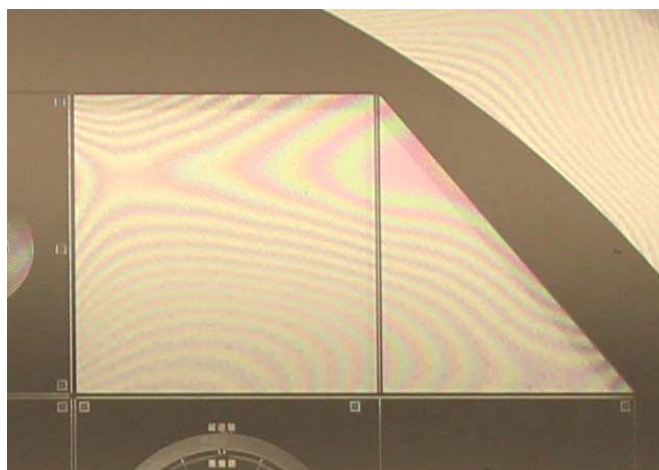


Figure 3.15 Transparent window of the mask.

In addition, in order to fit the cathode sample holder of the electroplating equipment and to form an electrical connection, the surrounding area of the wafer must not be covered with photoresist. Therefore, the opaque area of the mask is smaller than 4 inch wafer, a transparent circle area with the width of 1cm is created to expose the wafer's outer area. Layout of the mask is shown in **Figure 3.16**.

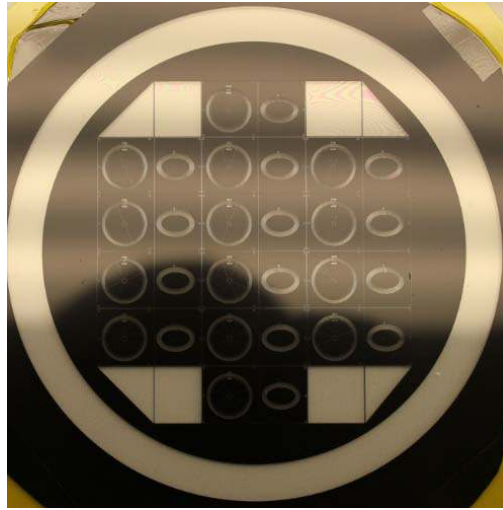


Figure 3.16 Mask designed for electroplating.

3.4 Microfabrication steps

In the following sections, steps of the process are explained in detail. Some of the difficulties and problems encountered in the process are also discussed.

3.4.1 Substrate pretreatment

To avoid any particles or chemical contamination, the substrate should be thoroughly cleaned. As we used Silicone substrate with 2um SiO_2 layer, the traditional RCA or HF cleaning process is not suitable. Instead, we used Nanostrip® solution to remove the organic contaminations. The Nanostrip solution was heated to 80°C to ensure the maximum effectiveness, the wafer was immersed in it for 3 minutes. Then the wafer was rinsing with de-ionized (DI) water. To make sure there is no residual chemicals, the wafer then was put into the Semitool wafer cleaning machine to rinse for 15 min and blow dry. Thereafter, the cleaned wafer was dehydrated in a oven at 150°C. Unlike traditional wafer

cleaning process, the wafer was not deposited the adhesion promoter HMDS (Bis(trimethylsilyl)amine) in the oven, because the wafer is covered with SiO_2 instead of Si.

3.4.2 Seeding layer sputtering

After cleaning, the wafer was put into the vacuum chamber of sputtering machine to do sputtering. In our experiment, the sputtering machine we use is Edwards Auto500 Sputter Deposition System, as shown below:

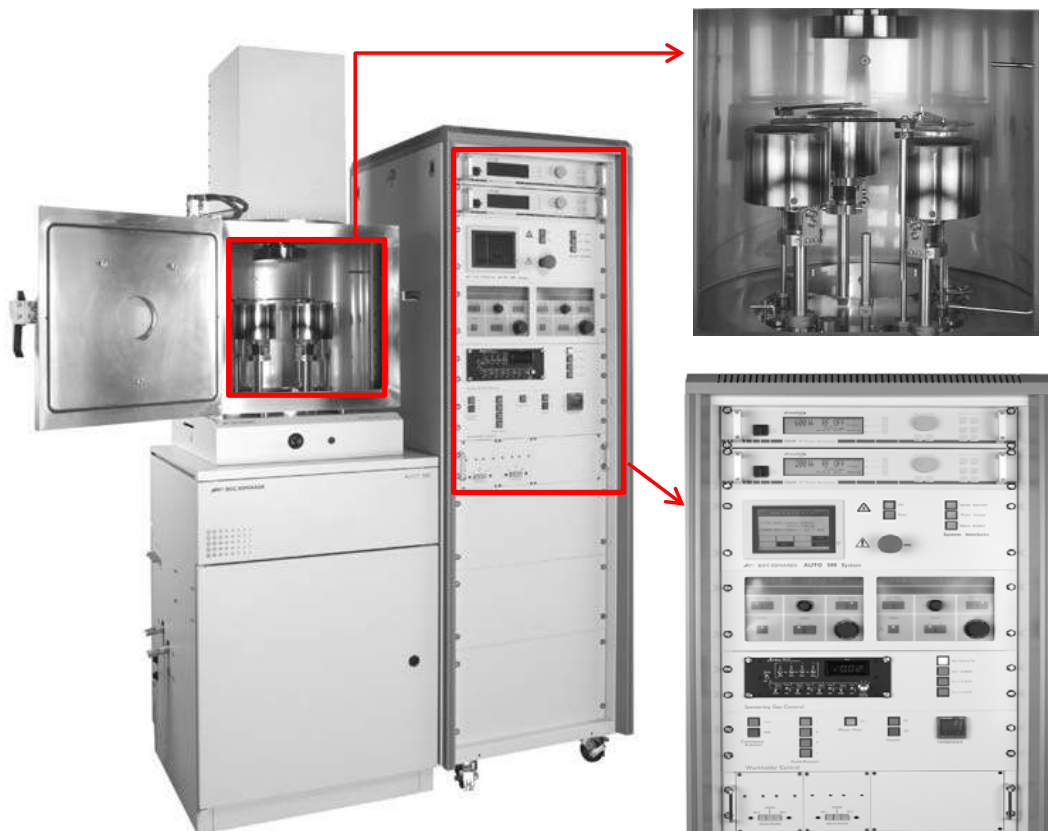


Figure 3.17 Photograph of Edwards Auto500 sputter deposition system. (Copied from [45])

In order to ensure the quality of the metal film, the vacuum chamber was pumped down to 5×10^{-5} bar before the sputtering started. The first step is to sputter a 50nm thick Titanium adhesion layer. There are several reasons for using Ti as an adhesion layer. The first one is Ti has good adhesion to silicon and silicon dioxide, as well as copper, therefore Ti could improve the adhesion between copper layer and SiO_2 layer; the second one is Ti can prevent electrical breakdown due to diffusion of copper atoms into the SiO_2 layer under high voltage or temperature [46, 47]. The Ti target was mounted on Cathode 3 which is driven by RF power source. Therefore, the Ti sputtering was done by RF sputtering mode with power of 100W. The duration of deposition is 15 minutes. Hereafter, copper was sputtered using DC sputtering mode with power of 150W for 15mins. The thickness of the copper layer was around 300nm. The sample holder rotated continuously at 10 rpm to ensure uniform deposition during the sputtering. The wafer with a copper seed layer is shown below, it can be seen that the copper layer is uniform and sturdy.

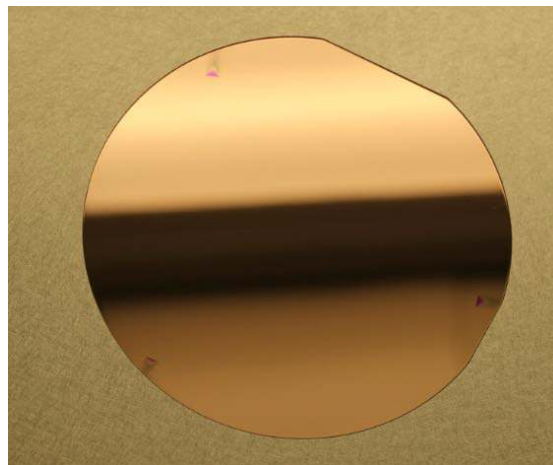


Figure 3.18 Wafer with copper seed layer.

3.4.3 First layer micromold photolithography

The following section will explain how to fabricate photoresist micromold on the wafer.

The nature of AZ9260 photoresist

AZ9260 photoresist is a DNQ-novolac based positive photoresist. There are three basic ingredients in it: novolac resin, diazonaphthoquinone (DNQ) type dissolution inhibitor and solvent [48]. Some properties of the photoresist, such as film forming characteristics, etch resistance and thermal stability, attribute to novolac resin (**Figure 3.19**).

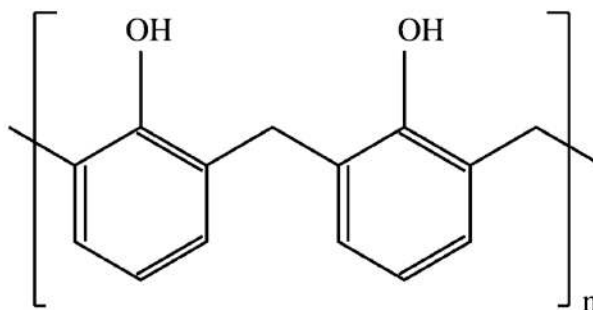


Figure 3.19 Structures of novolac resin. (Copied from [27])

Diazonaphthoquinone (DNQ) is the photo-sensitizer. DNQ inhibits the novolac resin dissolve in base solution. Upon exposure to UV light, the quinonediazide decomposes. The decomposition product is base-soluble, in addition, Nitrogen generated from the reaction produce a porous structure (as shown in **Figure 3.20**), allow the developer to diffuse, resulting in increased solubility.

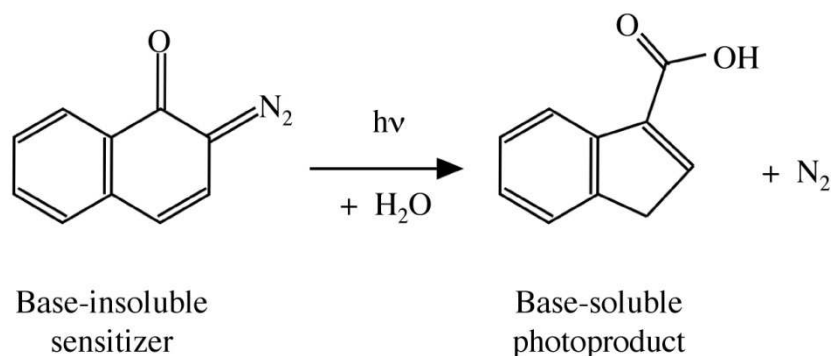


Figure 3.20 Photochemical reaction of DNQ upon exposure. (Copied from [27])

The solvent allows the photoresist to stay in liquid state and to be spin coated on the wafer to form uniform thin films.

After exposure and developing, the exposed photoresist is washed away; as a result, the patterned structures are left on the substrate.

To avoid any particle contamination, the process of patterning AZ9260 is done in cleanroom. Unprocessed AZ9260 photoresist should be stored in tightly closed containers in a cool, dry environment, and kept away from light at 4-21°C.

AZ9260 spin coating

The thickness of AZ9260 resist can be adjusted by changing the spinning speed of the spin coating equipment. The datasheet provided by the company shows the relation between the spinning speed and thickness (**Figure 3.21**).

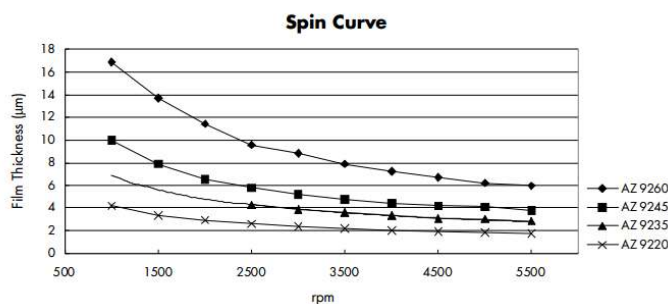


Figure 3.21 Spinning speed vs thickness. (Copied from [49])

From the previous experiments experience, if the spinning speed is under 1000rpm, the photoresist film is not uniform. Therefore, the spinning speed should be above 1000rpm.

The spin coating process is:

(1). Dispense: squeeze 2ml AZ9260 resist on the substrate, make the liquid form a round pool which can cover 1/3 of the whole wafer. If the resist pool is not round before spinning, some of the area will not be covered during spinning due to the un-even spread of the photoresist.

(2). Spread cycle: Ramp to 500 rpm at 100 rpm / sec acceleration and hold for 10 sec.

(3). Spin cycle: Ramp to spin speed 1000rpm at an acceleration of 500 rpm/s and hold for 50 sec.

The spinning process is done by spinner Solitec 5110 in the cleanroom. The target thickness of the film is 15μm.

Soft bake

After coating photoresist, the wafer was put on a hotplate to evaporate the solvent prior exposure; this process is called soft-bake. At the beginning, the wafer is put on the unheated room-temperature hotplate, then the hotplate is turned on and the temperature slowly ramps up to 110 °C. The reason for doing so is: for a 15 μm thick resist, ramping up the temperature slowly from room temperature can prevent bubbles generation caused by application of sudden high temperature. By doing this, the adhesion of the photoresist film is improved. The wafer is baked at 110 °C for 3mins. Then the power of hotplate was turned off, and the wafer was left on the hotplate cooling down to room temperature.

Exposure

A photomask is required to define the microstructure. The plastic mask we ordered from CAD/Art Service Inc is stucked on the 5-inch square glass with its ink side facing outwards. The side of the plastic mask should be carefully examined under the microscope to distinguish which side is the ink side. The reason for doing so is: the plastic mask itself has a certain thickness, the ink side should be adjacent to the substrate, otherwise the light will be scattered inside the plastic sheet as shown below (as shown in **Figure 3.21**). If the mask were installed by the wrong side, the quality of the patterns would be worse.

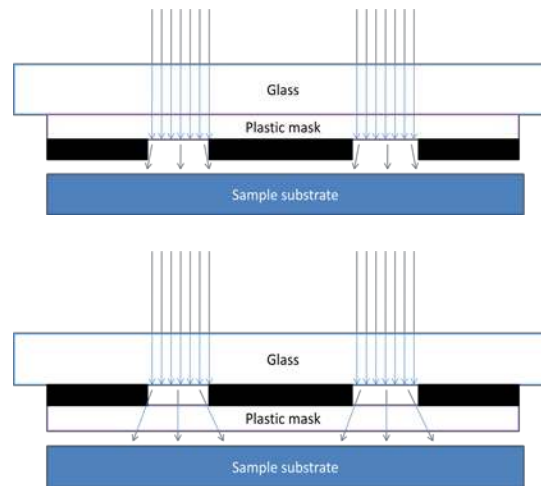


Figure 3.22 The difference between ink side facing glass and facing substrate.

Karl Suss MA6 Mask Aligner was used in lithography to align the sample and photomask as well as providing parallel light source (**Figure 3.23**). UV light generated by the Mercury lamp goes through a series of optical regulation systems, becomes parallel and irradiate the photomask perpendicularly, eventually reaches the photoresist. The MA6 system uses proximity expose method, thus the proximity gap between the photomask and the substrate must be keep as small as possible. By removing the bead or placing the mask in the right direction, the gap can be reduced even smaller to reduce the diffraction errors. Otherwise the diffraction would cause the exposed area is larger than it should be.



Figure 3.23 Karl SussMA6 mask aligner for photolithography.

For the first layer copper micromold, Mask 1 was used for the patterning, layout of mask 1 is shown in **Figure 3.24**.



Figure 3.24 Layout of mask 1

For the 15 μm thick photoresist, the exposure dose should be around $2100\text{mJ}/\text{cm}^2$. The intensity of the UV light is $12\text{mJ}/\text{cm}^2$ in our experiment, the exposure time is $2100/12=177$ seconds.

Develop

Following the exposure, the sample was immersed in the developer AZ400K for developing while agitation is applied. The developing time for the same thickness AZ9260 is around 4 minute according to datasheet. However, we found the development time is related to agitation rate, environment temperature, baking time, exposure time, etc. The developing should be carefully controlled, otherwise, if the sample is over-developed, the patterns will become inaccurate, and some small gap will disappear. The development is completed or not can be more reliably judged by the color of the underneath copper layer. Once the development is completed, the copper is covered by photoresist at the exposed area, thus that area is visible with metal luster. Developing can be easily monitored by observing the transparent window area (Figure 3.15), in which a big area of copper metal can be seen.

Based on our experience, the development time varies a lot in winter and in summer. In winter, the development takes about 15~20 min, in summer, it only takes 5~6 min.

Rinse and dry

The wafer should be rinsed carefully with DI water, and dried with gently application of compressed air. Although the surrounding area of the wafer is intentionally exposed, the

edge bead is so thick that it cannot be removed by development. The residual edge bead photoresist is removed by acetone using Q-tip.

O₂ plasma RIE

Some of the residual photoresist cannot be completely removed by development. The sample has to be thoroughly cleaned by O₂ plasma RIE. The residual photoresist can react with the oxygen plasma, and then the reactant products can be expelled with exhaust.

The patterning of micromold is completed after the RIE cleaning. Parts of the microstructure are shown below. The photoresist film is 15 μm thick, which is measured by profiler. Pattern of micromold is shown in **Figure 3.25**.

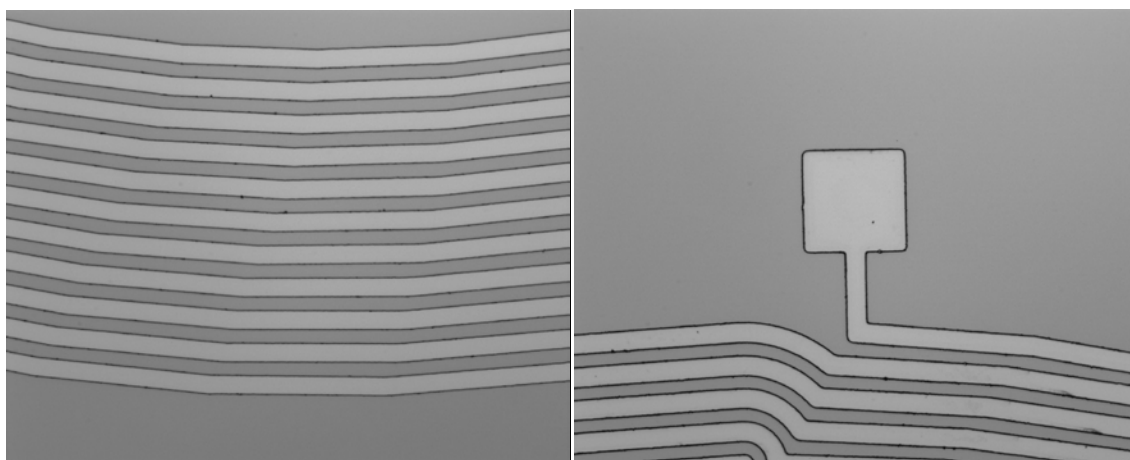


Figure 3.25 Part of the patterned micromold under microscope

3.4.4 Electroplating

Electroplating is usually used for metal coating on a big surface. In this study, electroplating is used to grow the copper microstructure, which is more challenging because a small plating defect could cause the failure of the microstructure.

To fabricate uniform, non-defect copper structures, some requirements have to be met in the electroplating process.

The first requirement is for the photoresist micromold. The photoresist must have good adhesion with the substrate. If not, the circulation of the electrolyte solution or anode vibration (some electroplating machine has a reciprocator to agitate the solution) could easily cause the photoresist to peel off with underplating consequently. To improve adhesion, the primary requirement is to choose the right photoresist, some of the photoresist such as AZ 1400, 4500, 9200 are good candidates, because they are optimized for electroplating, and show an improved adhesion to many substrate materials [50]. Optimum soft-bake parameters also improve the adhesion: the baking time could be extended another 1 or 2 min; to prevent the formation of cracks, when soft bake is done, the sample should be cooled down to room temperature gradually rather than removed from hotplate instantly. A prolonged baking time can also evaporate the solvent in the photoresist more thoroughly. If the residual solvent release to the electrolyte, the solvent may hinder the electro-chemical process and result in a reduced deposition rate. Moreover, the photoresist must be chemically stable in acidic electrolyte solution, the novolac resin in the AZ9260 ensure that the resist remains intact in the solution. The sample should also be fully developed and rinsed, and etched by O_2 plasma to make sure there is no thin, invisible thin layer residual resist staying on the substrate to prevent proper contact between the substrate and the deposited metal.

The second requirement is to optimized electroplating parameters. Electroplating can be operated in DC mode or pulse-reverse mode; the plating power source can be regulated by current or voltage. Only the optimum combination ensures a fast, reliable result.

Last but not least, a proper electroplating solution has to be carefully prepared to function as the reliable source of copper and stable chemical reaction circumstance.

Electroplating bath solution

The chemical composition of acid sulphate bath includes: copper sulphate pentahydrate, sulfuric acid and additives.

The metal ions come from the copper sulphate. Sulfuric acid increases the solution conductivity and helps to prevent the formation of basic cuprous or cupric crystals. If sulfuric acid is not sufficient, some defects like poorer leveling and nodular growth will happen [51]. The concentration of copper sulphate must be appropriate. If the concentration of copper sulfuric is too small, the solution resistivity increases and anode and cathode polarization is reduced. If the concentration is too big, copper will crystallize in the solution instead of on the sample. To produce a bright copper, additives must be added. For example, Hydrochloric acid is added to inhibit formation of rough nodular plate. Low chloride can cause loss of brightness, and high chloride causes streaks. Additives like carrier can help increase throwing power in to holes and other surface features. Brighteners can control the grain structure.

The recipe of plating bath used in our experiment is:

225 g/L CuSO_4 , 50 g/L H_2SO_4 , 50 ppm HCl , 8 ml/L Brightener, 8 ml/L Carrier.

Electroplating process

IKOTM Classic electroplating system is utilized in our experiment (**Figure 3.26**). The system includes a solution tank, a power source and a control box that can control the anode reciprocator and the heater in the solution tank. The sample holder is the cathode, thus it connects the negative cable of the power source. The anode is an inert electrode, which is covered by conductive sponge to increase the contact area with plating solution.



Figure 3.26 IKO electroplating system. (Copied from [52])

To begin with, the sample wafer is fixed on the electroplating sample holder (**Figure 3.27**). The hollow circle in the upper part is slightly smaller than the 4-inch wafer in order to secure the wafer as well as expose most of the wafer in the plating solution. The lower part is fastened by screws on the upper part to hold the wafer tightly. The sample should be approximately positioned concentric with the hollow circle in order to form a good connection between the sample and flexible electrode around the circle edge.

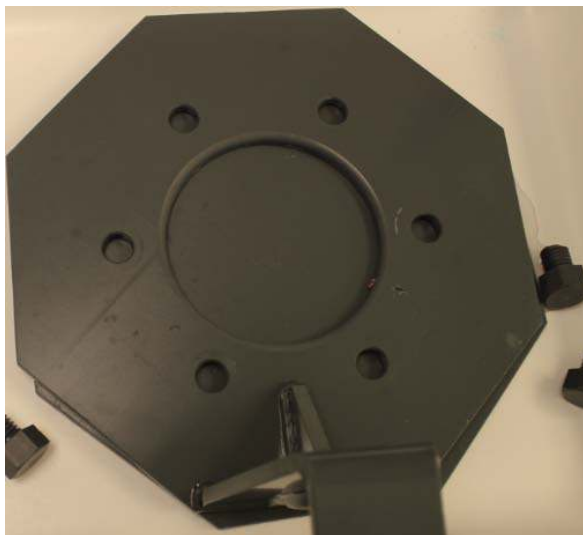


Figure 3.27 Sample holder

At the beginning, 40ml of brightener is added (brightener should be added every time before the electroplating process because it is consumed during the process). Then the system is turned on to let the pump circulate the solution for 5min. Thereafter, the sample holder is immersed into the solution. After cathode and anode is connected to the power source, the process can be commenced by turning on the power supply regulator. Although the anode reciprocator can reciprocate to agitate the plating bath for a better quality, but we found severe vibration caused by continuing agitation will damage some structure with small size. Therefore, the reciprocator stayed still during the electroplating, anode electrode was lifted up a little from the sample for the solution circulation.

The electroplating power source is regulated by current rather than voltage, because as the process continues, the concentration of the plating bath, as well as the resistivity changes, if the process is regulated by voltage, the total current will be changed accordingly.

The plating process should be completed as fast as possible with good quality. However, a compromise between speed and quality has to be made. Increase the current could accelerate the plating process, the metal grain will grow much faster, more nucleation will occur at the same time. If the high current continues, the copper film will become rough and dots will appear on the surface of the metal with application of excessive current, as shown in **Figure 3.28**.

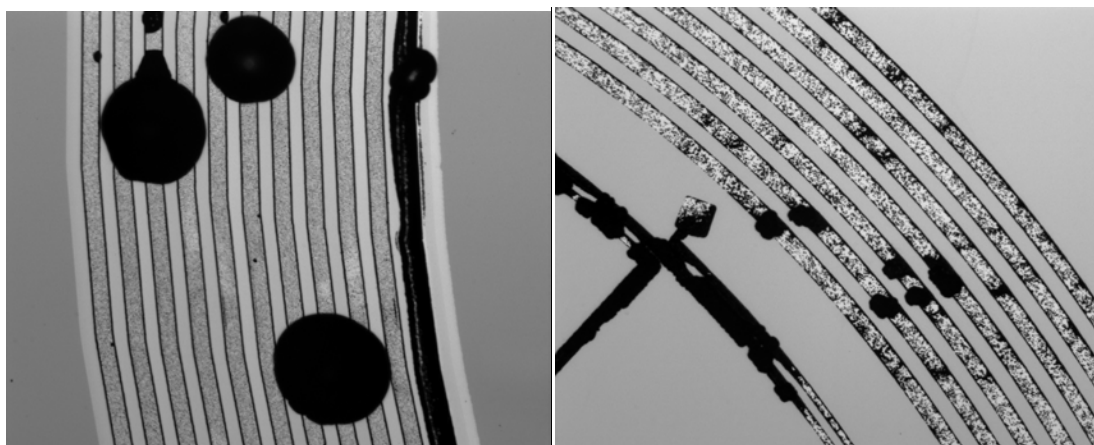


Figure 3.28 Defects caused by excessive current.

The recommended current density is $20\text{--}40\text{ mA/cm}^2$, the total pattern area is approximately 3cm^2 measured by CAD software. After running many samples with different parameter, the applicable parameters are summarized below:

Table 3.1 Parameters for electroplating.

	Brightener added	Total current	Current density	Duration	Final thickness
Recipe 1	30ml	50	17 mA/cm ²	3 hours	12 μ m
Recipe 2	60ml	120	40 mA/cm ²	2 hours	20 μ m
Recipe 3	80ml	160	53 mA/cm ²	2 hours	25 μ m

All three recipes can guarantee uniform, bright and defect-free copper. As the current increases, more brightener needs to be added. Considering the efficiency of the process, the Recipe 3 is used in our device fabrication. Although the copper thickness is almost twice of the micromold thickness, the morphology of the over-plating copper is controlled by the Brightener additive from over-growing horizontally. The coil turns remain separated rather than connect to each other. When the electroplating is finished, the sample is removed from the sample holder, rinsed for 5 min under DI water to remove the plating solution thoroughly, and then blew dry by compressed air. The morphology of the copper grown by electroplating is shown in **Figure 3.29**.

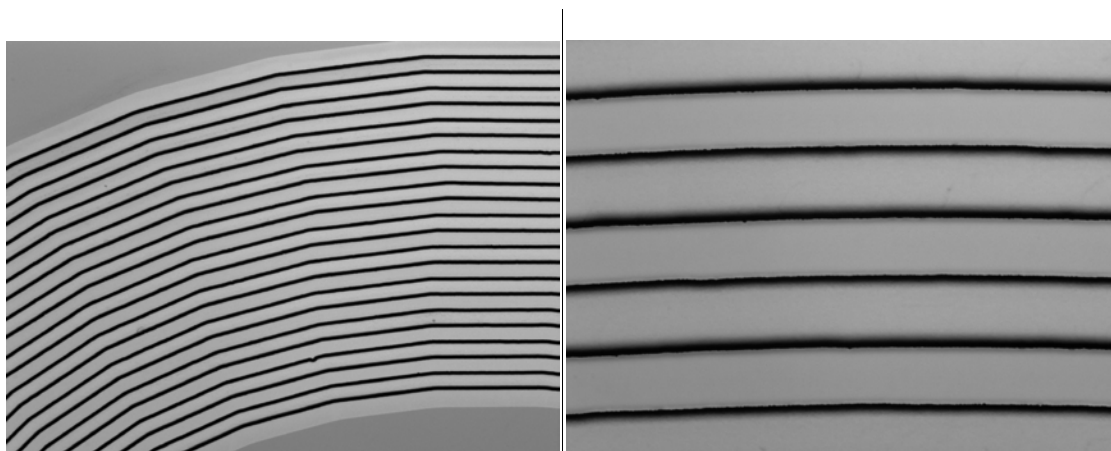


Figure 3.29 Copper grown by electroplating in micromold.

3.4.5 Strip photoresist

In order to remove the seed layer, the photoresist must be stripped off. As novolac resin is soluble in Acetone, so acetone is used as the photoresist strip.

The photoresist will be dissolved instantly once the sample is dipped in the acetone. To make sure there is no residual photoresist, the sample was kept in the acetone for 2 min while agitating. Followed by rinsing with acetone, the sample then was rinsed by IPA to wash off the acetone. Eventually, the sample was rinsed by DI water and then blow dry.

3.4.6 Etching seed layer

The seed layer need to be etched off, otherwise the circuit is shorted. Both Cu and Ti layer need to be removed by wet etch. The electroplated copper is much thicker than the seed layer, therefore, the electroplated copper behaves as the mask for the wet etch. APS-100 copper etchant provided by Transene is used in copper etch. The same as developing, whether the Cu wet etch is completed is judged by the color change during the process. A few second after the sample is put in the etchant, the copper seed layer turned black then short after the color fades away, the color of substrate is visible. Even the color of Cu is

completely gone, the sample is still need to be etched another 3~5 seconds to avoid any residual copper seed layer remaining on the substrate. A small copper residual can easily short the coils, therefore, the etched wafer should be carefully examined by microscope. If a small residual copper is observed, the sample needs to be etched another several seconds until it is completely done. This procedure is repeated until the coil is completely separated. The sample was cleaned and blow dry after Cu etch.

Then Ti layer was etched by Titanium etchant TFTN. Titanium etchant contains HF, the process have to be done in the well-vented fumehood with safety glass and rubber gloves. Ti layer is only 50nm, judging by color change is very difficult since the Ti layer is almost transparent. Yet we have another method to monitor the process: in the seed layer sputtering step, the wafer was fixated on the sample holder by three clips, the area beneath the clip will not be deposited metal so three clip shadow marks were left there. The Ti etch could be ascertained to be finish when the shadow marks disappear. Finally, the sample was cleaned and blow dry. The first layer copper is completed here. The images of the first layer copper structure are shown in **Figure 3.30**. The 10 μm width structures with 20 μm gaps can be clearly seen on the picture, it means that the quality of copper structures are very good.

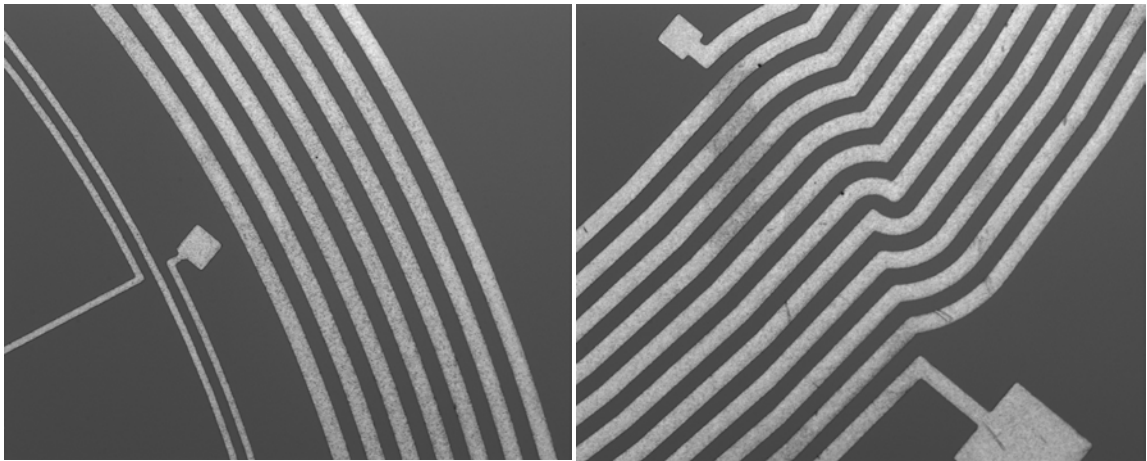


Figure 3.30 Details of the first layer copper

3.4.7 Insulating layer preparation

Nature of HD4100 Polyimide

Polyimide has the properties such as high heat resistance, good chemical resistance, good thermal stability and solvent resistant. The main physical properties of polyimide are presented in the following table.

Table 3.2 Physical properties of the HD4100 negative tone Polyimide [43].

Characteristics	Value
Tensile strength	200Mpa
Tg	330 °C
Elongation	45%
Modulus	3.4Gpa
Coefficient of Thermal Expansion	35ppm/°C
Decomposition temperature	600 °C
Initial (1%) weight loss	430 °C
Residual stress	34Mpa
Dielectric Constant (1Mhz)	3.36
Surface Resistivity (50V)	3.3×10^{16}
Volume Resistivity (50V)	2.4×10^{16}
Dissipation factor (1Mhz)	0.001
Dielectric strength	250kV/mm

From the **Table 3.2**, we know that Polyimide can endure high temperature, has high resistivity and superior elongation properties. All those properties make Polyimide a suitable material for our application.

HD4100 is provided by Dupont®. As a negative tone photo-definable Polyimide, HD4100 can be processed the same way as the common negative photoresist.

Sample pretreatment

Before photolithography, the sample was heated on hotplate at 110 °C for 3 min. The purposes of doing this are: (1). evaporate the humidity on the wafer surface, increase the Polyimide adhesion. (2). Oxidize the surface of the copper coils, form a thin CuO protection layer. (3). In the following spin coating, heated substrate also decrease the viscosity of liquid Polyimide, the film is more uniform on a heated wafer than on a unheated wafer.

Spin coating

The spinning curve provided by the vendor is shown in **Figure 3.31**.

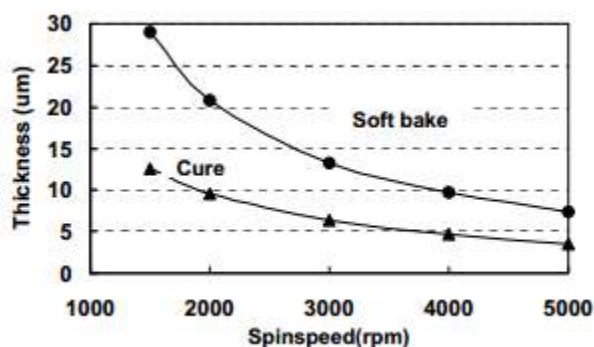


Figure 3.31 Spinning curve of HD4100 (Copied from [43]).

According to spinning curve, the coating procedures include:

- (1). The heated wafer was put in spin coater and fixated by vacuum.
- (2). Squeeze the HD4100 on the wafer. Let the Polyimide flow and cover all the patterned copper coils. If the Polyimide was only squeezed on to the center area, the copper coils with height of 25 μ m can obstruct the spreading of Polyimide during spinning, resulting in a poorly covered sample.
- (3). Spread cycle: Ramp to 500 rpm at 100 rpm / sec acceleration and hold for 10 sec.
- (4). Spin cycle: Ramp to spin speed 1500rpm at an acceleration of 500 rpm/s and hold for 50 sec.

Soft bake

Like photoresist, the Polyimide need to be soft baked to drive off solvents and provide sufficient chemical resistance and adhesion prior lithography. The soft bake includes two phases: the sample was put on an un-heated hotplate at the beginning, and then the hotplate was turned, the temperature gradually ramp up to 90°C. The sample is baked at 90°C for 90 sec. Then the temperature ramp up to 110°C, the sample is baked for another 90 sec.

Exposure

The purpose of exposure is to crosslink the Polyimide as well as created via holes in the film.

The exposure process begins with the sample loading. After the wafer is loaded in MA6, an alignment process has to be done very carefully to make sure the opaque area on the mask fully cover the via area on the sample, preventing the UV light to irradiate the via area. Layout of Mask 2 is shown in **Figure 3.32**.

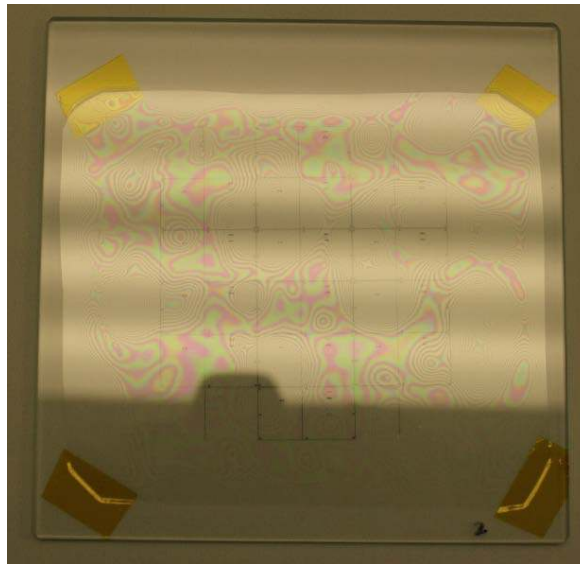


Figure 3.32 Layout of Mask 2 used in Polyimide photolithography.

The procedure of alignment includes:

1. Align microscope objectives to mask alignment marks. In the split view, the two alignment marks should be parallel to each other.
2. Move the wafer alignment mark close to a mask alignment mark. If the pre-alignment is done, this step should be easy since the alignment marks on the wafer should not be far from the alignment on the mask.

3. Use the fine X-Y movement and rotation to refine the alignment. Once the alignment marks of the wafer match to the alignment marks of the mask, it means the wafer has been perfectly aligned.

According to the datasheet, for the 30 μm thick photoresist the exposure dose should be around $300\text{mJ}/\text{cm}^2$. The intensity of the UV light is $6\text{mJ}/\text{cm}^2$ in our Fab, the exposure time is 50 seconds.

Post exposure bake (PEB)

After exposure, a post exposure bake (PEB) should be performed on a hot plate to further increase the adhesion and selectively crosslink the exposed parts of Polyimide. Without the post exposure bake, the un-crosslink part of the Polyimide can be easily attacked or delaminated by the developer. A 3 min baking at $100\text{ }^{\circ}\text{C}$ is need for the post exposure bake. To avoid cracks caused by thermal stress, the sample was cool down gradually to room temperature with the hotplate rather than took off the hotplate instantly after the baking.

Develop

When the sample is completely cooled down to room temperature, the sample can be immersed into PA-401D for developing. The develop process takes 10 min while agitation is applied. After developing, the sample is better to be checked under the microscope to make sure the via is not covered by residual Polyimide. In the via hole, the copper lustre and metal texture should be seen if the developing is successful (as shown

in **Figure 3.33**), if not, the sample should be developed again. Eventually, the sample was rinse by PA-400R Rinser, and then blew dry.

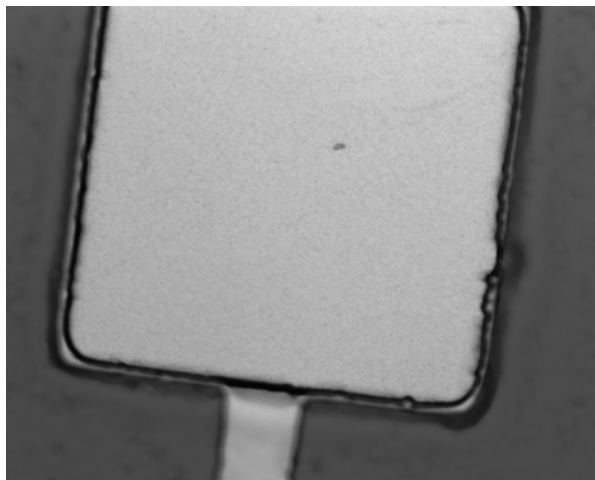


Figure 3.33 Microscope image of a well developed via area.

O₂ plasma RIE

Followed by developing, the sample was plasma etched to completely remove the residual Polyimide, most importantly, roughen the surface of Polyimide film for better Ti/Cu seed layer adhesion in the next step. Increasing the surface roughness can increase the contact area between the seed layer and the film, therefore adhesion is improved accordingly

Cure

The objectives of cure are: (1), Remove the residual solvents, (2), complete the imidization process that changes the precursor into a polyimide, (3), improve adhesion, (4), remove the photosensitive ingredients. Curing was performed at 250 °C for 20 min.

3.4.8 Sulfuric acid etch

Before depositing the second seed layer on the polyimide, sulfuric acid etch is necessary. Copper can be easily oxidized in the air, especially during cure with high temperature and plasma etching with high energy oxygen ions, the Cu atom can react with oxygen to generate CuO. The CuO layer is so thin that it is invisible under the microscope, the via still reveals a metallic lustre but actually the conductivity is already diminished. The device will not be functional if the CuO layer is not removed. CuO can react with sulfuric acid, and the reactant products are soluble.



Sulfuric acid with concentration of 10% was used; the sample was immersed in the sulfuric solution for 3 min then blew dry.

3.4.9 Second seed layer sputtering

After sulfuric etch, the sample should be put into the sputtering and pump down immediately to prevent any oxidization. The second seed layer is still Cu/Ti bi-layer structure, the sputtering parameter such as power or Argon flow rate is the same as the first seed layer. However, the thickness of Ti layer increases from 50 nm to 120 nm. The reason is: as the polyimide film's surface roughness is increased by RIE, some sharp, needle-like peaks form on the surface. Increasing the thickness of Ti can compensate the roughness, form a more smooth adhesion interface with copper, and generate a rigid bond with polyimide as well as copper.

The thickness of copper seed layer remains 300nm by using the same sputtering parameter.

3.4.10 Second layer copper coil fabrication

AZ9260 is spin coated on the sample with the second seed layer using the same coating and baking parameter. Mask 3 is used to fabricate the second micromold. The alignment is divided into two steps: a pre-alignment and a fine alignment. The transparent window is utilized to facilitate the pre-alignment. Through the window, underneath structure could be seen without microscope. By adjust the position, the sample's previous window shape pattern could be easily matched the window on the mask. Once the window pattern matches, the alignment marks on the sample and on mask are not far from each other, a fine alignment could be easily performed after the pre-alignment rather than search the entire mask for the underneath alignment marks. Layout of Mask 3 is shown in **Figure 3.34**.

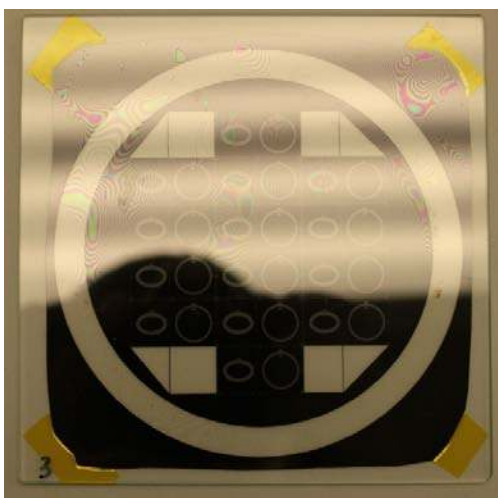


Figure 3.34 Layout of Mask 3.

A 177 sec exposure with intensity of $12\text{mJ}/\text{cm}^2$ is used to expose the photoresist. Followed by exposure, the sample is developed, rinsed and dried. After cleaned by O_2 plasma RIE, electroplating was performed using the same current and time. Then the

photoresist is stripped off, and seed layer is removed by wet etch. The images of the device are shown in **Figure 3.35**; double-layer structure can be seen in the picture.

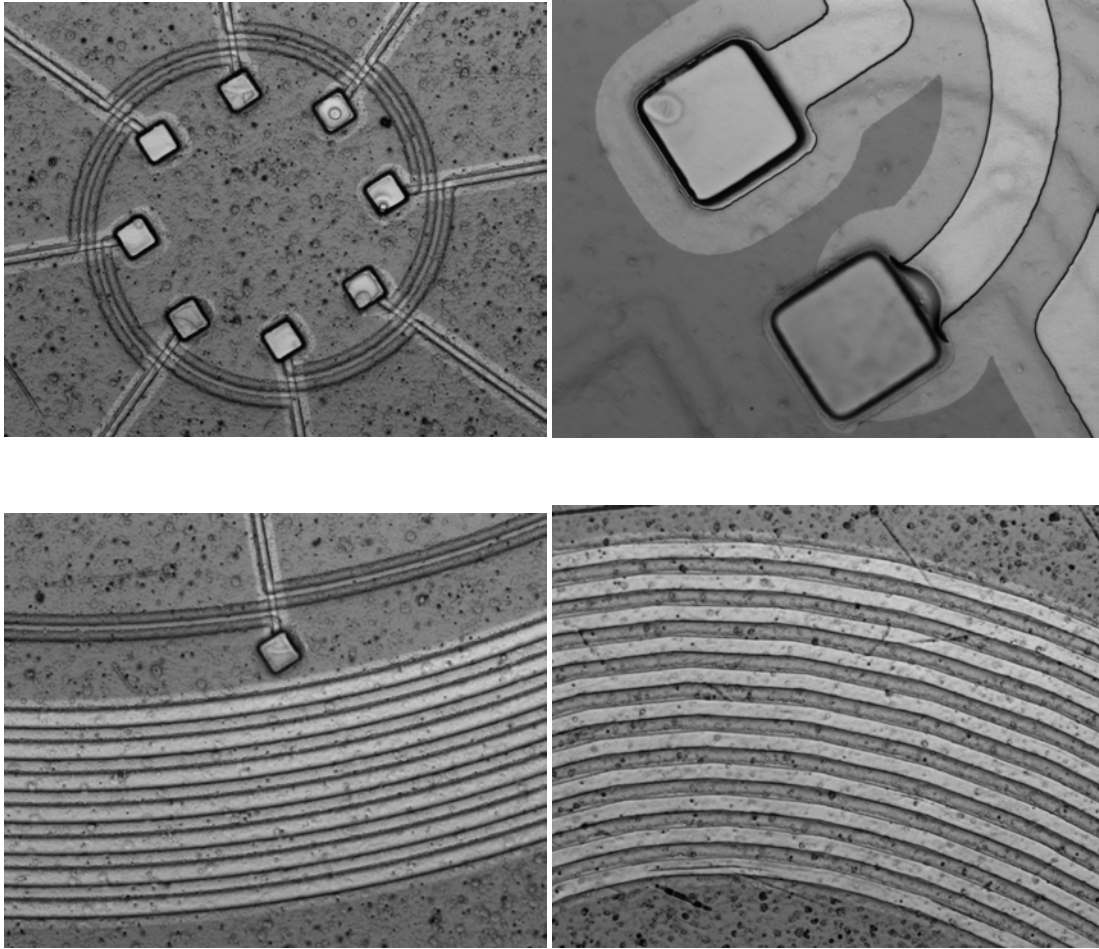


Figure 3.35 Images of two layer structure under the microscope.

If no defects were observed by microscope checking, the sample is spin coated another layer of polyimide, and then exposed to unveil the solder pad and cured. The top polyimide layer is used to protect the copper from oxidization, as well as prevent any mechanical damage due to careless handling.

Figure 3.36 shows the finished wafer before dicing. On a 4-inch silicon wafer, 14 pairs of device can be fabricated simultaneously.

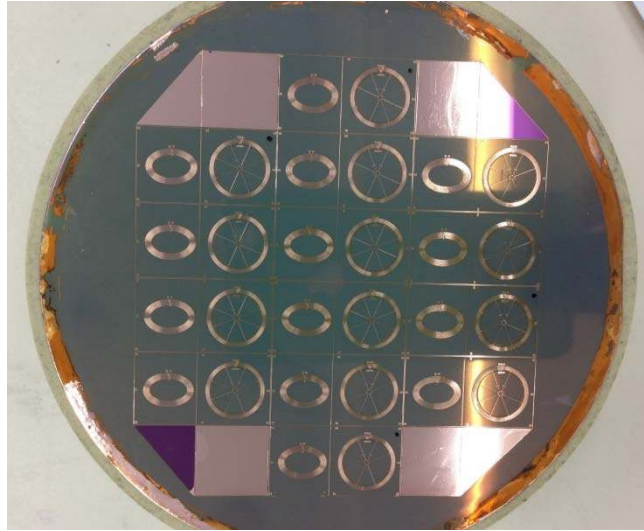


Figure 3.36 Image of finished sample.

At last, the wafer was dices into small pieces by dicing saw. Separated devices are shown in the **Figure 3.37**.

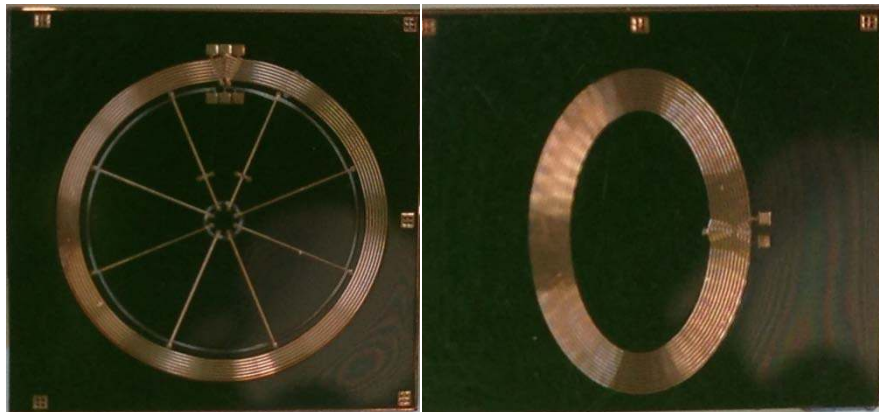


Figure 3.37 Image of devices after dicing.

3.5 Conclusions

In this chapter, the processes of fabricating multilayer inductive sensor coils are introduced. Through combining microfabrication technology, sputtering process and electroplating technique, coils with thickness over 10 μm was well achieved. Briefly, the silicon wafer with 2 μm SiO_2 was sputtered with Cu/Ti as a seed layer, then the positive photoresist AZ9260 was patterned with conventional photolithography process as the micromold for the following electroplating. The first copper layer then is fabricated by electroplating within the photoresist micromold. After removing the photoresist and seed layers, Polyimide was spin-coated and patterned to function as an insulating layer. Before sputtering the second seed layer on the polyimide, oxidization layer in the via pad is removed by sulfuric acid. The second copper layer was fabricated by the same way as the first layer through electroplating process. At last, another layer of polyimide was fabricated for protecting the copper coils. In one batch, 14 pairs of devices can be fabricated together. Upon completion, the wafer is diced into pieces to separate each device for the following test application.

Chapter 4

4 Quality characterization

4.1 Introduction

Although the morphology of the devices were checked after upon finishing of every step by microscope to make sure the devices were free of defects, the electrical properties, such as inductance and resistance, need to be measured and compared with simulation results to verify the performance of the devices. The preliminary tests were performed on LCR tester. Then further tests were performed on Agilent 4294A impedance analyzer at high frequency. After calculating the resonance frequency, the devices were integrated in the processing circuit with capacitor and other electronic components, and then the outputs were measured by oscilloscope.

4.2 Inter-procedure test and low frequency test by LCR meter

The fabrication of the device comprises many individual steps, the result of the previous step is very important for the next step. In order to verify the result of the process, a quick test should be done after every fabrication process. For example, after the first layer copper coil is finished, inductance and resistance of the copper coils should be measured to make sure the coil is not shorted by the un-etched copper, and the inductance is approximately the same as simulation. By doing this, some of the mistakes can be corrected during the procedures instead of leading the failure of the entire devices. LCR meter and probe station was used in the inter-procedure because we do not need to bond

wire on the device for this measurement, we can use the needles of the probe station to measure the device without causing any surface damage.

Measurements of first layer copper

After the first layer of copper was done, measurements were made to test the performance of the coil. The circuit schematics of the first layer coil are shown below. The round activation part includes two separate coils, which can be considered as two inductors; the eclipse coupler part includes one coil, which can be considered as one inductor (**Figure 4.1**).

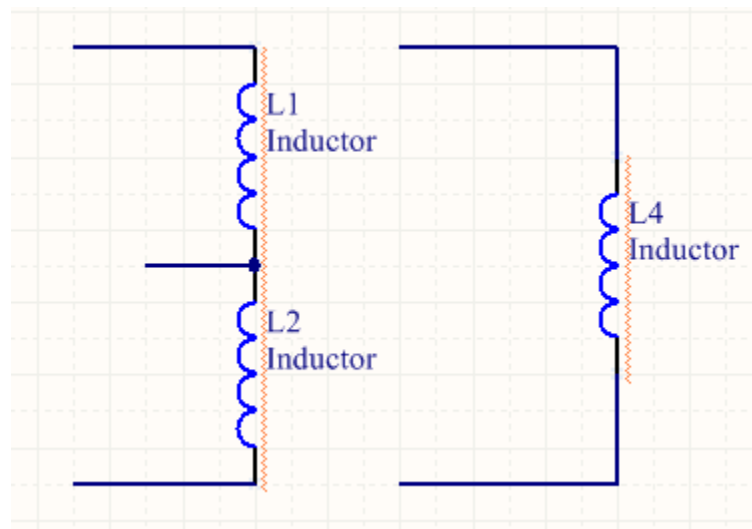


Figure 4.1 The circuit schematics of the first layer coil.

For the first layer copper, L1, L2 represent the two coils inductors of the round excitation coil, L4 represents the coil inductor of the eclipse coil. Since the pads of device are very small, probe station needs to be used for the measurement. The LCR meter, GWINSTEK LCR-821, is connected to probe station for measuring the parameters of the coils (**Figure 4.2**).

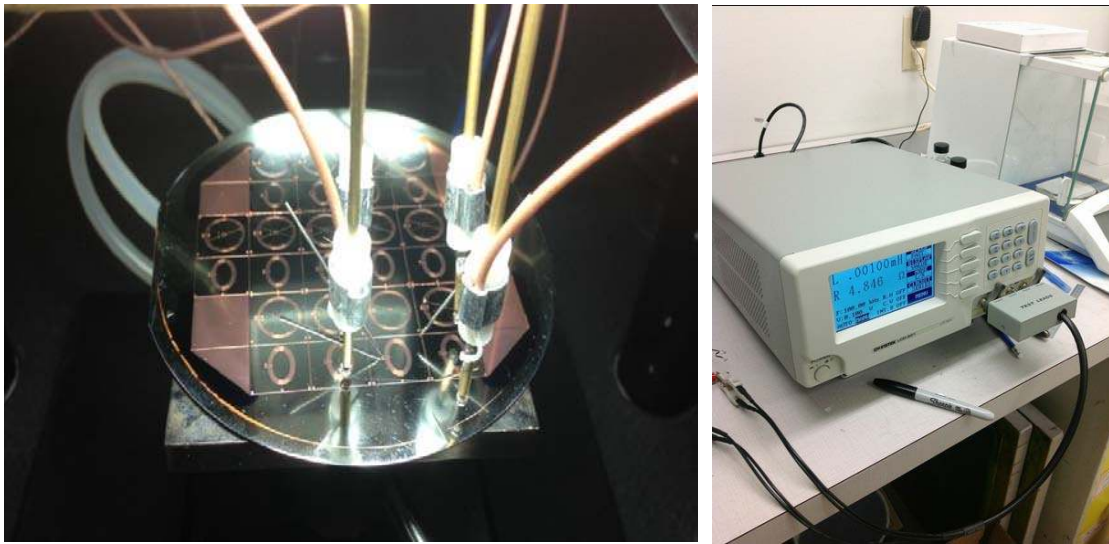


Figure 4.2 Probe station and LCR meter used in the measurement.

The needles were connected to the pad with a little compression force to minimize the contact resistance. The wires which connect the needle and LCR meter have their own inductance, comparing to the device coils to be measured, the inductance of wires are the same or larger than the coils. Therefore, at the beginning of the measurement, two steps of compensation, which include open compensation and short compensation, need to be done to eliminate the influence of wire inductance. The tests result are shown below:

Table 4.1 Test result of first copper coils

Excitation coil				Eclipse coil	
L1		L2		L4	
Inductance	Resistance	Inductance	Resistance	Inductance	Resistance
0.50 μ H	2 Ω	0.50 μ H	2 Ω	2.10 μ H	5 Ω

The maximum frequency of the LCR meter is 200 kHz, it is smaller than the working frequency of 4MHz, however the resistance results match the simulation result. It means fabrication of the first layer is successful.

Measurements of insulating layer

The same measurements need to be done again after the Polyimide insulating layer is prepared. These measurements are performed to ensure that the via holes are not covered by invisible Polyimide thin film. If the test results are the same as the previous ones, it means the via holes are fully exposed.

However, the CuO thin layer coverage cannot be discovered in this step because the needle contacts the pad with pressure force, therefore, the CuO thin layer is penetrated by the needle.

Measurements of devices

After the whole process was done, measurements were performed to test the inductance and resistance of the devices. In the first batch, the resistance of the round activation coil

was 40Ω , which was larger than simulation. After examining every possibility, we realized the problem was caused by the copper oxidization during the process, then sulfuric acid etch was introduced to remove the oxidization layer. The final test results are shown below:

Table 4.2 Test result of the device.

Excitation coil						Eclipse coil	
L1'		L2'		L1'+L2'		L4'	
Inductance	Resistance	Inductance	Resistance	Inductance	Resistance	Inductance	Resistance
1.00 μ H	4 Ω	1.00 μ H	4 Ω	4.00 μ H	8 Ω	4.20 μ H	10 Ω

In **Table 4.2**, L1' and L2' represent the two coil inductors of the round excitation coil, L4' represent the coil inductor of the eclipse coil. When L1 and L2 are both applied current, they are in series connection. The measured inductance includes their own inductance and mutual inductance, so the total inductance is much larger than the sum of the L1' and L2's inductance.

The test results were approximately the same as the simulation result. In the next step, further tests were performed on the impedance analyzer at high frequency.

4.3 High frequency test by impedance analyzer

The high frequency test were preformed on Agilent 4294A in KSR International Co. (**Figure 4.3**). 4294A is capable of testing inductance, resistance and impedance from 40Hz to 11MHz.

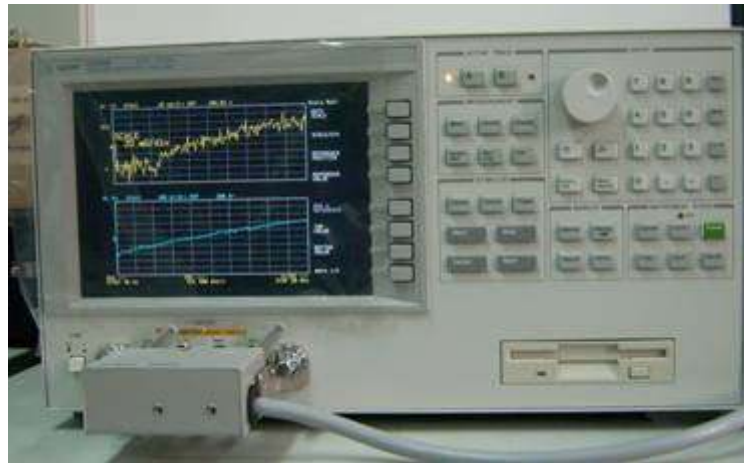


Figure 4.3 Agilent 4294A impedance analyzer.

The same as LCR meter, compensation need to be done before the test to calibrate the 4294A as well as eliminated the error caused by connecting wire. The compensation procedures include a short compensation, an open compensation and calibration of a 50Ω standard resistor. After the compensation, device was connected to the analyzer, the sweeping frequency is from 1 MHz to 6 MHz. The tests results are shown in **Figure 4.4**, **Figure 4.5**, **Figure 4.6** and **Figure 4.7**:

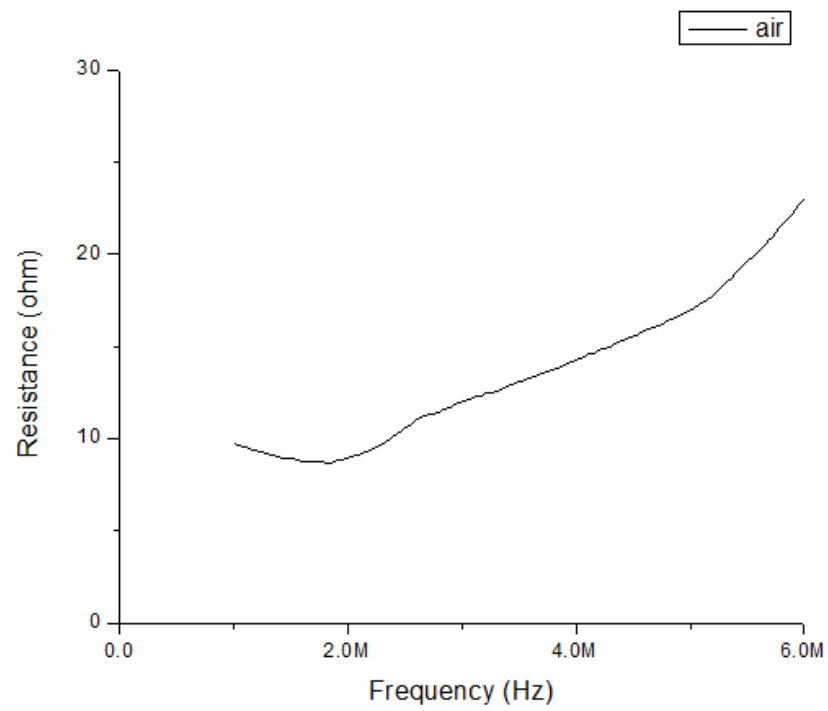


Figure 4.4 Resistance of the eclipse coil.

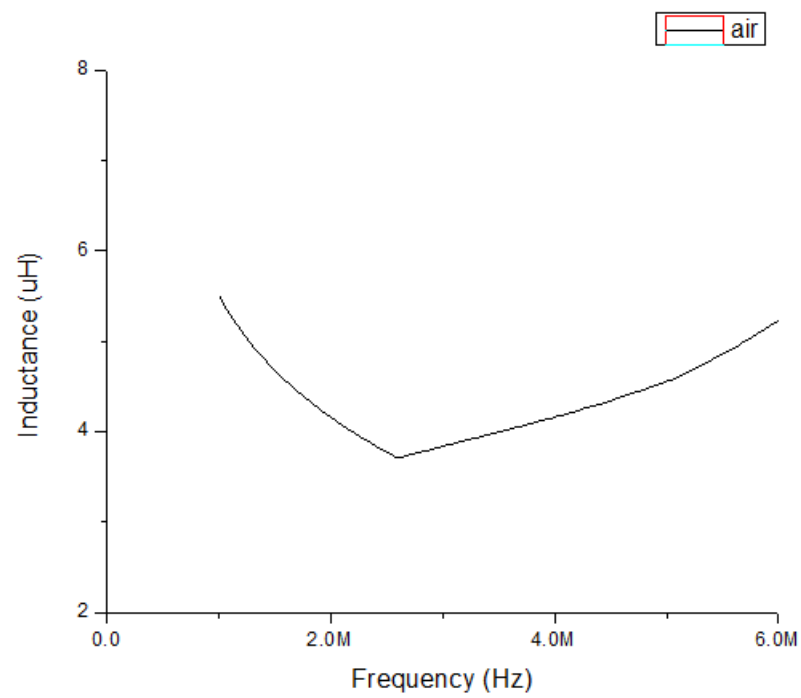


Figure 4.5 Inductance of the eclipse coil.

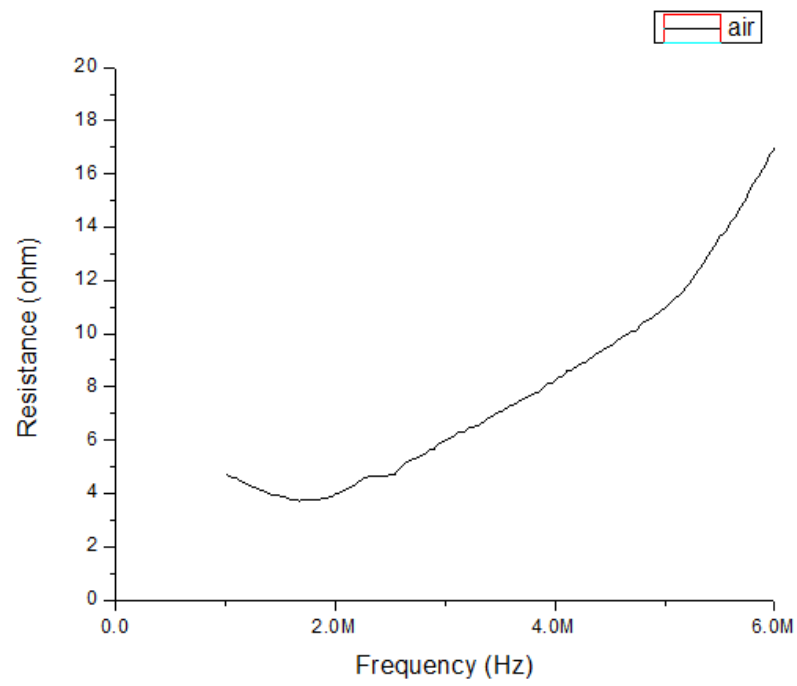


Figure 4.6 Resistance of the round excitation coil.

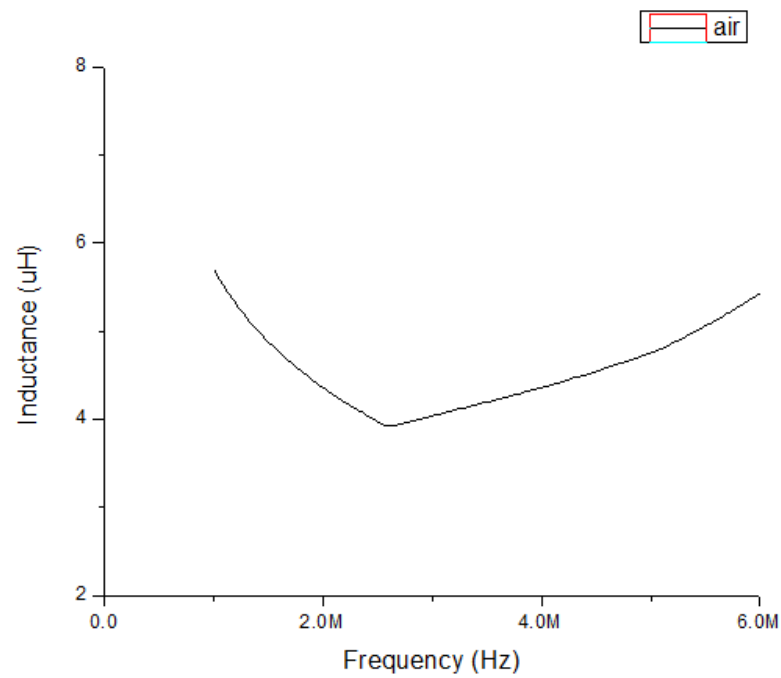


Figure 4.7 Inductance of the round excitation coil.

By comparing the inductance and resistance data with the simulation results, it can be seen that the measured results were very close to the simulation results. The comparisons of the results are listed below:

Table 4.3 Comparison of simulation results and test results.

	Measurement		Theoretical	
	Inductance	Resistance	Inductance	Resistance
	μH	Ohm	μH	Ohm
Ellipse coil	4.56	12.87	4.86	10
Round excitation coil	4.60	8	4.82	8.44

4.4 Circuit integration

The electrical properties proved that the device's fabrication process is reliable and successful. However, to make the inductive sensor work, the devices need to be integrated into the PCB system.

A PCB board is designed to integrate the device, peripheral electronic components and ASIC chip. This ASIC (Application-Specific Integrated Circuit) chip is customized by KSR International Co., the product number of this ASIC is AA800B. PCB board not only provides mechanical support, also provides electrically connections using copper signal traces. Before the measurements, SMT (surface-mount technology) capacitors, resistors and AA800B are soldered on the PCB. The layout of PCB is shown in **Figure 4.8**:

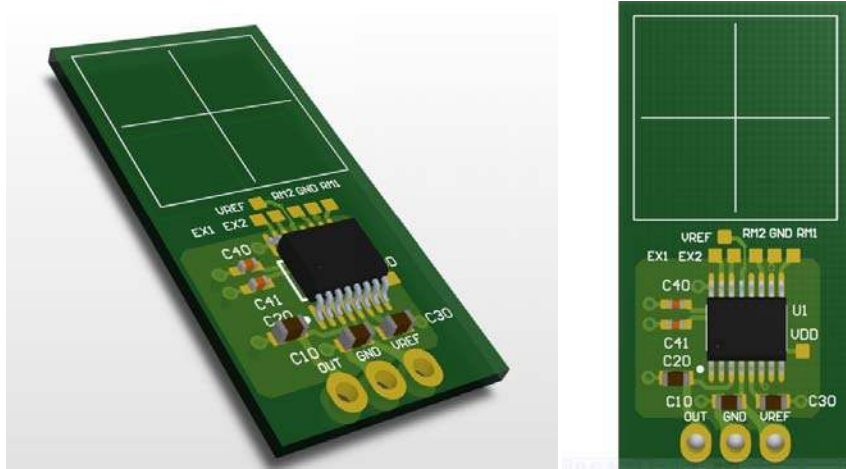


Figure 4.8 Layout of PCB.

A capacitor is working in series with the excitation coil inductor to form a LC oscillator. Another capacitor is soldered in series with the eclipse coil to form the coupler LC loop. When the coupler is put at a proper position, the coupler LC loop and activation LC loop will resonance at a designated frequency. A voltage is induced in the sensing coil by the alternating resonance magnetic field. According to Faraday's Law, when the coupler changes position, the magnetic flux in the sensing coils changes, therefore, the induced voltage changes. There is a driving circuit in the AA800B to drive the excitation LC loop to oscillate, there are also a modulation, de-modulation and signal processing circuit for processing the signal transferred from sensing coil. The schematic of resonance circuit and the sensing coil are shown in **Figure 4.9**, L1 and L2 represent the two coils in excitation coil, L4 represents eclipse coil and L3 represents sensing coil. The resonance frequency can be calculated by the following equation:

$$f = \frac{\omega}{2\pi} = \frac{1}{2\pi\sqrt{LC}} \quad \text{Eq 4.1}$$

For the excitation coil or eclipse coil alone, we assume their oscillate frequency is 5MHz, according to **Eq 4.1**, the calculated capacitor's capacitance is 220pF and 200pF respectively. When the two LC loops approaches each other, they will resonance at the same frequency, which is $\frac{\sqrt{2}}{2} \times f = \frac{\sqrt{2}}{2} \times 4.8 = 3.39MHz$.

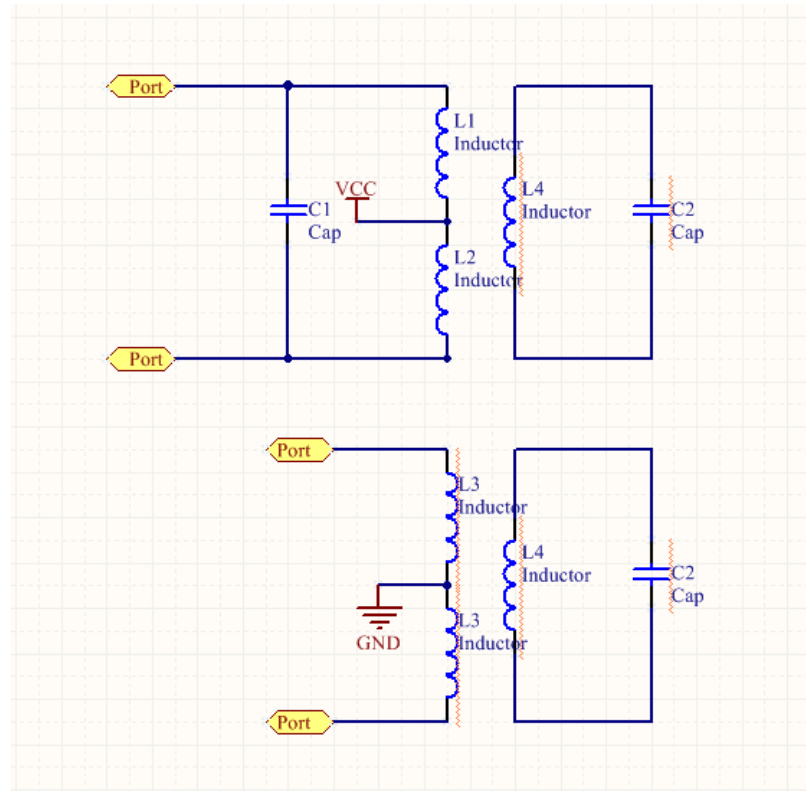


Figure 4.9 Schematic circuitry of excitation coil, LC coupler and sensing coil.

In order to connect the device to PCB assembly, a precise wire bonding method is needed. Traditional wire soldering or surface-mount (SMT) is not applicable because of two reasons: 1. The pad is very small, it is hard to apply soldering paste for SMT or soldering iron. 2. Heat dissipation on Si is faster than PCB because Si is a relatively good heat transfer medium, the temperature of the heat gun is not enough to melt the solder paste

applied on the device pads. Therefore, gold wire ball bonding is used to accomplish the task. Wire bonding is performed by the machine shown in **Figure 4.10** in McMaster University.



Figure 4.10 Wire bonder used to bond device to PCB.

35 μm diameter gold wire is used for the wire bonding because gold does not oxide easily. The wire is fed through a needle-like tool call capillary. Once the length of the wire tail outside the capillary reaches 1-2 mm, a high voltage electric charge is applied to the wire to melt the wire at the tip of the capillary, making the tip of the wire to form into a ball. Then the capillary is lowered to the surface of the pad, there is a certain distance between the capillary and the pad to avoid the ball touching the pad surface, otherwise the ball will fall. Alignment is done by the user through microscope to make sure the capillary is at the right bonding position. If the alignment is good, the user hits the bonding button and the machine pushes down the capillary and applies ultrasonic energy. The

combination of pressure and ultrasonic energy create a weld between gold ball and the surface of the pad. Then the capillary is moved to the next bonding position, the same procedure performed again, but this time without making a ball so that the wire is crushed between the second pad and the tip of the capillary. In the final step, the machine feeds out a small length of wire and tears the wire using a clamp. Again, the tail is applied high-voltage charge and next bonding can be performed. Morphology of good bonding result is shown in **Figure 4.11**.



Figure 4.11 Morphology of good bonding result and the bonding parameter-setting panel.

The parameters for the ball bonding are listed below:

Table 4.4 Bonding parameter.

	Loop	Search	Force	Time	Power
Bonding 1	4	1	3.0	7	8.20
Bonding 2		1	6.0	5	5.30

After the bonding is done, along with the peripheral components and AA800B are soldered on the PCB, the circuit is ready for test. The PCB board size is 15×30mm. The peripheral electronic components and AA800B are better to be soldered before wire bonding, because the heat of the blow gun may damage the fragile gold wire. Otherwise, the welding points need to be covered by epoxy for protection.

Pin definitions of the AA800B are shown in Figure 4.12, the activation LC loop connects to EX1 Pin and EX2 Pin; sensing coil connects to RM1 Pin and RM2 Pin. VHV Pin connects to power source, PPS Pin is the output Pin. AA800B is driven by 5V voltage by connecting VHV Pin to power source and GND Pin to ground. Output PPS is measured by oscilloscope.

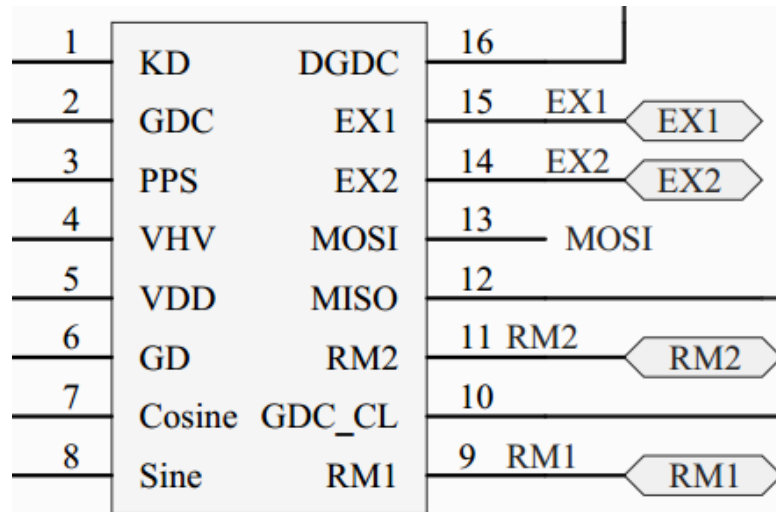


Figure 4.12 Pin definitions of AA800B

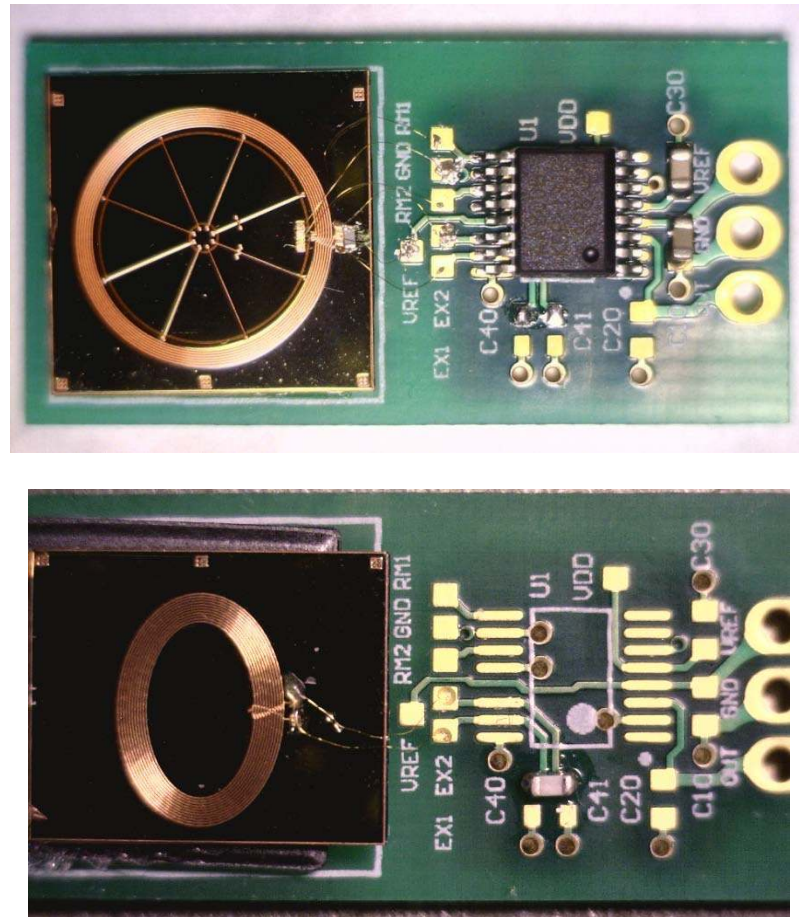


Figure 4.13 Image of the sensors assemblies.

The output is measured by oscilloscope through EX1 or EX2 Pin, screenshot of the waveform of the excitation coil individually is shown below. Sine waveform can be observed from the oscilloscope, which means the excitation can be driven by the AA800B to oscillate. From the waveform, we knew that the oscillate frequency is 4.8 MHz, output voltage of peak-to-peak is about 4.33V.

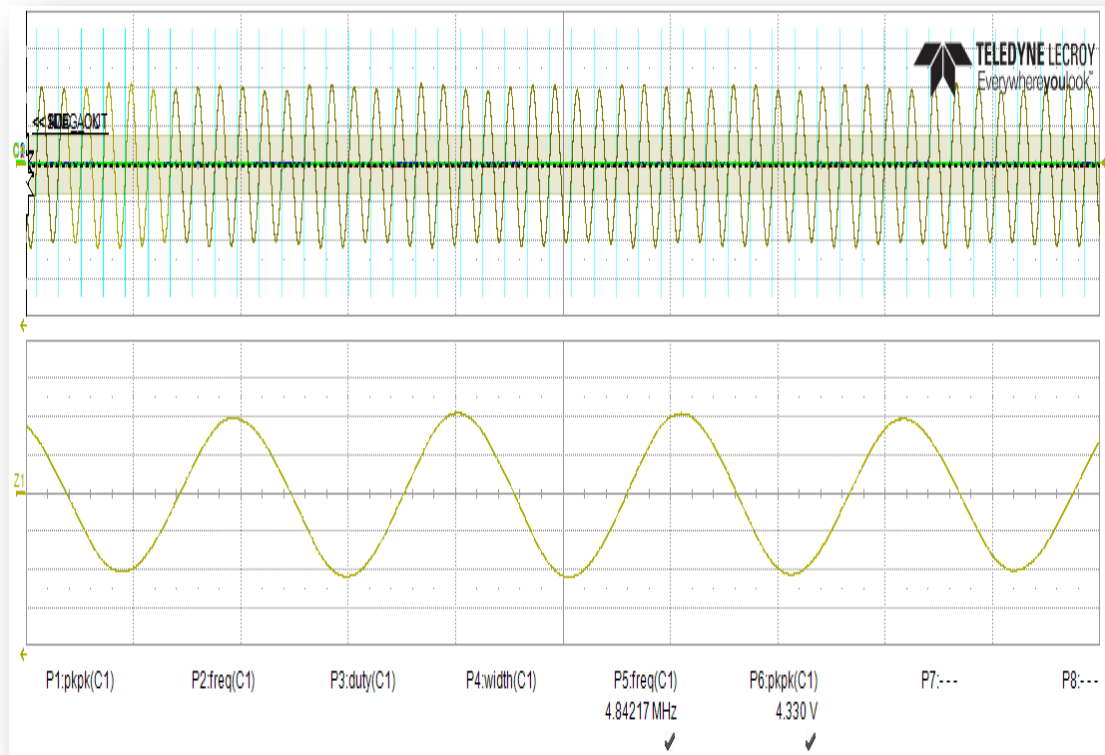


Figure 4.14 Screenshot of the waveform of the excitation coil alone

When the coupler LC circuit approaches, they will resonance at another frequency. As shown below, the resonance frequency is about 3.6 MHz, the output voltage measured from excitation coil is 3.7V.

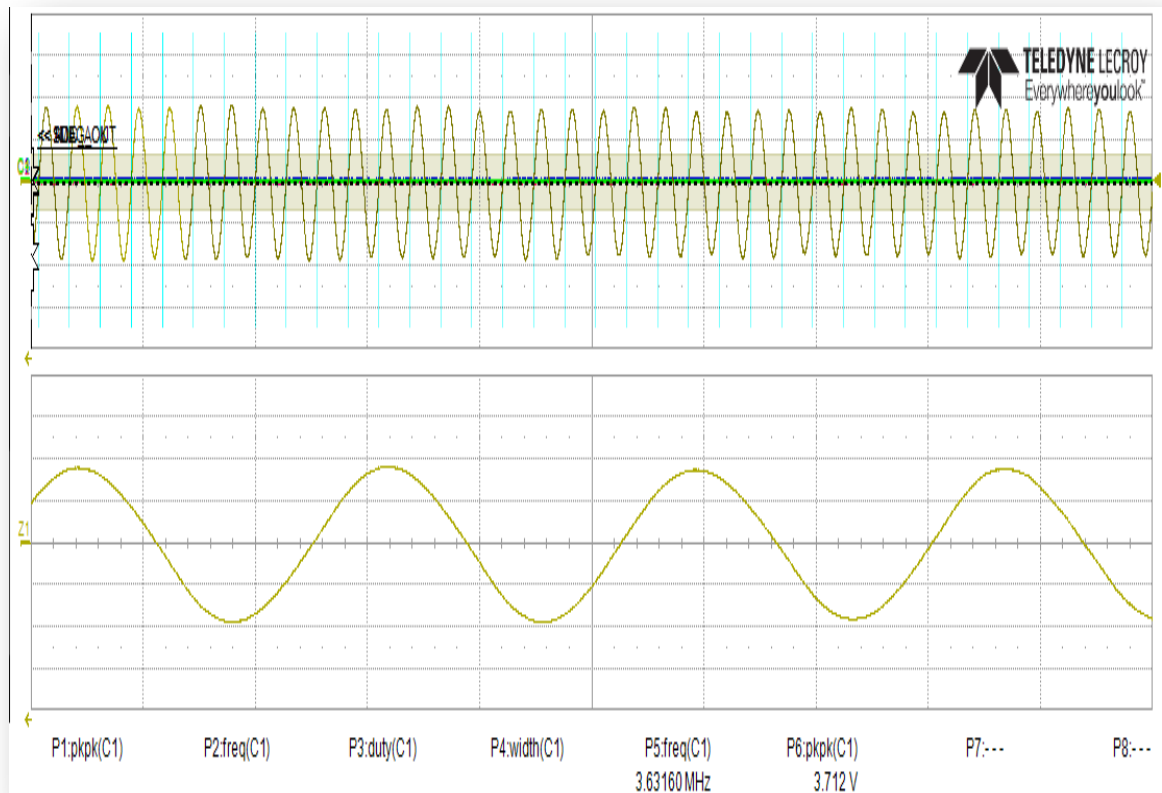


Figure 4.15 Screenshot of the waveform of the excitation coil with coupler.

The resonance frequency matches the calculation, the output voltage approximately at the same level with the PCB prototype manufactured by KSR.

Signals from the two sensing coils are also measured by oscilloscope through RM1 or RM2 Pin.

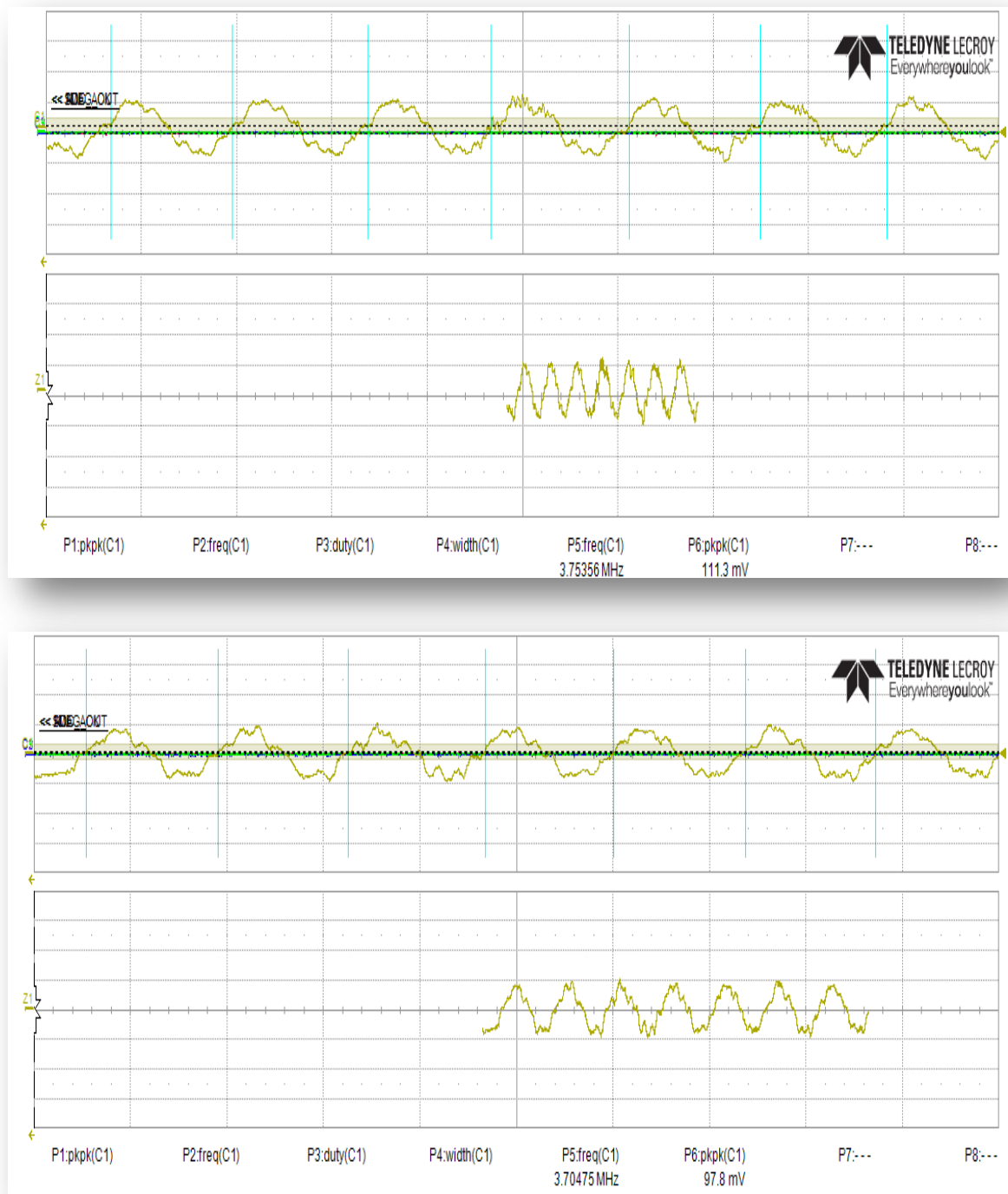
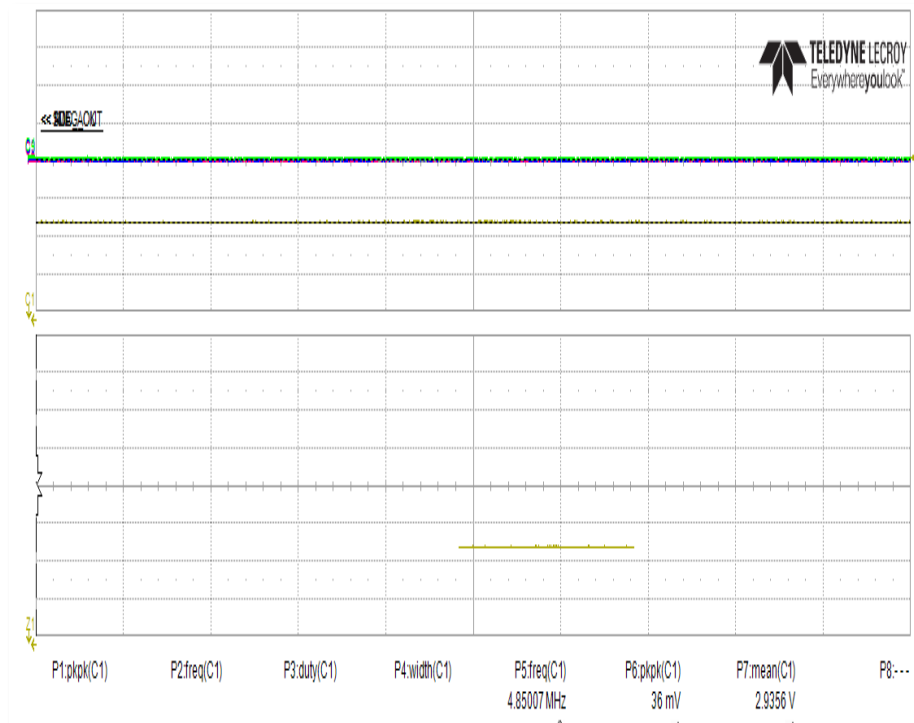
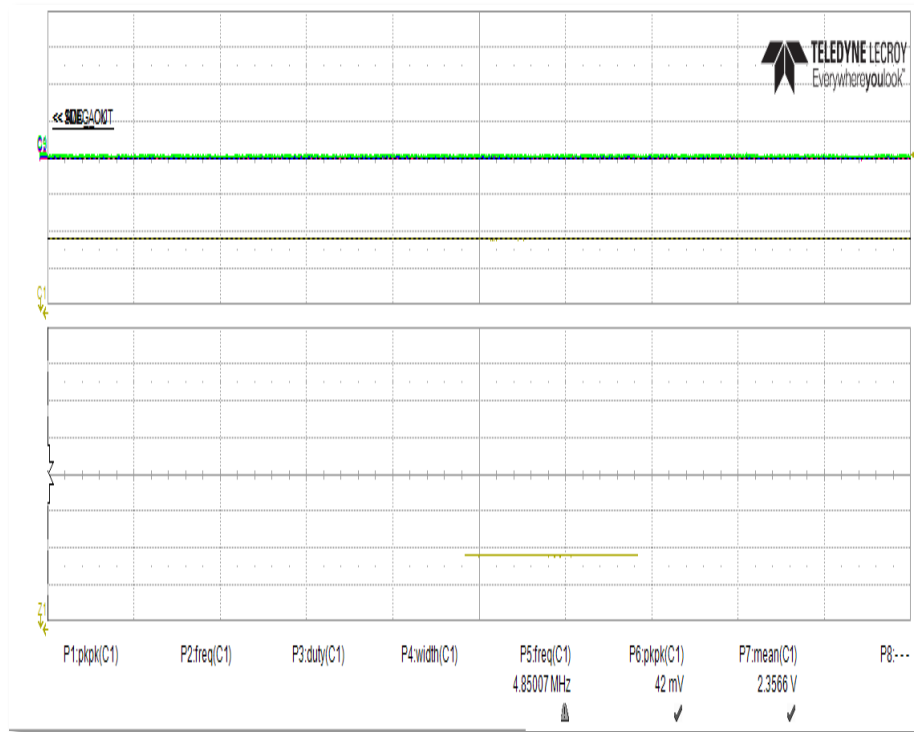


Figure 4.16 Waveform of the sensing coil.

The output voltage of the sensing coil is above 100mV, which satisfy the AA800B processing requirements. The signal strength is about the same level as the PCB peer product. By changing the position of the coupler, magnetic flux of in the sensing coils changes, therefore, the induced voltage changes accordingly in the sensing coil. Then the changing voltage is captured by AA800B, after filtering, modulation and demodulation and processing, a voltage signal is output at PPS pin to illustrate the relative position of the coupler. The PPS voltage should change between 0V to 5V as the position of the coupler changes.

In our case, as the position of the coupler changes, the output voltage of PPS changes from 2.3V to 3.1V. The output cannot change full range from 0V to 5V because the length of bonding wire is approximately the same as the sensing coil, therefore, the bonding wire forms another loop of sensing coil, and this sensing loop can pick up magnetic signals as well. Thus, the induced voltage in the sensing coil is influenced by the induced voltage in the bonding wires; the noise ratio is also increased by the bonding wire loop. To improve the performance of the device, the configuration of the coil needs to be optimized to eliminate the influence of the bonding wires.



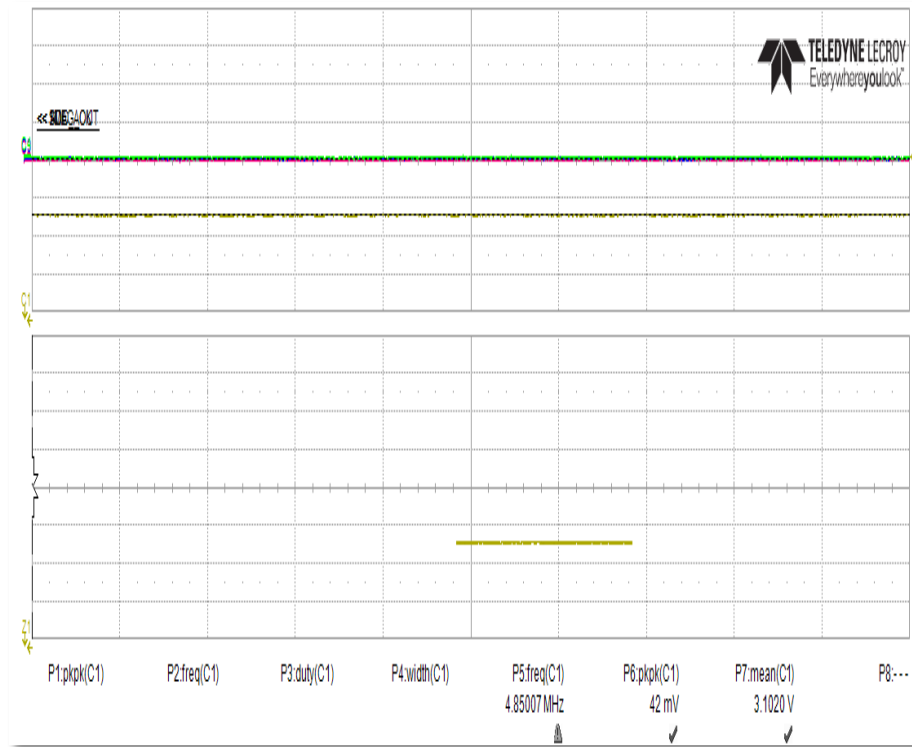


Figure 4.17 Sensor output measured from PPS port.

The result proves that the device is compatible with the AA800B; the working principle of the device is feasible.

4.5 Conclusion

Thanks to inter-procedure test, the fabrication flaws can be quickly identified and solved during the fabrication processes, which indeed increases the efficiency and accuracy of the procedures. Upon completion, the devices were tested by impedance analyzer at high frequency. The tests result showed that the resistance and inductance of the device match very well with the simulation results, which means the fabrication is quite successful. Then the devices were also integrated with the peripheral components and AA800B, the resonance frequency, voltage, and the output of AA800B were measured. The results

show that AA800B can drive the LC circuit to oscillate, and the excitation LC circuit and coupler LC circuit can resonate as expected. The output of excitation coil was over 4V and the resonance frequency matched with the calculation. The output of the PPS also changed as the position of coupler changed, this proves that the principle for the inductive sensor can work and the device is also compatible with the AA800B. These characterization tests are very encouraging to employ the newly designed coils for micro inductive sensors.

Chapter 5

5 Conclusions

5.1 Summary of results

In this thesis, the micro-fabrication process of the miniaturized inductive sensors and small volume production of inductive sensor devices were studied in detail. Based on calculation, simulation, and preliminary fabrication tests, proper parameters and key procedures were determined. Three layers coil structures, including two copper layers and an insulating layer, were built up by micro-fabrication process. During the fabrication process, LCR meter was used to measure the resistance and inductance of the devices. Upon completion, impedance analyzer was used to measure the inductance and resistance at high frequency. Eventually, the devices were integrated in the circuit, and the output of the LC excitation coils, sensing coils and AA800B output were measured.

The miniaturized micro inductive sensors were successfully fabricated by micro-fabrication and electroplating technique. A reliable, efficient micro-fabrication process was developed. At the beginning, the key parameters such as line width, gap and copper thickness were calculated with consideration of size, fabrication limit and skin effect at high frequency. Electroplating was chosen to fabricate the copper layer instead of sputtering, because electroplating is capable of fabricating over 10 μm thick copper, while the maximum thickness could be achieved by sputtering is only 3 μm . AZ9260 was chosen as the micromold material because of its good adhesion with copper and capability of forming thick film. Photomasks were specifically designed for the following

electroplating and lithography by adding some features such as transparent ring and transparent pre-alignment windows.

A silicon wafer with 2 μm SiO_2 and sputtered Cu (300nm)/Ti (50nm) seed layer was used as the substrate for the photolithography. AZ9260 was spin coated on the substrate, then exposed and developed to form a 15 μm thick patterned micromold. Electroplating was used to grow the copper layer in the micromold because of its relatively high growth rate. By regulating the electroplating current and adding additives like brightener and carrier, uniform and bright copper structures were formed. After stripping off the micromold photoresist, Cu and Ti seed layers were removed by wet etch respectively by carefully observing the color change.

Once the first layer copper was done, polyimide was spin coated on the sample. Polyimide has the advantages such as high heat resistance, solvent, acid and base resistance, high resistivity, good elasticity, therefore, it is a very unique material for insulating layer. In this project, a negative tone photo-definable polyimide HD4100 was used. The coated polyimide film was soft baked, exposed, developed and post baked to form via holes as well as polymerize the film. The polyimide was etched with O_2 plasma in order to increase the adhesion and remove the residual polyimide in the via holes. Followed by RIE, the polyimide was cured to further increase the adhesion between polyimide and wafer, as well as completely polymerized the film.

Before depositing the second seed layer, the sample needs to be washed by sulfuric acid solution to remove the invisible oxidization layer on top of the via copper surface which was formed in the previous baking and O_2 plasma etch steps.

The second layer of Cu/Ti seed layer was deposited by sputtering right after the sulfuric acid etch. The thickness of Ti layer was intentionally increased to increase the adhesion between polyimide film and Cu. Then the micromold and the copper were fabricated by the same way as the previous steps. Upon fabrication of copper layer was finished, another polyimide was coated and patterned for protecting the copper from oxidization and mechanical damage.

During the process, LCR meter and probe station were used to verify the properties of the device. Using probe station, the test can be performed without damaging the surface. The inter-procedure tests helped us to identify the surface oxidization problem, therefore assured the success of the fabrication.

After all the procedures were finished, devices were tested by the impedance analyzer at high frequency. The measurements showed that the inductance and resistance of the devices were consistent with simulation, which mean the microfabrication process was reliable and accurate.

Eventually the devices were integrated in the PCB with peripheral components and AA800B. Based on the inductance result and working frequency, the capacitance of the capacitor in the LC oscillate circuit was calculated. The output of the activation coil, sensing coil and AA800B were measured by oscilloscope. When the circuit was powered, sine waveform can be seen from the oscilloscope, which means the AA800B can drive the excitation coil to oscillate. When coupler approached, the two LC loops resonance. The resonance signal can be pick-up by the sensing coil. The output of the sensing coil

was above 100mV level, the output of AA800B change with the rotation of the coupler, which means the device worked and the prototype principle was feasible.

In conclusion, the test results of the measurements presented in this study are consistent well with our simulation and fulfill the objective. The microfabrication procedures developed for the inductive sensor are reliable and efficient. Some of the key parameters in the process are digged out and some valuable fabrication experiences are gained. Hence, the results obtained demonstrate the feasibility of prototyping. The methodology and the experimental parameters shown in the present study can also be further optimized and considered to benefit the mass production in the future.

5.2 Thesis contributions

The original contributions of this thesis are summarized as follows:

- (1). Developed a series of microfabrication procedures with combination of electroplating process which can fabricate two or multiple layers of patterned metal with higher thickness that traditional microfabrication technique can't achieve.
- (2).Successfully fabricated the miniaturized micro inductive sensor.
- (3).Performed systematic measurements to verify the performance of fabrication process and evaluated the performance of the newly designed inductive sensor.

5.3 Suggestions for future research

The work has already shown that the microfabrication process developed for the inductive sensor is reliable and efficient. The performance and the production yield would be better if he following aspects can be done in future.

First of all, the layout of the inductive sensor design needs to be optimized. Although the current design is functional, the not-well-positioned pads increase the complexity of wire bonding. The bonding wire may intertwine and cause the circuit short and increase the noise ratio.

Secondly, the plastic masks should be replaced by the chromium masks to increase the resolution. Although the plastic masks we are using are produced using the highest resolution, the edge of the pattern is still rough. The resolution of chromium masks are much better because they are fabricated by laser or electron beam rather than printing. The plastic mask also decomposes due to repeated UV exposure. The chromium mask is more reliable and stable comparing to plastic mask.

Thirdly, although AZ9260 is good enough for fabricating the 20 μm copper, other thick resist options need to be explored. If in the future, thicker copper layer is required, AZ9260 is not good enough. If the growth time is increased, the seed layer grows thicker and it cannot be removed when the copper thickness is over 40 μm . Some other photoresist, such as AZ® 10XT [53], AZ® 125nXT [54] are capable of forming thicker film, which will benefit the electroplating for thicker metal growth.

Last but not least, ferrite substrate may be used to substitute the silicon wafer, or integrated in the packaging to enhance the signal strength and EMC performance. If ferrite can be integrated in the device, it can reduce the dissipation of magnetic field. Therefore, signal/noise ratio can also be improved accordingly.

References

1. Barron, M.B. and W.F. Powers, *The role of electronic controls for future automotive mechatronic systems. Mechatronics, IEEE/ASME Transactions on*, 1996. *1*(1): p. 80-88.
2. www.ksrint.com. [Accessed: Sept. 19, 2013]
3. Fleming, W.J., *Overview of automotive sensors. Sensors Journal, IEEE*, 2001. *1*(4): p. 296-308.
4. Toyota Auto Sales, U.S.A, Inc. *Position Sensors*. p.3.
5. Wikipedia, *Hall effect*. http://en.wikipedia.org/wiki/Hall_effect. [Accessed: Sept. 19, 2013]
6. Consys.com. <http://consys.com.ua/electropedalseng.htm>. [Accessed: Sept. 19, 2013]
7. Honeywell.com. *Hall Effect Sensing and Application*. p. 3-4.
8. Honeywell.com. *Application of Magnetic Position Sensors*. p. 1.
9. Treutler, C.P.O., *Magnetic sensors for automotive applications. Sensors and Actuators A: Physical*, 2001. **91**(1–2): p. 2-6.
10. BMW Education. *Automotive Sensors*. p.5.
11. Ripka, P. and J. Humr. *Inductive distance sensor for biomedical applications. in Sensors, 2008 IEEE*. 2008.

12. Roux, A., et al., *The Search Coil Magnetometer for THEMIS. Space Science Reviews*, 2008. **141**(1-4): p. 265-275.
13. Lichtenberger, J., et al., *Automatic Whistler Detector and Analyzer system: Automatic Whistler Detector. Journal of Geophysical Research: Space Physics*, 2008. **113**(A12): p. A12201.
14. Hayakawa, M., K. Hattori, and K. Ohta, *Monitoring of ULF (Ultra-Low-Frequency) Geomagnetic Variations Associated with Earthquakes. Sensors*, 2007. **7**(7): p. 1108-1122.
15. Kamenicky, P. and P. Horsky, *An Inductive Position Sensor ASIC, in Analog Circuit Design*. 2008, Springer. p. 33-53.
16. Robertson, C.T., *Printed Circuit Board Designer's Reference: Basic*. 2004: Prentice Hall PTR.
17. Cheng, H., *ULSI Technology*, eds. CY Chang and SM Sze, 1996, McGraw-Hill, Singapore.
18. Sze, S., *VLSI Technology*, 2nd, 1988, New York: McGraw-Hill.
19. Sze, S.M., *Semiconductor devices: physics and technology*. 2008: John Wiley & Sons.
20. Voldman, J., M.L. Gray, and M.A. Schmidt, *Microfabrication in biology and medicine. Annual review of biomedical engineering*, 1999. **1**(1): p. 401-425.

21. Petersen, K.E., *Silicon as a mechanical material. Proceedings of the IEEE, 1982. 70(5): p. 420-457.*
22. Menz, W., J. Mohr, and O. Paul, *Microsystem technology. 2008: Wiley-VCH.*
23. Kovacs, G.T., *Micromachined Transducers Sourcebook McGraw Hill. New York, 1998.*
24. Madou, M.J., *Fundamentals of microfabrication: the science of miniaturization. 2002: CRC Press LLC.*
25. Brown, A.D., et al., *Patch antennas on ferromagnetic substrates. Antennas and Propagation, IEEE Transactions on, 1999. 47(1): p. 26-32.*
26. Li, G., et al., *Analysis of frequency-selective surfaces on a biased ferrite substrate. International journal of electronics, 1995. 78(6): p. 1159-1175.*
27. Barron, A.R., *Composition and Photochemical Mechanisms of Photoresists. <http://cnx.org/content/m25525/latest/>. [Accessed: Sept. 19, 2013]*
28. Pimpin, A. and W. Srituravanich, *Review on micro-and nanolithography techniques and their applications. Engineering Journal, 2011. 16(1): p. 37-56.*
29. Robinson, M. and R. Behrisch, *Sputtering by particle bombardment I. Topics in Applied Physics, 1981. 47: p. 73.*
30. Oxford Vacuum Science. *Sputter Deposition. http://www.oxford-vacuum.com/background/thin_film/sputtering.htm. [Accessed: Sept. 19, 2013]*

31. Wikibooks. *Microtechnology/Additive Processes*. http://en.wikibooks.org/wiki/Microtechnology/Additive_Processes. [Accessed: Sept. 19, 2013]
32. Kanani, N., *Electroplating: basic principles, processes and practice*. 2004: Elsevier Science.
33. Franssila, S., *Introduction to microfabrication*. 2004, John Wiley & Sons Ltd.
34. Ansys. *Ansys HFSS product introduction*
35. Singh, J. and D.E. Wolfe, *Review Nano and macro-structured component fabrication by electron beam-physical vapor deposition (EB-PVD)*. *Journal of Materials Science*, 2005. **40**(1): p. 1-26.
36. Tisone, T. and J. Bindell, *Step coverage in the vacuum deposition of thin metal films*. *Journal of Vacuum Science and Technology*, 1974. **11**(1): p. 72-76.
37. Microchem. *LOR and PMGI Resists Datasheet*.
38. Lorenz, H., et al., *High-aspect-ratio, ultrathick, negative-tone near-UV photoresist and its applications for MEMS*. *Sensors and Actuators A: Physical*, 1998. **64**(1): p. 33-39.
39. Lee, C. and K. Jiang, *Fabrication of thick electroforming micro mould using a KMPR negative tone photoresist*. *Journal of Micromechanics and Microengineering*, 2008. **18**(5): p. 055032.

40. Bhushan, B., S.P. Murarka, and J. Gerlach, *Stress in silicon dioxide films deposited using chemical vapor deposition techniques and the effect of annealing on these stresses. Journal of Vacuum Science & Technology B: Microelectronics and Nanometer Structures*, 1990. **8**(5): p. 1068-1074.
41. MicroChem. *SU-8 Product Bulletin*.
42. Wikipedia. Polyimide. <http://en.wikipedia.org/wiki/Polyimide>. [Accessed: Sept. 19, 2013]
43. HD Microsystems. *HD-4100 Series Product Bulletin*.
44. Microchem. *SU-8 table of properties*.
45. Edwards Sputtering System. *Auto 500 sputtering systems for research and development*.
46. Kirchner, E., et al. *Ultra Thin Sacrificial Diffusion Barriers-Control of Diffusion Across the Cu-SiO₂ Interface. in MATERIALS RESEARCH SOCIETY SYMPOSIUM PROCEEDINGS*. 1994. Cambridge Univ Press.
47. McBrayer, J.D., R. Swanson, and T. Sigmon, *Diffusion of metals in silicon dioxide. Journal of The Electrochemical Society*, 1986. **133**(6): p. 1242-1246.
48. Dammel, R., *Diazonaphthoquinone-based resists. Vol. 11*. 1993: SPIE Press.
49. AZ Electronic Materials. *AZ9200 Series Datasheet*.
50. MicroChemicals. *Electroplating with Photoresist Masks*.

51. Davis, J.R., *Copper and copper alloys*. 2001: ASM international.
52. Western Nanofabrication Facility
Website. <http://www.uwo.ca/fab/equipment/equipment/page53/index.html>. [Accessed:
Sept. 19, 2013]
53. AZ Electronic Materials. AZ® 40 XT datasheet.
54. AZ Electronic Materials. AZ® 125 nXT - Ultra-Thick Negative Resist for Plating.

Curriculum Vitae

Name:	Xueguang Han
Post-secondary Education and Degrees:	<p>Harbin Institute of Technology Harbin, Heilongjiang, China 2002-2006 B.A.</p> <p>Tsinghua University Beijing, China 2007-2010 M.Eng.</p> <p>The University of Western Ontario London, Ontario, Canada 2011-2013</p>
Honours and Awards:	Connect Canada Internship Program 2013
Related Work Experience	Research Assistant The University of Western Ontario 2011-2013